AD-A230 427

DTIC FILE COPY

(1)

DTIC
ELECTE
JAN 07 1991
D
D

DETERMINATION OF THE OPTICAL PROPERTIES OF ORGANIC THIN FILMS BY SPECTROSCOPIC ELLIPSOMETRY

THESIS

Mark L. Sward, Captain, USAF

AFIT/GEP/ENP/90D-8

DISTRIBUTION STATEMENT A
Approved for public release
Distribution Unlimited

DEPARTMENT OF THE AIR FORCE
AIR UNIVERSITY
AIR FORCE INSTITUTE OF TECHNOLOGY

Wright-Patterson Air Force Base, Ohio

91 1 3 106

AFIT/GEP/ENP/90D-8

DTIC
ELECTE
JAN 07 1991
S D
D

DETERMINATION OF THE OPTICAL PROPERTIES OF ORGANIC THIN FILMS BY SPECTROSCOPIC ELLIPSOMETRY

THESIS

Mark L. Sward, Captain, USAF

AFIT/GEP/ENP/90D-8

Approved for public release; distribution unlimited

AFIT/GEP/ENP/90D-8

DETERMINATION OF THE OPTICAL PROPERTIES OF ORGANIC THIN FILMS BY SPECTROSCOPIC ELLIPSOMETRY

THESIS

Presented to the Faculty of the School of Engineering
of the Air Force Institute of Technology
Air University
In Partial Fulfillment of the
Requirements for the Degree of
Master of Science in Engineering Physics

Mark L. Sward, B.S.
Captain, USAF

December 1990

Accesion For
NTIS CRA&I
DTIC TAB
Unannounced
Justification
By
Distribution /
Avail
Dist
A-1

Approved for public release; distribution unlimited

Preface

The purpose of this thesis was to determine the feasibility of using the 4x4 matrix method developed by Dwight Berreman in a Spectroscopic Ellipsometry model to examine the optical properties of organic and polymer thin films. When it was presented as a possible thesis project, it sounded too good to be true. Unfortunately, that turned out to be the case. It was more difficult than it sounded, much like the entire AFIT program. My getting married between the fourth and fifth quarter didn't make things any easier (at school or at home).

There was more coding than you could shake a stick at (in MATLAB, no less). Considering I hadn't written any code since I was 12 (and that was in BASIC), it's a wonder I didn't go totally bald. Fortunately, my wife Diane and my thesis advisor Captain James D. Targove kept me from going insane. They made me focus on one problem at a time. And for that I am eternally grateful.

I must also thank the Materials Laboratory of the Wright Research and Development Center for providing the equipment and samples necessary to complete this thesis.

Mark L. Sward, Esq.

Table of Contents

Abstract

This thesis demonstrated the feasibility of determining the optical properties of organic and polymer thin films through the use of Spectroscopic Ellipsometry (SE). Tan Ψ and cos Δ data from 300-800 nanometers (nm) were taken with a Rudolph Research s2000 spectroscopic ellipsometer on four samples: indium tin oxide (ITO) coated glass; five layer poly-benzyl-L glutamate (PBLG) organic film on ITO coated glass; eight layer PBLG film on ITO coated glass; and a thiophene polymer film on a microscope slide. The data sets were fit to a choice of four computer models based on a paper written by Dwight Berreman in 1972. The four models were written in MATLAB to take advantage of its matrix manipulative capabilities. The models were: a single layer isotropic film on an isotropic substrate; a single layer anisotropic film (with random orientation of optical axes) on an isotropic substrate; two isotropic films on an isotropic substrate; and two anisotropic films (with random orientation of optical axes) on an isotropic substrate. Using only tan Ψ data over a restricted wavelength region, all four data sets were fit to variances of 0.01 or less.

I. Introduction

Thin films (thicknesses less than 5000 Å) have been recognized and used for well over a century now. Whether naturally occurring or man-made, thin films affect the electro-magnetic properties of almost all materials used in today's advanced science. Recently, the use of organic thin films (including liquid crystal and polymer thin films) has been considered in non-linear signal processing as switches, modulators, and wave-guides(1). In order to predict the properties of these non-linear devices, one must first have a good grasp of the optical properties of the thin films themselves.

The optical properties of interest are usually the complex index of refraction (N=n-ik) or the complex dielectric function ($\epsilon=\epsilon_1+i\epsilon_2$) in a frequency region of interest. An important way of obtaining these parameters for thin films is ellipsometry. Ellipsometry is a non-destructive technique that measures the relative change in polarization upon reflection from a sample. The reflectance of a sample depends on many parameters: the frequency of the incident light; the angle of incidence; the number of films on the substrate; the thickness of the films; the indices of refraction (or dielectric functions) of the films at that frequency and that angle of incidence; whether the films are anisotropic; the orientation of the optical axes with respect

to the film/substrate surface; the optical activity of the films; surface roughness; whether the films are homogeneous; and so on.

Once the reflectance measurements are in hand, the optical properties and thickness of any thin films are determined through computer modeling of the sample. The models allow for a certain structure of the film and include as many parameters as possible. The parameters are adjusted through a non-linear least-squares fitting routine until the model reflectance matches the measured reflectance (within acceptable tolerance).

So, in order to understand the optical properties of organic thin films, one must have a complete description of the complex indices of refraction (or dielectric function) over an extended frequency region. One also must know how the films are oriented with respect to each other, or the sample surface, in order to obtain the desired optical response. Unfortunately, the ellipsometry models constructed to date for organic thin films have not taken these needs into account. Typically, the models allow for only one frequency; and therefore only one value of the index of refraction (or dielectric function) is calculated.

This thesis was undertaken to correct some of these deficiencies. Four models were constructed to allow for the determination of the complex indices of refraction across an

optical frequency range. These models were successfully tested against published data. Finally, the models were used to reduce data taken from multiple layer organic films (five and eight layers of poly benzyl L-glutamate (PBLG)). These samples were mounted on an indium tin oxide coated glass substrate. The models were also used on a film of thiophene mounted on a microscope slide.

Although multiple wavelength (frequency) and multiple angle of incidence data were taken and successfully reduced (as mentioned above), the models used were hardly complete. Three of the model's inherent capabilities (accounting for optical rotation, paramagnetic effects and random orientation of the optical axes) were not taken advantage of. Maybe most importantly, the models' accounted for neither surface roughness nor inhomogeneous indices of refraction. Nonetheless, the assumptions made in modeling the organic thin films here are sound; and the calculated data match the measured data well.

II. Background

Ellipsometry measures the change in polarization of light upon reflection from or transmission through a sample. This thesis dealt exclusively with reflection ellipsometry. The change in polarization, as measured by an ellipsometer, is typically characterized by the two parameters tan Ψ and cos Δ. Tan Ψ represents the relative amplitudes of the perpendicular component of reflection (R_s), and the parallel component of reflection (R_p). Cos Δ is the difference in phase between these two components. The defining equation is

$$\rho = \frac{R^*_p}{R^*_s} = \frac{|R_p|}{|R_s|} e^{i(\delta_p - \delta_s)} = \tan\Psi e^{i\Delta} \qquad (1)$$

Note that the reflection coefficients can be complex. Good precision is expected, since tan Ψ and cos Δ are parameters based on a relative measurement.

Previous ellipsometric studies of organic thin films have concentrated on biological samples (2),(3). Although interesting, few biological samples have properties analogous to the polymer and liquid crystal thin films needed to produce non-linear optical devices. The exceptions are biological samples produced as Langmuir-Blodgett (LB) films. These are films in which the individual molecules typically attach themselves to the substrate at one end, and the molecule itself is more or less perpendicular to the substrate surface

(see Figure 1).

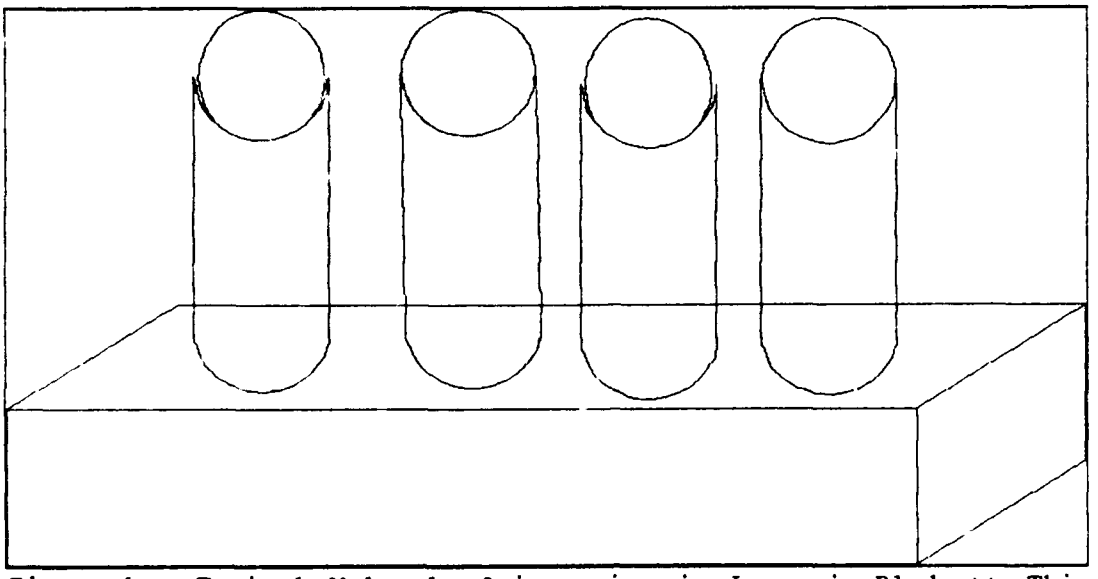

Figure 1. Typical Molecule Orientation in Langmuir-Blodgett Thin Films

Biological LB films do resemble the polymer LB films necessary for non-linear effects. They are deposited in the same fashion, and both are best modeled as uniaxial (two different indices of refraction in different directions) thin films. However, previous ellipsometric studies of biological LB films (4) restricted themselves to null ellipsometry. Typical null ellipsometry has a polarizer, compensator, sample and analyzer (PCSA) setup. The compensator is adjusted such that the measured reflectance at each angle of incidence and each frequency is zero. (For a complete description of null ellipsometry, see Azzam and Bashra (5).) Unfortunately, multiple frequency determinations are exceedingly slow in null ellipsometry. Therefore, null ellipsometry lacks any realistic chance of yielding the necessarily complete optical

properties of polymer or liquid crystal thin films. A different type of ellipsometry is required.

A Rotating Analyzer/Polarizer Ellipsometer (RAE) measures the reflected intensity from a sample and Fourier decomposes the signal into a calculated tan Ψ and cos Δ. This technique does not require a "null" determination. By taking advantage of the computer required for the Fourier decomposition, one can cover a large frequency range in a short period of time. When using RAE, one measurement is obtained at each frequency, with two resulting data points (tan Ψ and cos Δ). RAE is the technique required to completely determine optical properties over a frequency spectrum.

Once tan Ψ and cos Δ at some frequency are in hand, the optical properties and thickness of any thin films are determined through computer modeling of the sample. The models allow for a certain structure of the film, to include as many parameters as possible. In RAE, the parameters can include indices of refraction, orientation of optical axes, optical rotation, paramagnetic effects, film thicknesses and surface roughness.

In order to best model an organic thin film, this thesis uses the matrix technique of Berreman (5). This models the optical properties of a thin film as a 6x6 matrix, eventually yielding the 4x4 reflection matrix for the entire sample. The model assumes the geometry of Figure 2, with the plane of

incidence the x-z plane.

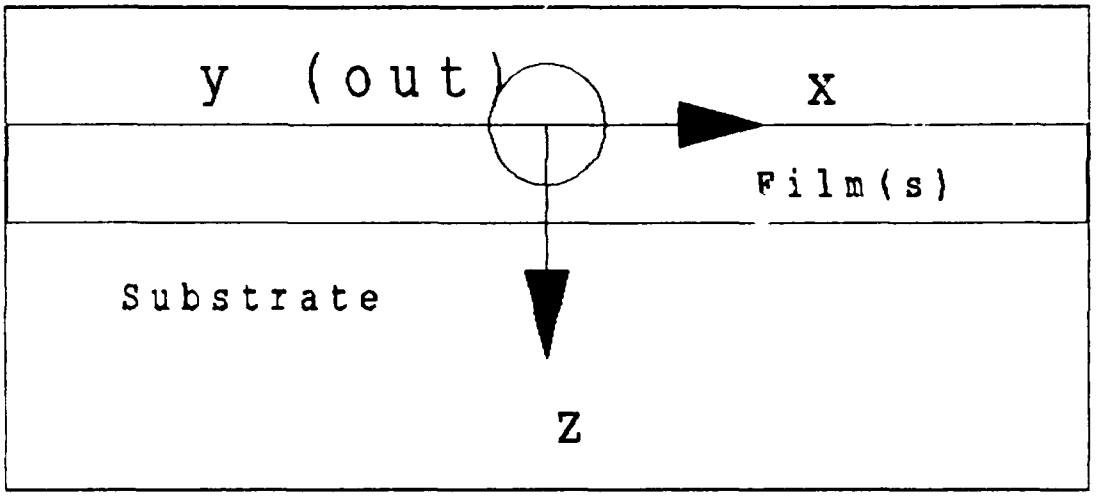

Figure 2. Assumed Geometry of Sample

The derivation of the optical matrix begins by casting Maxwell's equations in a 6x6 matrix (assuming rationalized MKS units and an $e^{i\omega t}$ time dependence):

$$\begin{bmatrix} 0 & 0 & 0 & 0 & -\frac{\partial}{\partial z} & \frac{\partial}{\partial y} \\ 0 & 0 & 0 & \frac{\partial}{\partial z} & 0 & -\frac{\partial}{\partial x} \\ 0 & 0 & 0 & -\frac{\partial}{\partial y} & \frac{\partial}{\partial x} & 0 \\ 0 & \frac{\partial}{\partial z} & -\frac{\partial}{\partial y} & 0 & 0 & 0 \\ -\frac{\partial}{\partial z} & 0 & \frac{\partial}{\partial x} & 0 & 0 & 0 \\ \frac{\partial}{\partial y} & -\frac{\partial}{\partial x} & 0 & 0 & 0 & 0 \end{bmatrix} \cdot \begin{bmatrix} E_x \\ E_y \\ E_z \\ H_x \\ H_y \\ H_z \end{bmatrix} - i\omega \cdot \begin{bmatrix} D_x \\ D_y \\ D_z \\ B_x \\ B_y \\ B_z \end{bmatrix} \qquad (2)$$

Substituting

$$\underline{\mathbf{0}} = \begin{bmatrix} 0 & 0 & 0 \\ 0 & 0 & 0 \\ 0 & 0 & 0 \end{bmatrix} \tag{3}$$

and

$$\underline{curl} = \begin{bmatrix} 0 & -\frac{\partial}{\partial z} & \frac{\partial}{\partial y} \\ \frac{\partial}{\partial z} & 0 & -\frac{\partial}{\partial x} \\ -\frac{\partial}{\partial y} & \frac{\partial}{\partial x} & 0 \end{bmatrix} \tag{4}$$

then Eq. (2) can be rewritten as

$$\begin{bmatrix} \underline{\mathbf{0}} & \underline{curl} \\ -\underline{curl} & \underline{\mathbf{0}} \end{bmatrix} \cdot \begin{bmatrix} E_x \\ E_y \\ E_z \\ H_x \\ H_y \\ H_z \end{bmatrix} = i\omega \cdot \begin{bmatrix} D_x \\ D_y \\ D_z \\ B_x \\ B_y \\ B_z \end{bmatrix} \tag{5}$$

or, shortened, as

$$\underline{\Omega} \cdot \underline{G} = i\omega \cdot \underline{C} \tag{6}$$

In the absence of nonlinear optical effects and inhomogeneity, the constitutive relation between $\underline{C}$ and $\underline{G}$ can generally be put as:

$$\underline{C} = \underline{M} \cdot \underline{G} \tag{7}$$

where

$$\underline{M} = \begin{bmatrix} \underline{\epsilon} & \underline{\rho} \\ \underline{\rho}' & \underline{\mu} \end{bmatrix} \tag{8}$$

$\underline{M}$ is the matrix that completely characterizes the optical properties of the thin film. $\underline{\mu}$ is the magnetic permeability tensor; $\underline{\rho}$ and $\underline{\rho}'$ are optical rotation tensors; and $\underline{\epsilon}$ is the dielectric permittivity tensor. Allowing for an anisotropic film with the optical axes randomly oriented (after rotation through Euler angles α, β and γ) as in Figure 3, $\underline{\epsilon}$ is given by

$$\underline{\epsilon} = \underline{A}^{-1} \cdot \underline{\epsilon}' \cdot \underline{A} \tag{9}$$

where ϵ_1, ϵ_2, and ϵ_3 are the principal dielectric constants

$$\underline{\epsilon}' = \begin{bmatrix} \epsilon_1 & 0 & 0 \\ 0 & \epsilon_2 & 0 \\ 0 & 0 & \epsilon_3 \end{bmatrix} \tag{10}$$

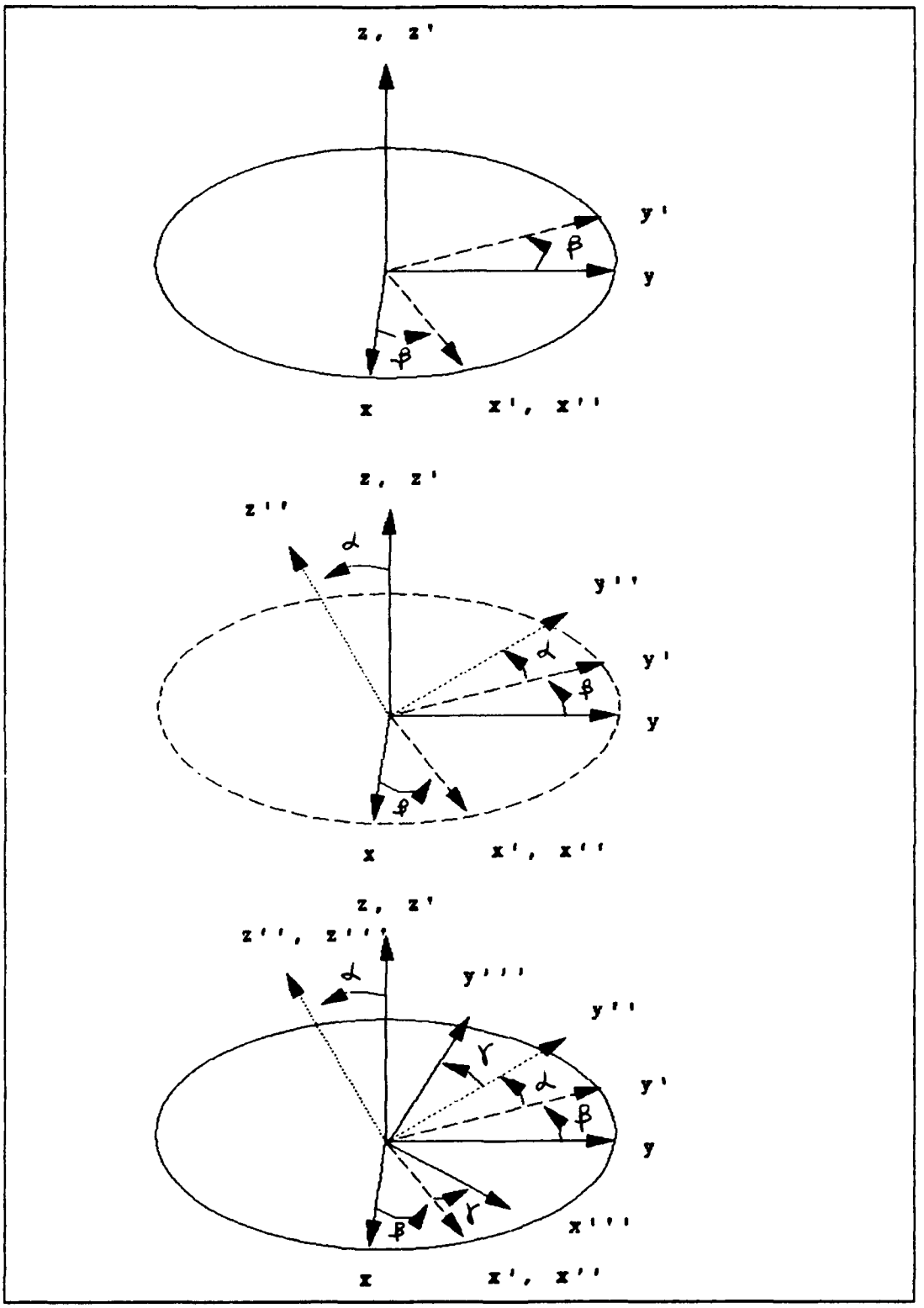

Figure 3 Definition of Coordinate Rotation

and the coordinate rotation is given by (6)

$$A = \begin{bmatrix} \cos\gamma\cos\beta - \cos\alpha\sin\beta\sin\gamma & \cos\gamma\sin\beta + \cos\alpha\cos\beta\sin\gamma & \sin\alpha\sin\gamma \\ -\sin\gamma\cos\beta - \cos\alpha\sin\beta\cos\gamma & -\sin\gamma\sin\beta + \cos\alpha\cos\beta\cos\gamma & \sin\alpha\cos\gamma \\ \sin\alpha\sin\beta & -\sin\alpha\cos\beta & \cos\alpha \end{bmatrix} \tag{11}$$

If the spatial and time dependence of $\underline{G}$ are separated into

$$\underline{G} = e^{i\omega t} \cdot \Gamma \tag{12}$$

then Eq. (6) can be rewritten as

$$\Omega \cdot \Gamma = i\omega M \cdot \Gamma \tag{13}$$

Look again at *Figure* 2. *From* the symmetry of the problem, there is no variation in the y direction of any field component, so

$$\frac{\partial}{\partial y} = 0 \tag{14}$$

For the tangential fields to match across the boundary at z=0,

$$\frac{\partial}{\partial x} = -i \frac{\omega}{c} N_0 \sin\theta_0 \tag{15}$$

where ω is the frequency of the incident light; c is the speed of light in a vacuum (in rationalized MKS units, c = 1); N_0 is the index of refraction from the ambient media; θ_0 is the

angle of incidence. Let

$$\xi = \omega N_0 \sin\theta_0 \tag{16}$$

Then Eq. (4) can be rewritten as

$$curl = \begin{bmatrix} 0 & -\frac{\partial}{\partial z} & 0 \\ \frac{\partial}{\partial z} & 0 & i\xi \\ 0 & -i\xi & 0 \end{bmatrix} \tag{17}$$

This eliminates E_z and H_z from Eq. (13). What remains is

$$\frac{\partial}{\partial z}\begin{bmatrix} E_x \\ H_y \\ E_y \\ -H_x \end{bmatrix} = -i\omega\underline{\Delta} \cdot \begin{bmatrix} E_x \\ H_y \\ E_y \\ -H_x \end{bmatrix} \tag{18}$$

or,

$$\frac{\partial}{\partial z}\underline{\Psi} = -i\omega\underline{\Delta} \cdot \underline{\Psi} \tag{19}$$

The components of $\underline{\Delta}$ are derived from $\underline{M}$, given by

$$
\begin{aligned}
\Delta_{11} &= M_{51}+(M_{53}+\eta)A_1+M_{56}A_5 \\
\Delta_{12} &= M_{55}+(M_{53}+\eta)A_4+M_{56}A_8 \\
\Delta_{13} &= M_{52}+(M_{53}+\eta)A_2+M_{56}A_6 \\
\Delta_{14} &= -M_{54}-(M_{53}+\eta)A_3-M_{56}A_7 \\
\Delta_{21} &= M_{11}+M_{13}A_1+M_{16}A_5 \\
\Delta_{22} &= M_{15}+M_{13}A_4+M_{16}A_8 \\
\Delta_{23} &= M_{12}+M_{13}A_2+M_{16}A_6 \\
\Delta_{24} &= -M_{14}-M_{13}A_3-M_{16}A_7 \\
\Delta_{31} &= -M_{41}-M_{43}A_1-M_{46}A_5 \\
\Delta_{32} &= -M_{45}-M_{43}A_4-M_{46}A_8 \\
\Delta_{33} &= -M_{42}-M_{43}A_2-M_{46}A_6 \\
\Delta_{34} &= M_{44}+M_{43}A_3+M_{46}A_7 \\
\Delta_{41} &= M_{21}+M_{23}A_1+(M_{26}-\eta)A_5 \\
\Delta_{42} &= M_{25}+M_{23}A_4+(M_{26}-\eta)A_8 \\
\Delta_{43} &= M_{22}+M_{23}A_2+(M_{26}-\eta)A_6 \\
\Delta_{44} &= -M_{24}-M_{23}A_3-(M_{26}-\eta)A_7
\end{aligned}
\tag{20}
$$

and

$$
\begin{aligned}
A_1 &= (M_{61}M_{36} - M_{31}M_{66})/D \\
A_2 &= [(M_{62}-\eta)M_{36} - M_{32}M_{66}]/D \\
A_3 &= (M_{64}M_{36} - M_{34}M_{66})/D \\
A_4 &= [M_{65}M_{36} - (M_{35}+\eta)M_{66}]/D \\
A_5 &= (M_{63}M_{31} - M_{33}M_{61})/D \\
A_6 &= [M_{63}M_{32} - (M_{62}-\eta)M_{33}]/D \\
A_7 &= (M_{63}M_{34} - M_{33}M_{64})/D \\
A_8 &= [(M_{35}+\eta)M_{63} - M_{33}M_{65}]/D \\
D &= M_{33}M_{66} - M_{36}M_{63} \\
\eta &= \frac{\xi}{\omega} = \frac{N_0}{c}\sin\theta_0
\end{aligned}
\tag{21}
$$

With $\underline{A}$ known from $\underline{M}$, ω, N_0, and θ_0, one can predict how the electric and magnetic waves will travel in the film.

In the general case, $\underline{M}$ is an arbitrary function of z and Eq. (19) cannot be solved analytically. However, assuming the film is homogeneous, $\underline{M}$ is independent of z. Then Eq. (19) can be integrated directly to give

$$\Psi(z + h) = L(h) \cdot \Psi(z) \tag{22}$$

where

$$L(h) = e^{-i\omega h\Delta} \tag{23}$$

is the 4x4 "layer" matrix for a thin film of thickness h. Eq. (22) gives the ability to model the reflection from a sample as a matrix and include it in ellipsometric calculations (as will be shown later).

If more film layers are present: add more "layer" matrices; multiply the "layer" matrices together; and use the resulting matrix as described below. Specifically, if the sample is to be modeled as in Figure 4, the overall layer matrix would be given by $\underline{L} = \underline{L}(h_2)*\underline{L}(h_1)$.

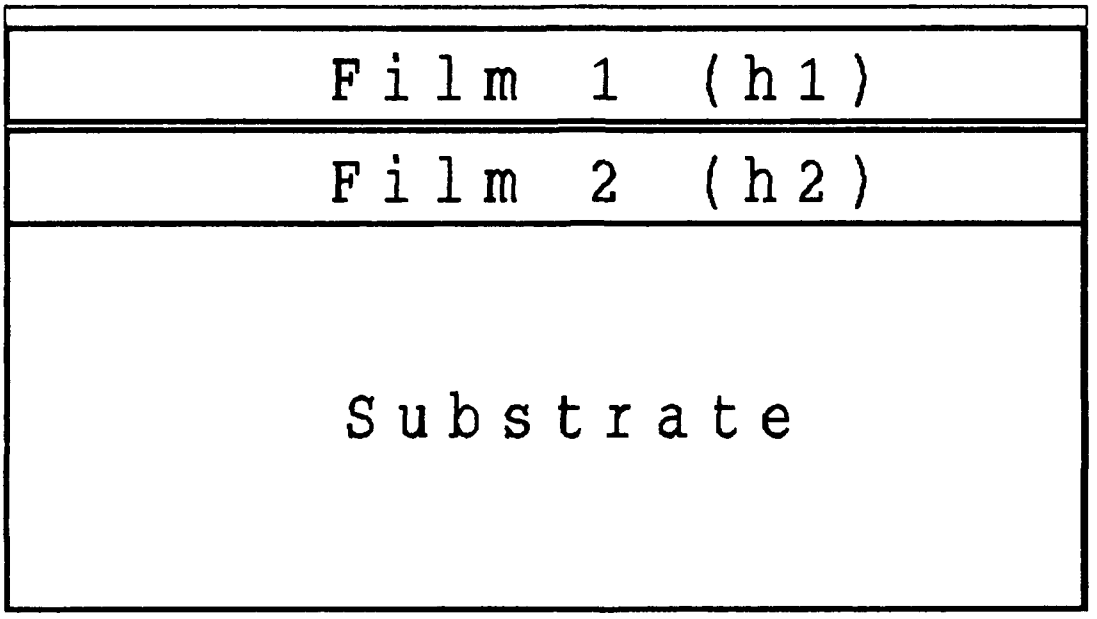

Figure 4. Modeling with Two Thin Films on a Substrate

As you can see, Berreman's technique allows for films to be modeled as anisotropic, optically rotating, paramagnetic, and homogeneous. All of the models used in this thesis assumed the following:

1) Films were non-magnetic (μ=1); smooth; homogeneous; and have no optical rotation.

2) The ambient refractive index (N_0) was 1.000.

3) All films were on isotropic substrates.

III. Computational Methods

It is still unclear how one gets from the layer matrix calculation (Eq. (23)) to the ellipsometric parameters tan Ψ and cos Δ. A diagram of the ellipsometric configuration used in this experiment is given in Figure 5:

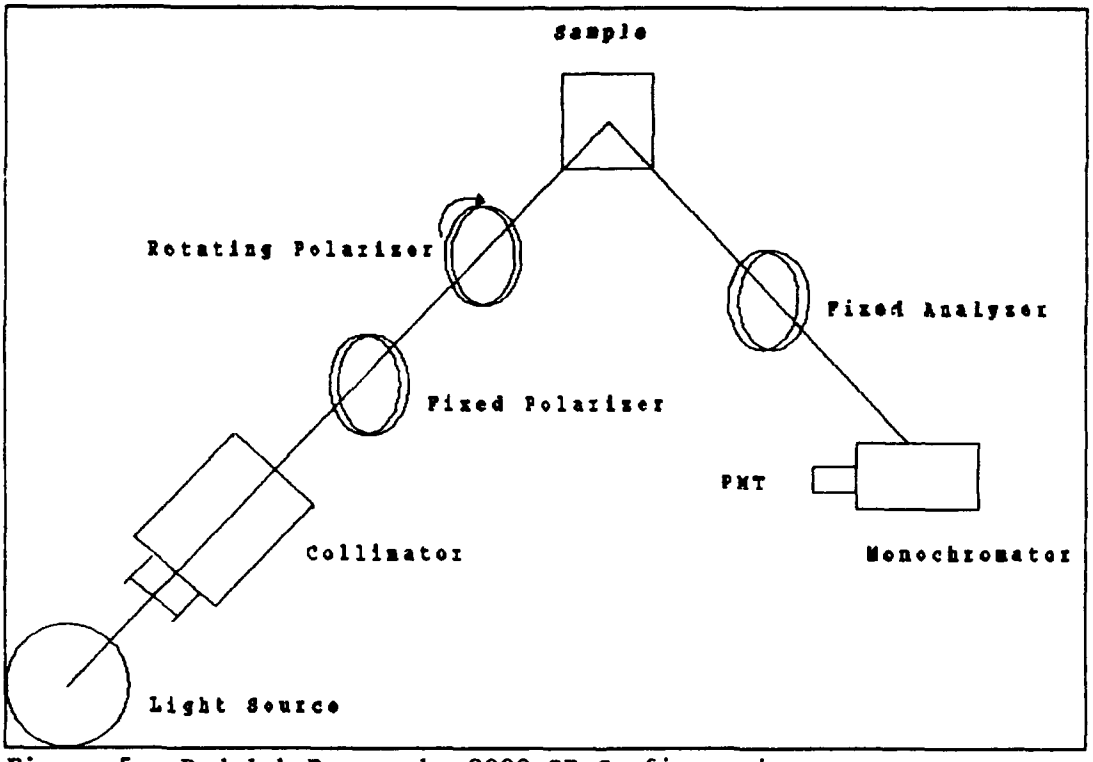

Figure 5. Rudolph Research s2000 SE Configuration

First, model the light through each optical device as a 4x4 matrix. Assume the light striking the fixed polarizer is entirely unpolarized (untrue; but it will be shown the fixed polarizer completely polarizes the light). The Stokes vector describing the light is given by

$$\mathbf{S} = \begin{bmatrix} 1 \\ 0 \\ 0 \\ 0 \end{bmatrix} \tag{24}$$

After passing through the fixed polarizer, the Stokes vector is now

$$\mathbf{S} = \frac{1}{2}\begin{bmatrix} 1 & 0 & 1 & 0 \\ 0 & 0 & 0 & 0 \\ 1 & 0 & 1 & 0 \\ 0 & 0 & 0 & 0 \end{bmatrix} \cdot \begin{bmatrix} 1 \\ 0 \\ 0 \\ 0 \end{bmatrix} = \frac{1}{2}\begin{bmatrix} 1 \\ 0 \\ 1 \\ 0 \end{bmatrix} \tag{25}$$

After passing through the second polarizer (rotating at an angular velocity of ϖ), the resulting Stokes vector becomes

$$\mathbf{S} = \frac{1}{2}\begin{bmatrix} 1 \\ 0 \\ 1 \\ 0 \end{bmatrix} \cdot \frac{1}{2}\begin{bmatrix} 1 & \cos 2\varpi & \sin 2\varpi & 0 \\ \cos 2\varpi & \cos^2 2\varpi & \sin 2\varpi \cos 2\varpi & 0 \\ \sin 2\varpi & \sin 2\varpi \cos 2\varpi & \sin^2 2\varpi 0 & 0 \\ 0 & 0 & 0 & 0 \end{bmatrix} \tag{26}$$

$$\mathbf{S} = \frac{1}{4}\begin{bmatrix} 1 + \sin 2\varpi \\ \sin 2\varpi \cos 2\varpi + \cos 2\varpi \\ \sin^2 2\varpi + \sin 2\varpi \\ 0 \end{bmatrix} \tag{27}$$

The next component in the optical path is the sample. If the sample surface is assumed to be homogeneous, it is characterized by ellipsometric parameters tan Ψ and cos Δ, its

Mueller matrix is given by (5):

$$\mathbf{R} = \begin{bmatrix} (\tan^2\psi+1) & (\tan^2\psi-1) & 0 & 0 \\ (\tan^2\psi-1) & (\tan^2\psi+1) & 0 & 0 \\ 0 & 0 & 2\cos\Delta\tan\psi & 2\sin\Delta\tan\psi \\ 0 & 0 & -2\sin\Delta\tan\psi & 2\cos\Delta\tan\psi \end{bmatrix} \tag{28}$$

So, the Stokes vector after reflection from the sample surface is given by

$$\mathbf{S} = \frac{1}{4}\begin{bmatrix} (1+\sin 2\varpi)(\tan^2\psi+1)+(\cos 2\varpi+\sin 2\varpi\cos 2\varpi)(\tan^2\psi-1) \\ (1+\sin 2\varpi)(\tan^2\psi-1)+(\cos 2\varpi+\sin 2\varpi\cos 2\varpi)(\tan^2\psi+1) \\ (\sin^2 2\varpi+\sin 2\varpi)(2\cos\Delta\tan\psi) \\ (\sin^2 2\varpi+\sin 2\varpi)(-2\sin\Delta\tan\psi) \end{bmatrix} \tag{29}$$

The light passes through the fixed analyzer, producing the Stokes vector that reaches the photomultiplier tube (PMT). The PMT measures the intensity, given by S(1):

$$\begin{aligned} \mathbf{S}(1) = \frac{1}{8}[&(1+\sin 2\varpi)(\tan^2\psi+1) \\ &+(\cos 2\varpi+\sin 2\varpi\cos 2\varpi)(\tan^2\psi-1) \\ &+(2\cos\Delta\tan\psi)(\sin^2 2\varpi+\sin 2\varpi)] \end{aligned} \tag{30}$$

Substituting

$$\begin{aligned} \sin 2\varpi\cos 2\varpi &= \frac{1}{2}\sin 4\varpi \\ \sin^2 2\varpi &= \frac{1}{2} - \frac{1}{2}\cos 4\varpi \end{aligned} \tag{31}$$

S(1) is rewritten as a truncated Fourier series:

$$S(1) = \frac{1}{16}\left[\begin{array}{l} 2(\tan^2\Psi+\tan\Psi\cos\Delta+1) \\ +2(\tan^2\Psi-1)\cos 2\varpi \\ +2(\tan\Psi\cos\Delta+\tan^2\Psi+1)\sin 2\varpi \\ -2(\tan\Psi\cos\Delta)\cos 4\varpi \\ +(\tan^2-1)\sin 4\varpi \end{array}\right] \tag{32}$$

Notice that S(1) is in the form

$$S(1) = a_0 + a_2\cos 2\varpi + a_4\cos 4\varpi + b_2\sin 2\varpi + b_4\sin 4\varpi \tag{33}$$

Solving for tan Ψ and cos Δ(7), if

$$k = \frac{b_2 + 2a_4 - a_2}{2} \tag{34}$$

then

$$\begin{aligned} \tan\Psi &= \sqrt{\frac{a_2}{k} + 1} \\ \cos\Delta &= -\frac{a_4}{k\tan\Psi} \end{aligned} \tag{35}$$

What is needed is the 4x4 Mueller matrix for the sample, $\tilde{\underline{M}}$. It is <u>not</u> the same as the layer matrix, $\underline{L}$. The technique is to go from the 4x4 layer matrix $\underline{L}$, to the 2x2 sample reflection matrix $\underline{R}$, where

$$\underline{R} = \begin{bmatrix} R_{pp} & R_{ps} \\ R_{sp} & R_{ss} \end{bmatrix} \tag{36}$$

to the 4x4 sample Mueller matrix $\underline{\tilde{M}}$. For any layered structure on an isotropic substrate (4), $\underline{R}$ is given by

$$\underline{R} = (a_{ss}b_{pp} - a_{ps}b_{ps})^{-1} \cdot \begin{bmatrix} (a_{ip}b_{ss} - a_{ss}b_{ip}) & (a_{is}b_{ss} - a_{ss}b_{is}) \\ (a_{pp}b_{ip} - a_{ip}b_{pp}) & (a_{pp}b_{is} - a_{is}b_{pp}) \end{bmatrix} \tag{37}$$

where

$$\begin{aligned}
a_{ip} &= N_0(L_{12}N_s - L_{22}\cos\theta_2) + \cos\theta_0(L_{11}N_s - L_{21}\cos\theta_2) \\
a_{pp} &= N_0(L_{12}N_s - L_{22}\cos\theta_2) - \cos\theta_0(L_{11}N_s - L_{21}\cos\theta_2) \\
a_{is} &= (L_{13}N_s - L_{23}\cos\theta_2) + N_0\cos\theta_0(L_{14}N_s - L_{24}\cos\theta_2) \\
a_{ps} &= (L_{13}N_s - L_{23}\cos\theta_2) - N_0\cos\theta_0(L_{14}N_s - L_{24}\cos\theta_2) \\
b_{ip} &= N_0(L_{32}N_s\cos\theta_2 - L_{42}) + \cos\theta_0(L_{31}N_s\cos\theta_2 - L_{41}) \\
b_{pp} &= N_0(L_{32}N_s\cos\theta_2 - L_{42}) - \cos\theta_0(L_{31}N_s\cos\theta_2 - L_{41}) \\
b_{is} &= (L_{33}N_s\cos\theta_2 - L_{43}) + N_0\cos\theta_0(L_{34}N_s\cos\theta_2 - L_{44}) \\
b_{ps} &= (L_{33}N_s\cos\theta_2 - L_{43}) - N_0\cos\theta_0(L_{34}N_s\cos\theta_2 - L_{44})
\end{aligned} \tag{38}$$

Now, the 4x4 sample Mueller matrix is given by (4):

$$\underline{M} = \underline{A} \cdot (\underline{R} \otimes \underline{R}^*) \cdot \underline{A}^{-1} \tag{39}$$

where

$$\underline{A} = \begin{bmatrix} 1 & 0 & 0 & 1 \\ 1 & 0 & 0 & -1 \\ 0 & 1 & 1 & 0 \\ 0 & i & -i & 0 \end{bmatrix} \tag{40}$$

$\underline{R}$ the 2x2 sample reflection matrix; $\underline{R}^*$ is the complex conjugate of $\underline{R}$; and $\underline{R} \otimes \underline{R}^*$ is a direct product, given by (8):

$$\underline{R} \otimes \underline{R}^* = \begin{bmatrix} R_{11}\cdot\underline{R}^* & R_{12}\cdot\underline{R}^* \\ R_{21}\cdot\underline{R}^* & R_{22}\cdot\underline{R}^* \end{bmatrix} \tag{41}$$

So, the Stokes vector after reflection from the sample surface is given by

$$S = \frac{1}{4}\begin{bmatrix} M_{11}(1+\sin 2\varpi)+M_{12}(\sin 2\varpi\cos 2\varpi+\cos 2\varpi)+M_{13}(\sin^2 2\varpi+\sin 2\varpi) \\ M_{21}(1+\sin 2\varpi)+M_{22}(\sin 2\varpi\cos 2\varpi+\cos 2\varpi)+M_{23}(\sin^2 2\varpi+\sin 2\varpi) \\ M_{31}(1+\sin 2\varpi)+M_{32}(\sin 2\varpi\cos 2\varpi+\cos 2\varpi)+M_{33}(\sin^2 2\varpi+\sin 2\varpi) \\ M_{41}(1+\sin 2\varpi)+M_{42}(\sin 2\varpi\cos 2\varpi+\cos 2\varpi)+M_{43}(\sin^2 2\varpi+\sin 2\varpi) \end{bmatrix} \tag{42}$$

The light passes through the fixed analyzer, producing the Stokes vector that reaches the photomultiplier tube (PMT):

$$S = \frac{1}{8}\begin{bmatrix} (M_{11}+M_{21})(1+\sin 2\varpi)+(M_{12}+M_{22})(\sin 2\varpi\cos 2\varpi+\cos 2\varpi)+(M_{13}+M_{23})(\sin^2 2\varpi+\sin 2\varpi) \\ 0 \\ (M_{11}+M_{21})(1+\sin 2\varpi)+(M_{12}+M_{22})(\sin 2\varpi\cos 2\varpi+\cos 2\varpi)+(M_{13}+M_{23})(\sin^2 2\varpi+\sin 2\varpi) \\ 0 \end{bmatrix} \tag{43}$$

Using Eq.(31), and recalling that S(1) is rewritten as a truncated Fourier series,

$$
\begin{aligned}
S(1) = & \frac{1}{8}\left[M_{11}+M_{31}+\frac{1}{2}\left(M_{13}+M_{33}\right)\right] \\
& + \frac{1}{8}\left(M_{12}+M_{32}\right)\cos 2\varpi \\
& - \frac{1}{16}\left(M_{13}+M_{33}\right)\cos 4\varpi \\
& + \frac{1}{8}\left(M_{11}+M_{31}+M_{13}+M_{33}\right)\sin 2\varpi \\
& + \frac{1}{16}\left(M_{12}+M_{32}\right)\sin 4\varpi
\end{aligned}
\tag{44}
$$

Comparison of Eq. (44) with Eq. (33), we see that

$$
\begin{aligned}
a_0 &= \frac{1}{8}\left[M_{11}+M_{31}+\frac{1}{2}\left(M_{13}+M_{33}\right)\right] \\
a_2 &= \frac{1}{8}\left(M_{12}+M_{32}\right) \\
a_4 &= -\frac{1}{16}\left(M_{13}+M_{33}\right) \\
b_2 &= \frac{1}{8}\left(M_{11}+M_{31}+M_{13}+M_{33}\right) \\
b_4 &= \frac{1}{16}\left(M_{12}+M_{32}\right)
\end{aligned}
\tag{45}
$$

Substituting the Fourier coefficients of Eq. (45) into Eqs. (34) and (35), the calculated tan Ψ and cos Δ are found.

Let the sample be measured over some wavelength region, giving a set of tan Ψ and cos Δ for each wavelength. Assume that a model with m parameters (indices of refraction, thickness, etc) was chosen. How is it known when the <u>best</u> estimate of the model parameters is obtained? More importantly, how is an initial guess at each of the m model parameters improved to get to the best estimate?

The usual method of minimizing the weighted sum of the

squared deviations (least-squares fit) is followed. Assume all measurement errors follow a normal (Gaussian) distribution. Then define a mean squared error, χ^2, as:

$$\chi^2 = \frac{1}{N-1} \sum_{i=1}^{N} \left[\frac{y_i^{ex} - y_i^{calc}}{\sigma_i} \right]^2 \qquad (46)$$

where N is the number of data points; y_i^{ex} is the experimentally determined value of either tan Ψ or cos Δ; y_i^{calc} is the calculated value (from the model) of tan Ψ or cos Δ; and σ_i is the standard deviation of the measured value.

According to the method of least-squares, the optimum values of the m model parameters $\vec{a} = a_1, a_2, a_3, \ldots, a_j, \ldots a_m$ are obtained by minimizing χ^2 with respect to each of the parameters simultaneously

$$\frac{\partial \chi^2}{\partial a_j} = \frac{\partial}{\partial a_j} \sum_{i=1}^{N} \left[\frac{y_i^{ex} - y_i^{calc}}{\sigma_i} \right]^2 = 0 \qquad (47)$$

χ^2 must be considered a continuous function of the m model parameters describing a hypersurface in m-dimensional space. This space must be searched for the appropriate minimum value of χ^2. One of the difficulties of such a search is there may be more than one local minimum for χ^2 within a reasonable range of values for the $\vec{a}$.

There are many methods of searching the parameter space.

Marquardt derived a method based on a suggestion by Levenberg (9). The Marquardt-Levenberg method has become the standard non-linear, least squares fitting routine. It varies between two different methods: "steepest descent" and "inverse Hessian".

The inverse Hessian method expands the "fitting function" y as a function of the m model parameters $\vec{a}$. Suppose y is expanded to second order in a Taylor's series as a function of $\vec{a}$:

$$y = y_0^{calc} + \sum_{j=1}^{m}\left[\frac{\partial y_0^{calc}}{\partial a_j}\,\delta a_j\right] + \sum_{j=1}^{m}\sum_{k=1}^{m}\left[\frac{\partial^2 y_0^{calc}}{\partial a_j \partial a_k}\,\delta a_j\,\delta a_k\right] \qquad (48)$$

If the derivatives of χ^2 with respect to the model parameter increments $\delta\vec{a}$ are set equal to 0, and neglecting all terms of order one or higher in δa_j, the resulting equations are

$$\begin{aligned}\beta_k &= -\frac{1}{2}\frac{\partial \chi^2}{\partial a_k} = \sum_{i=1}^{N}[y_i^{ex} - y_i^{calc}]\left[\frac{\partial y_i^{calc}}{\partial a_k}\right] \\ \alpha_{jk} &= \frac{1}{2}\frac{\partial^2 \chi^2}{\partial a_j \partial a_k} = \sum_{i=1}^{N}\left[\frac{\partial y_i^{calc}}{\partial a_j}\frac{\partial y_i^{calc}}{\partial a_k}\right] - [y_i^{ex} - y_i^{calc}]\frac{\partial^2 y_i^{calc}}{\partial a_j \partial a_k}\end{aligned} \qquad (49)$$

and

$$\beta_k = \sum_{j=1}^{m}\delta a_j\,\alpha_{jk} \qquad (50)$$

where $\vec{\beta}$ is called the gradient vector and $\underline{\alpha}$ is called the curvature matrix. Eq. (48) is equivalent to approximating the χ^2 hypersurface with a parabolic surface.

The problem with the inverse Hessian method (named because the matrix $\underline{\alpha}$ is a Hessian matrix) is calculating the step sizes $\delta\vec{a}$. The step sizes must be large enough to prevent round-off error in the computation, and small enough to furnish reasonable results near the minimum where the derivatives may be changing rapidly with the parameters.

If the model parameters are close enough to the minimum to invoke parabolic approximation, then Eq. (50) can be solved directly to yield the parameter step sizes $\delta\vec{a}$ such that χ^2 should be minimized by $\vec{a}+\delta\vec{a}$. If the starting point is close enough to the minimum that higher-order terms in the expansion can be neglected, inverse Hessian is an accurate and precise method. But if the starting point is not close enough to the minimum, the parabolic approximation is invalid and the results are in error.

In contrast, the steepest descent method is ideally suited for approaching the minimum in χ^2 from far away, but does not converge rapidly when in the immediate neighborhood. In this method, all of the parameters $\vec{a}$ are incremented simultaneously, with the relative magnitudes adjusted so that the resultant travel in parameter space is along the gradient (the direction of maximum variation) of χ^2.

The gradient of χ^2, $\nabla\chi^2$, is given by

$$\nabla\chi^2 = \sum_{j=1}^{m}\left[\frac{\partial\chi^2}{\partial a_j}\right] \tag{51}$$

In order to determine the gradient, the variation of χ^2 in the neighborhood of the starting point is sampled independently for each parameter to yield an approximate value for the first derivative

$$(\nabla\chi^2)_j = \frac{\partial\chi^2}{\partial a_j} \approx \frac{\chi^2(a_j+\Delta a_j) - \chi^2(a_j)}{\Delta a_j} \tag{52}$$

Note that the dimensions (and units) of all of the model parameters are not the same. This is solved by letting

$$b_j = \frac{a_j}{\Delta a_j} \tag{53}$$

Define a dimensionless gradient γ

$$\gamma_j = \frac{\frac{\partial\chi^2}{\partial b_j}}{\sqrt{\sum_{k=1}^{m}\left(\frac{\partial\chi^2}{\partial b_k}\right)^2}} \tag{54}$$

$$\frac{\partial\chi^2}{\partial b_j} = \frac{\partial\chi^2}{\partial a_j}\Delta a_j$$

The method of steepest descent follows the opposite direction of the dimensionless gradient γ

$$\delta a_j = -\gamma_j \Delta a_j \tag{55}$$

Note the similarities between Eq. (49) and Eq. (54). Here is where the two methods are combined to get the best features of both. If the diagonal of the curvature matrix $\underline{\alpha}$ is increased by a factor of λ, Eq. (49) becomes

$$\beta_j = \sum_{j=1}^{m} \delta a_j \, \alpha'_{jk} \tag{56}$$

where

$$\alpha'_{jk} = \begin{cases} \alpha_{jj}(1+\lambda) \\ \alpha_{jk} \end{cases} \qquad (j \neq k) \tag{57}$$

If λ is small, Eq. (56) acts like an inverse Hessian. If λ is large, the diagonal terms of the curvature matrix dominate and the matrix equations become gradient equations (i.e., steepest descent). The solution for the step sizes in either case is given by

$$\delta a_j = \sum_{k=1}^{m} \beta_k \, [\alpha']^{-1}_{jk} \tag{58}$$

where $\underline{\alpha'^{-1}}$ is the inverse of the augmented curvature matrix. The inverse of the $\underline{\alpha}$ matrix is called the error matrix. It is used to calculate the 90% confidence limits of the model parameters.

Thus, given an initial set of m parameters, $\vec{a}$,

1) Compute $\chi^2(\vec{a})$;

2) Start with $\lambda = 0.001$;

3) Compute $\chi^2(\vec{a}+\delta\vec{a})$;

4) If $\chi^2(\vec{a}+\delta\vec{a}) \geq \chi^2(\vec{a})$, increase λ by a factor of 10 and redo 3);

5) If $\chi^2(\vec{a}+\delta\vec{a}) \leq \chi^2(\vec{a})$, decrease λ by a factor of 10; update the values of $\vec{a} = \vec{a}+\delta\vec{a}$; and redo 3).

Once a minimum in χ^2 is reached, the set $\vec{a}$ contains the parameters that best fit the model.

How is one certain the set of $\vec{a}$ parameters are truly the best fit? The error matrix allows one to calculate the standard error and 90% confidence intervals for each parameter. The standard error of each model parameter is given by:

$$\sigma_{a_i} = \sqrt{\frac{\chi^2}{N-1} \cdot \alpha_{ii}^{-1}} \qquad (59)$$

and the 90% confidence interval for each model parameter varied one at a time is given by (10)

$$\delta_i = \sigma_i \sqrt{2.71} = 1.65\,\sigma_i \qquad (60)$$

Thus, the signs of a good fit are:

1) small χ^2 ($<<1$);

2) reasonable 90% confidence intervals (i.e., <u>not</u> $t_f = 100 \pm 75$ Å, or $n_f = 1.51 \pm 1.25$).

However, there is an inherent problem with SE data taken at only one angle of incidence. Assume a model has five parameters. At any one wavelength, only two data points (tan Ψ and cos Δ) are obtained for each measurement. Unfortunately, the laws of statistics dictate that for a good fit to m model parameters, at <u>least</u> (m+2) data points must be used. Therefore, multiple angle of incidence (MAI) data is needed at each wavelength in order to obtain a good fit.

The models used in this thesis were written in MATLAB® to take advantage of its powerful and straight-forward matrix capabilities. A simplified flow chart of the models is given in Figure 6.

Four models were constructed, with the following parameters:

1) One isotropic, absorbing film ($n_f(\lambda)$, $k_f(\lambda)$, t_f) on an isotropic, absorbing substrate ($n_s(\lambda)$, $k_s(\lambda)$);

2) One anisotropic, absorbing film ($n_x(\lambda)$, $k_x(\lambda)$, $n_y(\lambda)$, $k_y(\lambda)$, $n_z(\lambda)$, $k_z(\lambda)$, α_f, β_f, γ_f, t_f) on an isotropic, absorbing substrate ($n_s(\lambda)$, $k_s(\lambda)$);

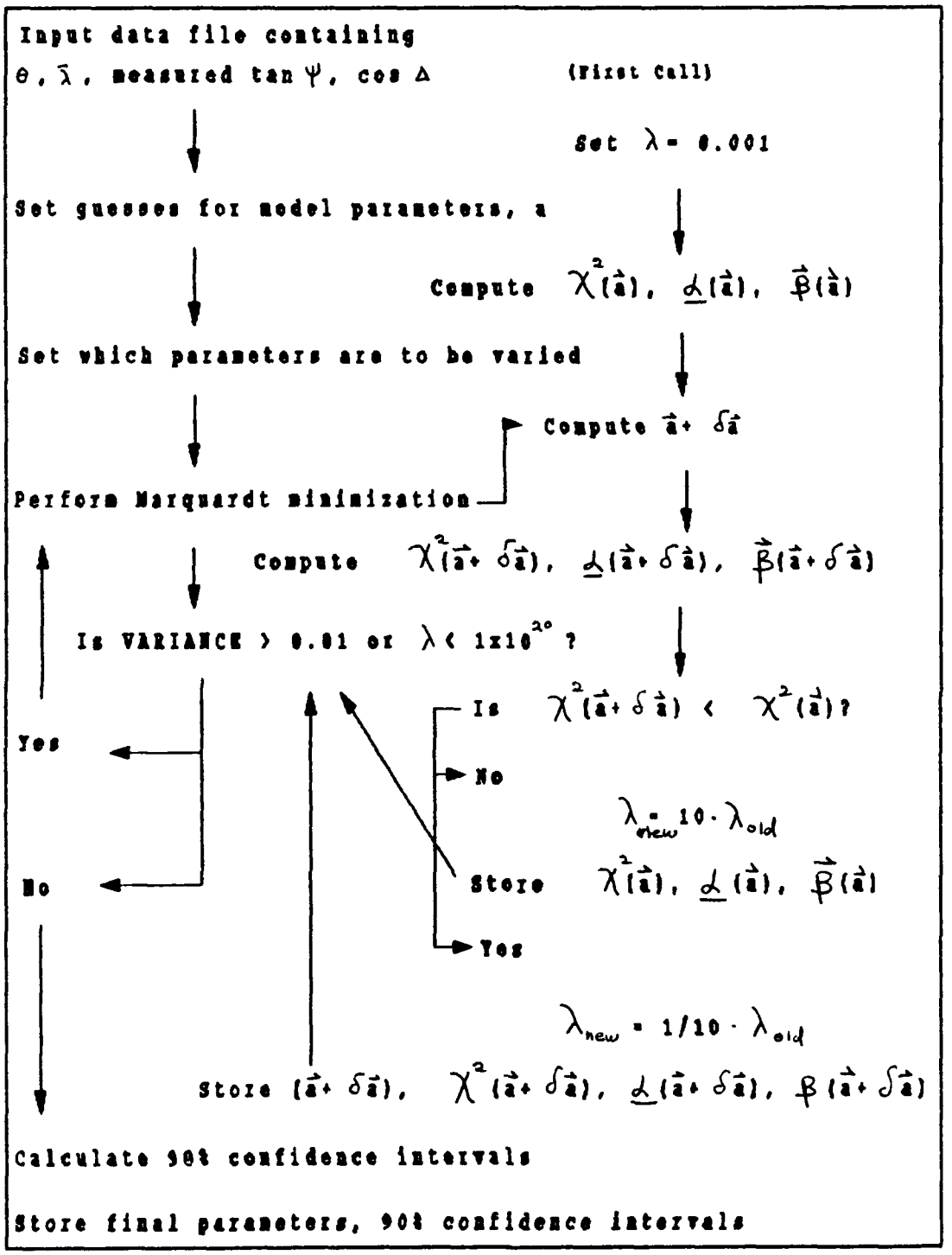

Figure 6. MATLAB SE Model Flow Chart

3) Two isotropic, absorbing films ($n_{f1}(\lambda)$, $k_{f1}(\lambda)$, t_{f1}, $n_{f2}(\lambda)$, $k_{f2}(\lambda)$, t_{f2}) on an isotropic, absorbing substrate ($n_s(\lambda)$, $k_s(\lambda)$);

4) Two anisotropic, absorbing films ($n_{x1}(\lambda)$, $k_{x1}(\lambda)$, $n_{y1}(\lambda)$, $k_{y1}(\lambda)$, $n_{z1}(\lambda)$, $k_{z1}(\lambda)$, α_1, β_1, γ_1, t_{f1} ,$n_{x2}(\lambda)$, $k_{x2}(\lambda)$, $n_{y2}(\lambda)$, $k_{y2}(\lambda)$, $n_{z2}(\lambda)$, $k_{z2}(\lambda)$, α_2, β_2, γ_2, t_{f2}) on an isotropic, absorbing substrate ($n_s(\lambda)$, $k_s(\lambda)$).

The basic models of the film(s)/substrate system were checked against a variety of published data (11),(12),(13),(14),(15),(16). The results matched very well and validated the basic code.

IV. Experimental Information

All of the data used in this thesis was taken with a Rudolph Research Corporation s2000 Spectroscopic Ellipsometer (7). A diagram of the machine layout was shown in Figure 5. The light source used in the s2000 was a 75 watt, high-pressure Xenon lamp. The fixed polarizer was an UV grade Glan-Thompson prism, set (for all thesis data taken) at 45.00 ± 0.01°. This polarizer converted the collimated light into linearly polarized light, with equal parallel (p) and perpendicular (s) components.

The rotating polarizer was also an UV grade Glan-Thompson prism. It converted the linearly polarized light into a beam whose intensity and polarization direction were modulated by the rotation of the prism. The fixed analyzer was also an UV grade Glan-Thompson prism set at 45.00 ± 0.01°. This converted the reflected beam into an output beam modulated in intensity only.

The monochromator used in the s2000 was a dual monochromator. The PMT was a Hammamatsu R928. A preamp/digitizer converted the current output from the PMT to a voltage signal and stored the intensity as a 12 bit word.

The s2000 measured the ellipsometric parameters tan Ψ and cos Δ as follows:

1) Set the monochromator to 0;

2) Drove the monochromator to the starting wavelength;

3) Adjusted the PMT voltage to get a signal between 5 and 7.5 volts;

4) Averaged measurements of tan Ψ and cos Δ until

- standard deviation less than 0.001, or
- 100 measurements were made;

5) Stored the wavelength, tan Ψ and cos Δ data; and continued to the next wavelength.

Four samples were analyzed for this thesis. Sample 1 was a indium tin oxide (ITO) coated glass substrate. Sample 2 was five layers of PBLG on a substrate of ITO coated glass. Sample 3 was eight layers of PBLG on a substrate of ITO coated glass. All of the substrates for these three samples had the same dimensions: 10 millimeters (mm) in length, 6 mm in width and 2 mm in thickness.

This substrate thickness was too small for the s2000 to resolve the differences between the front and back surface reflections. Since directly mounting the samples on the s2000 vacuum chuck didn't solve the problem, a different approach was tried. The substrates were affixed to a fused silica (SiO_2) block with index matched NYOGEL®. This allowed the front and back surface reflections to be resolved. A test with a similar thickness of BK7 glass mounted with NYOGEL to the fused silica block validated the technique.

Sample 4 was a film of thiophene mounted on a microscope slide. The back side of the slide was spray painted black in

order to eliminate the back surface reflections. The slide was mounted directly onto the vacuum chuck and the film analyzed.

Each of the four samples were analyzed from 300 to 800 nanometers (nm) at every 5 nm. Measurements were taken across the spectrum at 60.00°, 65.00°, 70.00°, 75.00° and 80.00° for all four samples. Plots of tan Ψ and cos Δ for all four samples at all five angles are given in Appendices A-D.

V. Results and Discussion

Additional data was taken to determine the repeatability of the measurements. This would also gave a range to which the data could be fit. There is no point to fit the data to a variance of 0.0001 when the data is only repeatable to 0.01.

Two sets of data were taken on the 5 layer PBLG film, one immediately after the other. The differences between the two tan Ψ and cos Δ, every 5 nm from 300-400 nm, are tabulated in Table 1. Note that the average change in tan Ψ measurements was 0.0021.

An example of two measurements made some time apart on different spots is given in Table 2. Again, two data sets were taken of the 5 layer PBLG film system. They were taken approximately 30 minutes apart, with the substrate in the same basic orientation. Again, the tabulated data are the differences between the two tan Ψ and cos Δ. The average change in tan Ψ measurements was about 0.0051.

This would seem to set a convergence criteria of about 0.01. In other words, when the variance is less than 0.01, then we can assume the fit is as good as another data set taken on the same sample.

TABLE 1

MEASUREMENT TO MEASUREMENT CHANGES (5 LAYER PBLG)

λ (nm)	δ(cos Φ)	δ(tan Ψ)
300	0.0054	0.0050
305	0.0039	0.0021
310	0.0001	0.0019
315	0.0001	0.0023
320	0.0033	0.0012
325	0.0051	0.0010
330	0.0019	0.0016
335	0.0056	0.0018
340	0.0130	0.0055
345	0.0651	0.0021
350	0.0468	0.0043
355	0.0951	0.0015
360	0.0488	0.0023
365	0.0257	0.0007
370	0.0240	0.0029
375	0.0158	0.0015
380	0.0286	0.0013
385	0.0127	0.0019
390	0.0029	0.0006
395	0.0140	0.0014
400	0.0050	0.0008
Average	0.0248	0.0021

TABLE 2

TIME TO TIME (OR SPOT TO SPOT) CHANGES (5 LAYER PBLG)

λ (nm)	δ(cos A)	δ(tan Ψ)
300	0.0134	0.0046
305	0.0082	0.0045
310	0.0196	0.0078
315	0.0354	0.0063
320	0.0390	0.0055
325	0.0442	0.0027
330	0.0388	0.0056
335	0.0613	0.0047
340	0.0590	0.0034
345	0.0735	0.0044
350	0.0684	0.0020
355	0.0501	0.0038
360	0.0707	0.0046
365	0.0440	0.0050
370	0.1176	0.0044
375	0.0394	0.0060
380	0.0415	0.0031
385	0.0504	0.0042
390	0.0174	0.0083
395	0.0198	0.0067
400	0.0191	0.0095
Average	0.0443	0.0051

Unfortunately, this also puts a restriction on the quality of the fit [see Eq. (59)]. For example, say a film had a small degree of anisotropy. Then let the difference in variance between data fitted with an isotropic model and data fitted with the correct degree of anisotropy be smaller than 0.01. The "true fit" would be impossible to determine accurately given the quality of data described above.

However, it appears from the data in this thesis that this might not be much of a problem. Note that the PBLG film layers had small degrees of anisotropy (0.03). The variances in the fits to these data sets were acceptable (less than 0.01) only when this anisotropy was accounted for.

Another restriction placed on fitting has to do with dispersion. Normally in the visible region of the electromagnetic spectrum, both the real and imaginary parts of the index of refraction for organic films decrease as λ increases. However, the models were not able to pull a dispersion profile out of a flat guess for samples that were known to be dispersive. The models, did however, improve a dispersive guess.

The sample measured in this thesis known to be dispersive was the ITO coated glass. Based on a priori knowledge of the ITO sample, it was determined that the best fit would come from the single isotropic film model. Examination of the ITO data showed at wavelengths greater than 370 nm, cos Δ and tan

Ψ results were not strongly influenced by the film. Use of data above this wavelength would be worthless. Hence all of the data used for the determination of the optical properties of the ITO films (Samples 1-3) was from 305 to 370 nm.

Additionally, since large changes in phase produce small changes in cos Δ when cos Δ is greater than $|0.707|$, this data is not normally used for accurate fitting. For some angles of incidence, all of the cos Δ data was greater than $|0.707|$. Therefore, it was decided to use only the tan Ψ data in reducing the data for all four samples.

In fine tuning the guesses made to fit data, some observations were made. If it is assumed all other parameters are fixed:

1) as the real part of the index of refraction (n_f) went up, tan Ψ went up and cos Δ went down, and vice versa;

2) as the complex part of the index of refraction (k_f) went up, tan Ψ went down and cos Δ went up, and vice versa;

3) as the film thickness (t_f) went up, tan Ψ went down and cos Δ went up, and vice versa;

4) for all of the samples used in this thesis, the fitted data was most sensitive to film thickness.

Since it was discovered that the models would not move automatically to the "true" minimum no matter what the initial guess, a search strategy was devised taking items 1-4 into

account.

First, since the models were most sensitive to film thickness, the complex part of the index of refraction would initially be set to zero and the real part of the index of refraction fixed at the same "arbitrary" value for all wavelengths. Arbitrary meant within 10% of the expected value of the real part of the index of refraction. Then the fit would be checked at different film thickness near the expected value.

Once the best fit with a given film thickness was determined, the thickness was fixed and the real part of the index of refraction was varied. The fits usually changed very little with a "flat" guess at index of refraction and fixed thickness. Once the best fit with a flat index profile and film thickness was set, the experimental data was examined to see if absorption appeared to be present. If so, then the complex part of the index of refraction was set at some small non-zero value and allowed to vary.

If the variance was still not less than 0.01 after all of this, a choice was made. In the case of films modeled as isotropic (i.e., ITO), some dispersion was added to the initial guess at the indices of refraction (both real and imaginary parts if necessary). In the case the films were to be modeled as anisotropic (i.e., PBLG 5 and 8 layer films on ITO), then the values from the isotropic models would be put

into the anisotropic model.

Dispersive guesses were made for both the real and imaginary parts of the index of refraction for the ITO coated glass. The final fitted parameters produced a variance of 0.0093. The film thickness was calculated to be 279 ± 3 Å. The measured and calculated data from 305-370 nm at all angles for the ITO coated glass are plotted in Appendix E. Additionally, the real and imaginary parts of the index of refraction, along with the corresponding 90% confidence intervals, are plotted versus wavelength for the ITO film in Appendix F.

The five and eight layer PBLG films were fit with the two layer anisotropic film model. They were both tried with the two layer isotropic film model, but the variances in the fits with the tan Ψ data was never less than 0.01. The smallest variance with the two layer isotropic film model was 0.014. The final variance in the fit for the five layer PBLG film was 0.0075, with flat indices of $N_x = 1.65 - 0.20*i$, $N_y = N_z = 1.62 - 0.10*i$, and film thickness of $T_f = 164 \pm 2$ Å. For the eight layer PBLG film, the final variance was 0.0056, with flat indices of $N_x = 1.65 - 0.18*i$, $N_y = N_z = 1.62 - 0.09*i$, and film thickness of $T_f = 216 \pm 2$ Å. The measured and calculated data from 305-370 nm at all angles of incidence for the five layer PBLG film are plotted in Appendix G. The measured and calculated data from 305-370 nm at all angles of incidence for

the eight layer PBLG film are plotted in Appendix H.

The thiophene film was fit with the single isotropic film model. In this case, neither dispersion nor absorption was needed to fit the data to within 0.0075. Here, the tan Ψ data from 500-800 nm was used. The data taken at 60° angle of incidence was not included in the fit because it appeared the back surface reflection was not removed by the black paint at that angle. The film thickness was calculated to be 3060 ± 7 Å, with an uniform index of refraction from 500-800 nm of N_{thio} = 1.68 - 0*i. The measured and calculated data from 500-800 nm at all angles for the thiophene film are plotted in Appendix I.

VI. Recommendations

Continuation of this work is mandatory to show the validity of the models chosen. In addition, new parameters may be added or new approaches tried to improve fitting the data.

First, the number of data sets taken at different angles of incidence should be increased. Five sets of tan Ψ data only fit the simplest model well. Many more data sets are needed for more complex models. Remember, one can never have too much data.

In order to improve the quality of data taken, long range measurement trends must be observed. This will give an indication on how far to trust the data, as well as giving the user insight into machine performance. Also, to use more of the data acquired, the compensator assembly that came with the machine could be used. This would allow the use of the cos Δ data $> |0.707|$. Another technique to use more of the measured data would be to mount the films on an absorbing substrate (say silicon).

At some point, the models used in this thesis will not be adequate. New models will have to be developed, probably to include more parameters. Two additional parameter sets immediately come to mind:

1) Accounting for surface roughness of each film layer. Much work has been done in assuming an Effective Medium

Approximation (EMA) for isotropic film(s)/substrates. No one has developed the formulae for an EMA in the anisotropic case.

2) Accounting for spatial dispersion (inhomogeneity) in the film(s)/substrate. Again, the models herein assume homogeneity. Once spatial dispersion is to be accounted for, the derivation must either be modified or a new derivation used.

Quality of data will affect both of the above mentioned changes. I predict that until the quality of data typically produced is improved by at least an order of magnitude, neither of the effects listed above will be accurately measured for anisotropic films.

Finally, a real computer programmer should take these models and make them "user friendly". A shell driving all of the models could easily be written by such a person. A look at the code written for this thesis shows this author is not such a person.

Appendices A-D

The following four appendices contain the four spectroscopic ellipsometry data sets used in this thesis. For each angle of incidence, tan Ψ and cos Δ data was taken every 5 nm from 300-800 nm, for a total of 202 data points.

Appendix A: ITO Spectroscopic Ellipsometry Data

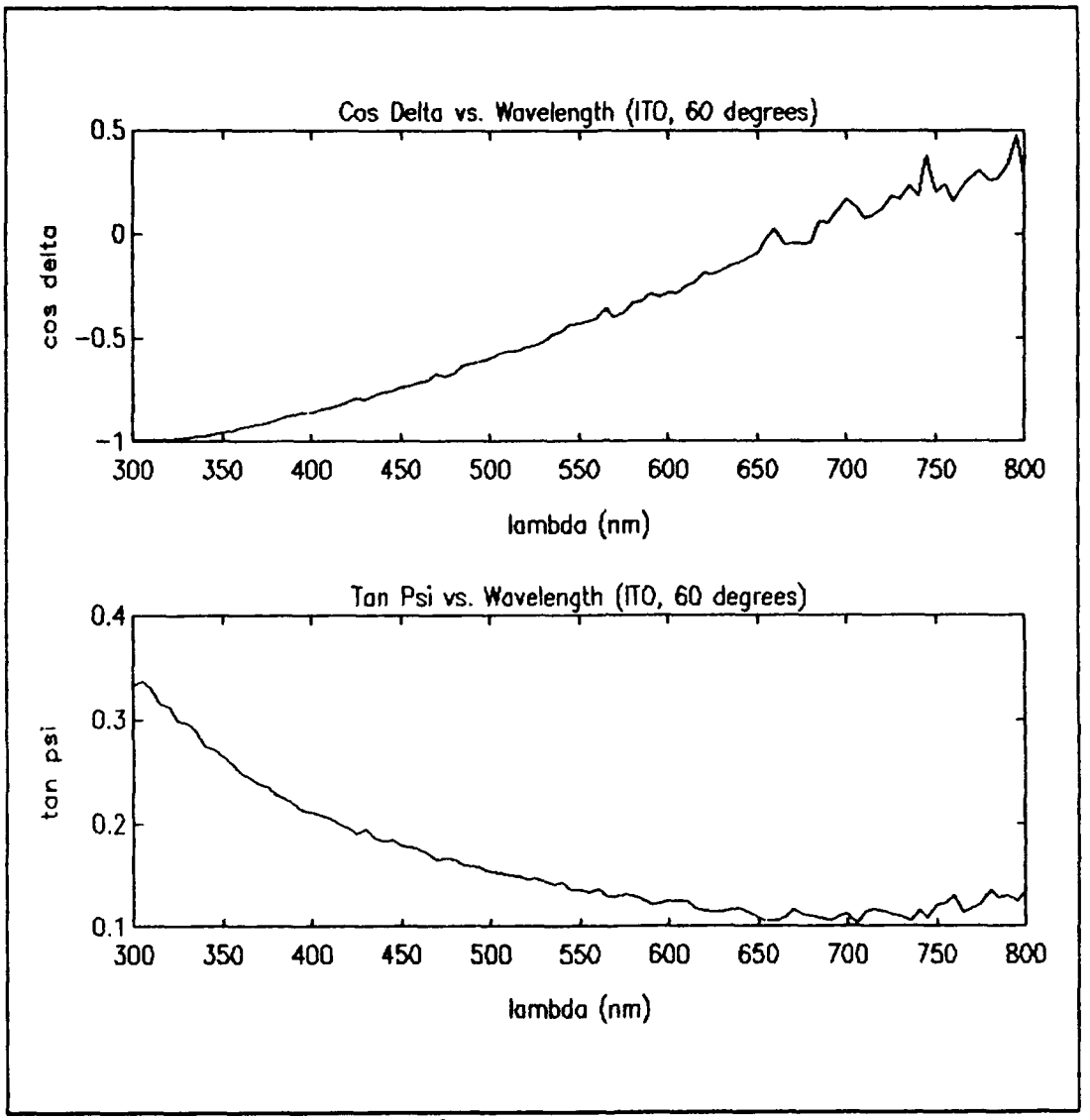

Figure 7 ITO SE Data at 60°

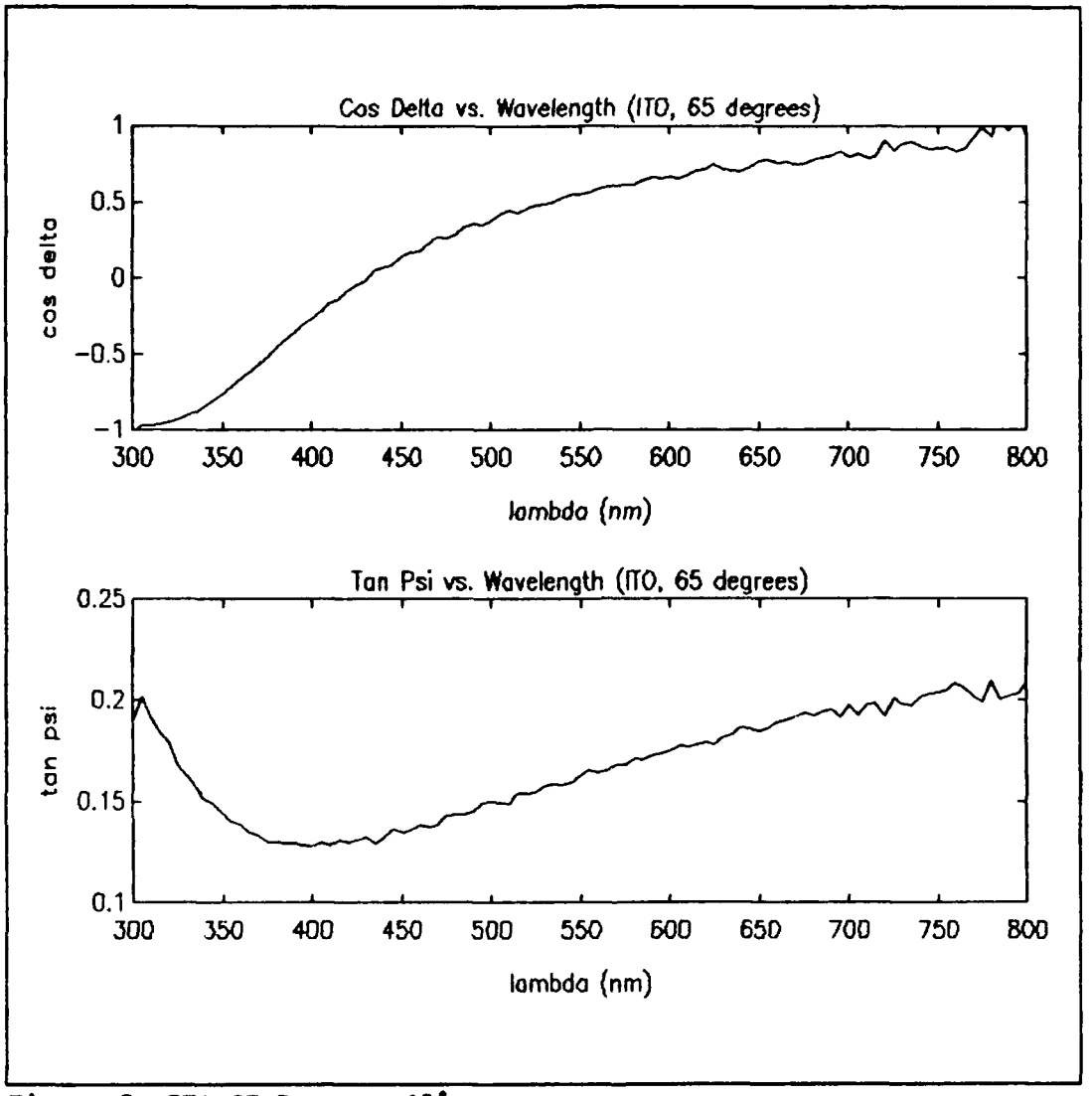

Figure 8 ITO SE Data at 65°

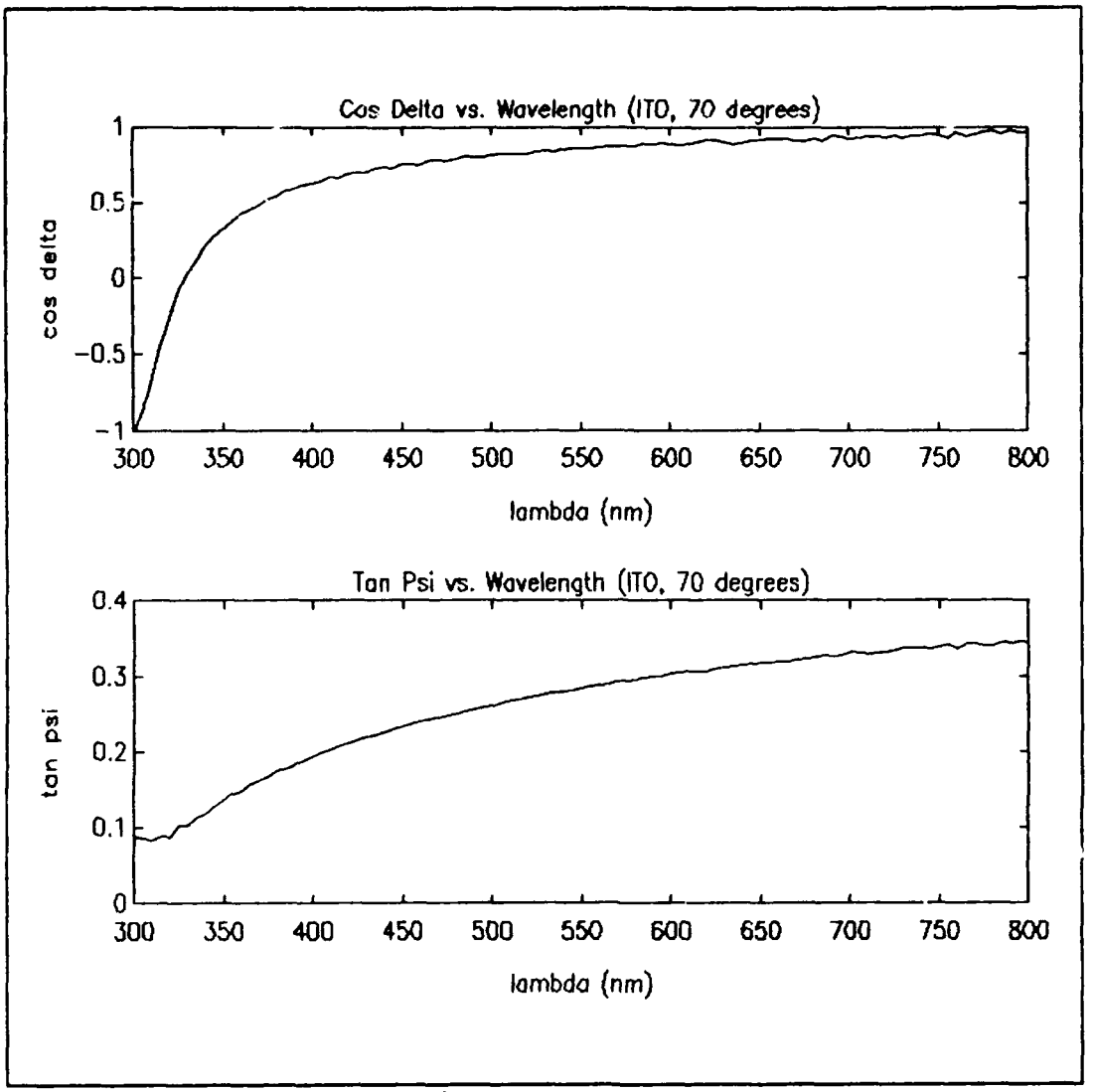

Figure 9 ITO SE Data at 70°

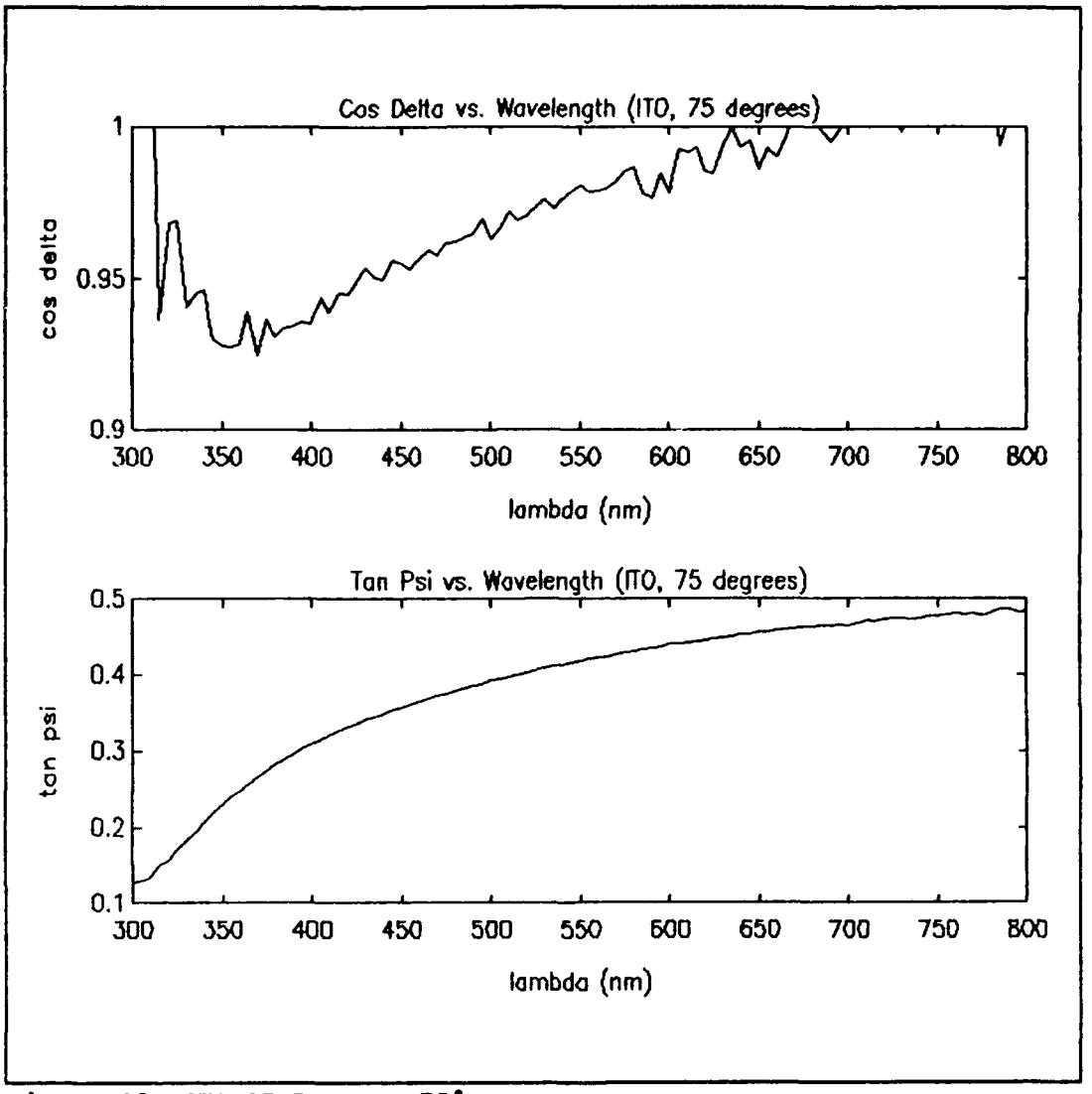

Figure 10 ITO SE Data at 75°

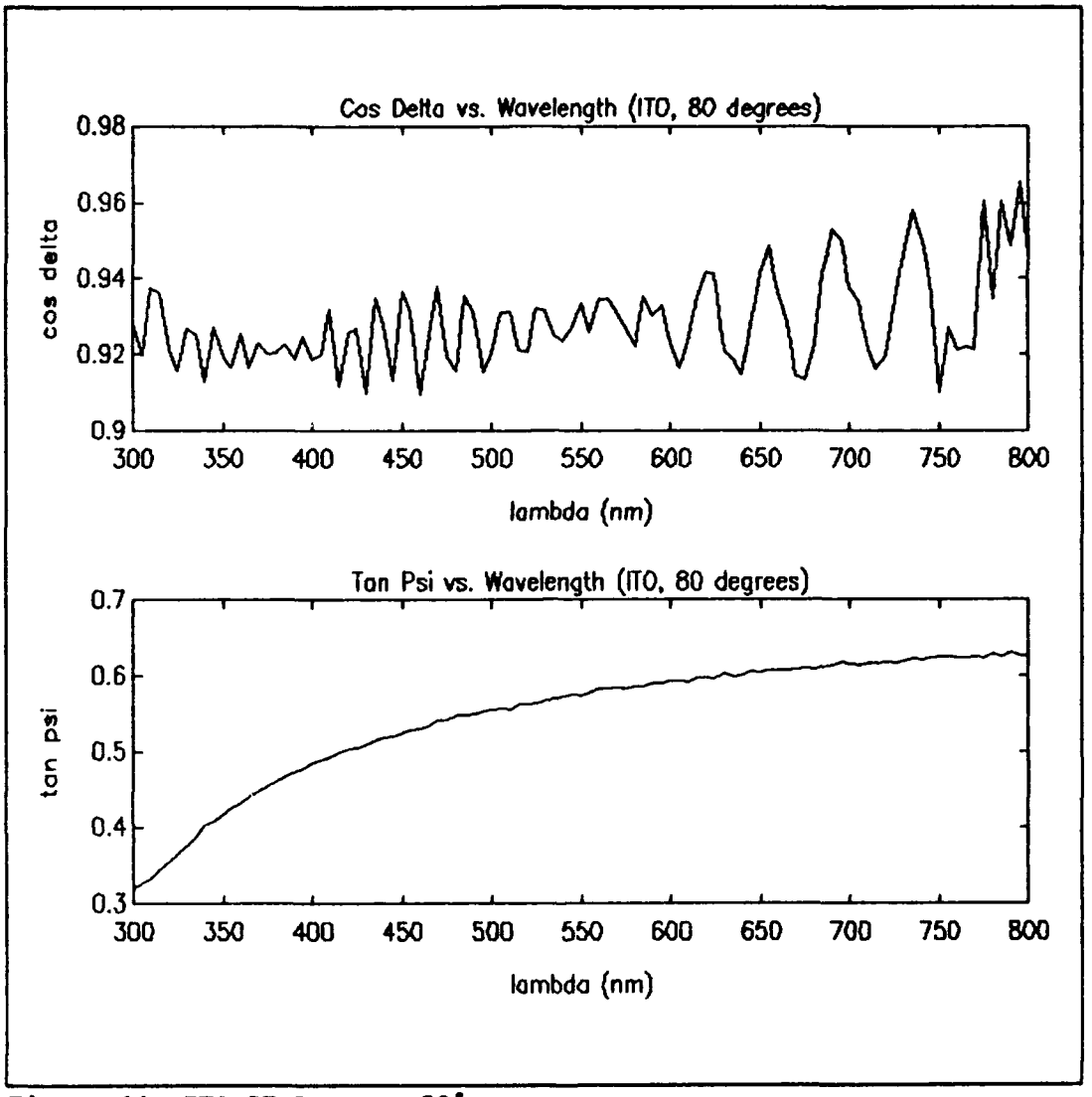

Figure 11 ITO SE Data at 80°

Appendix B: PBLG 5 Layer Spectroscopic Ellipsometry Data

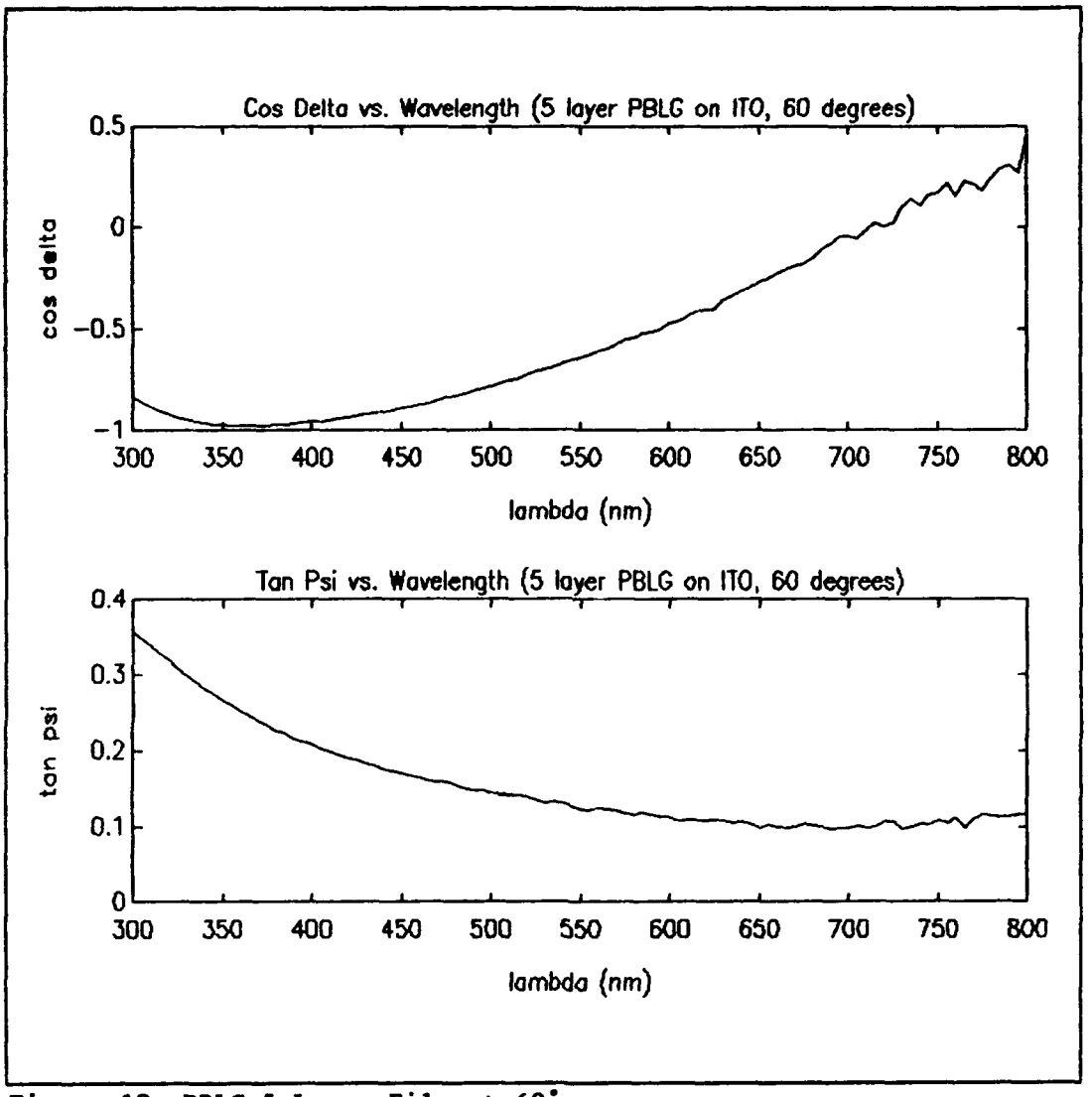

Figure 12 PBLG 5 Layer Film at 60°

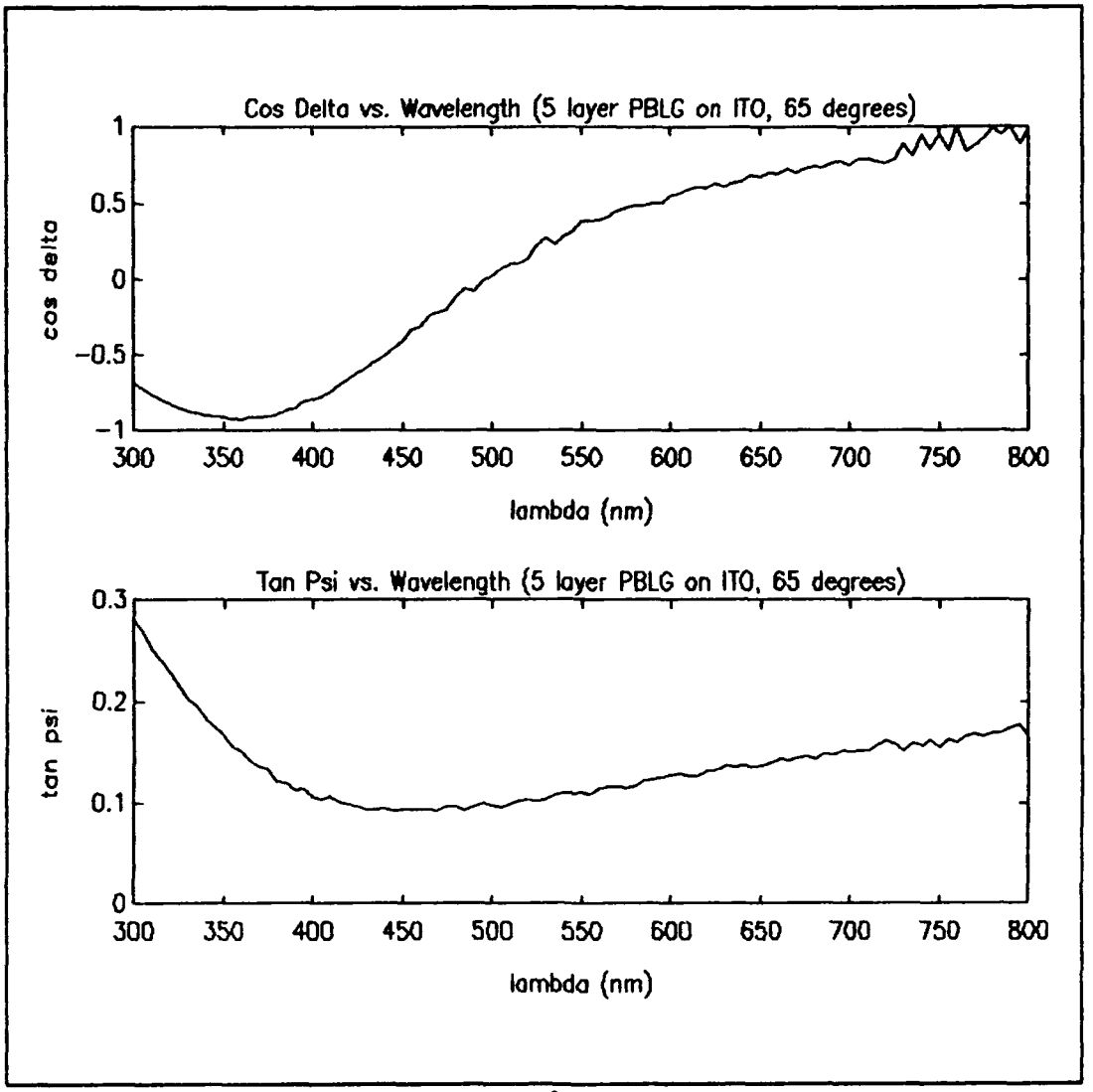

Figure 13 PBLG 5 Layer Film at 65°

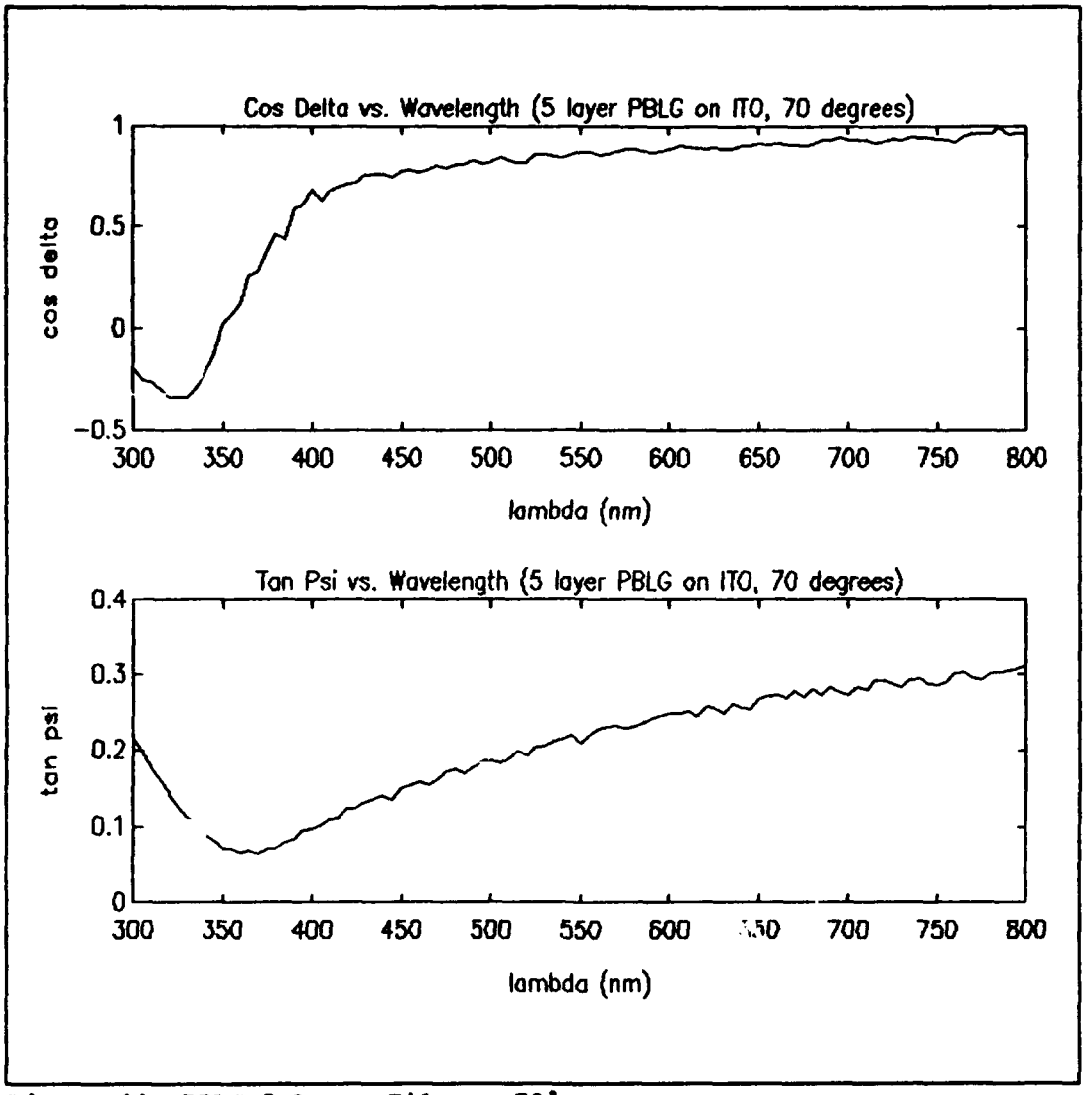

Figure 14 PBLG 5 Layer Film at 70°

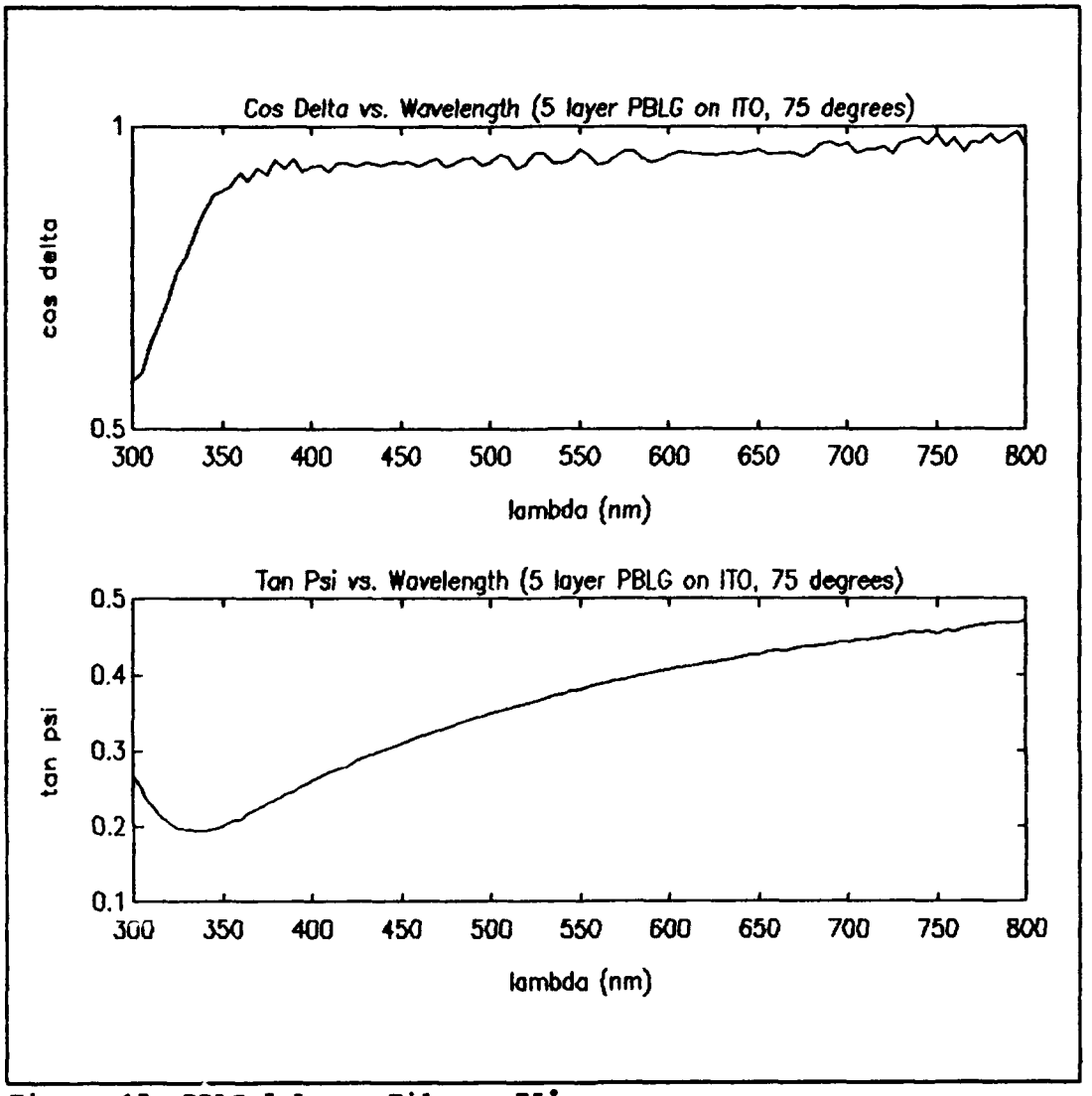

Figure 15 PBLG 5 Layer Film at 75°

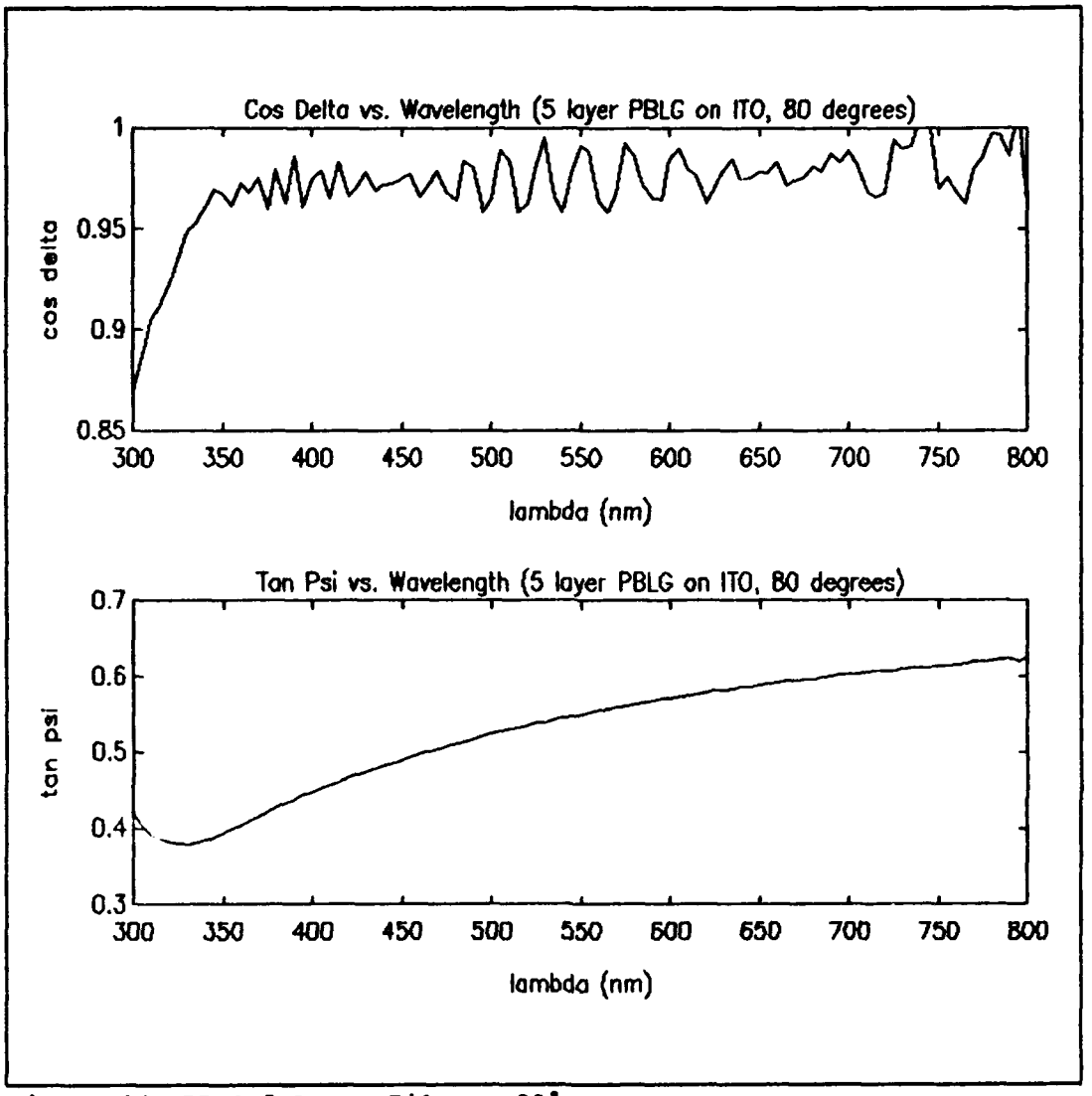

Figure 16 PBLG 5 Layer Film at 80°

Appendix C: PBLG 8 Layer Spectroscopic Ellipsometry Data

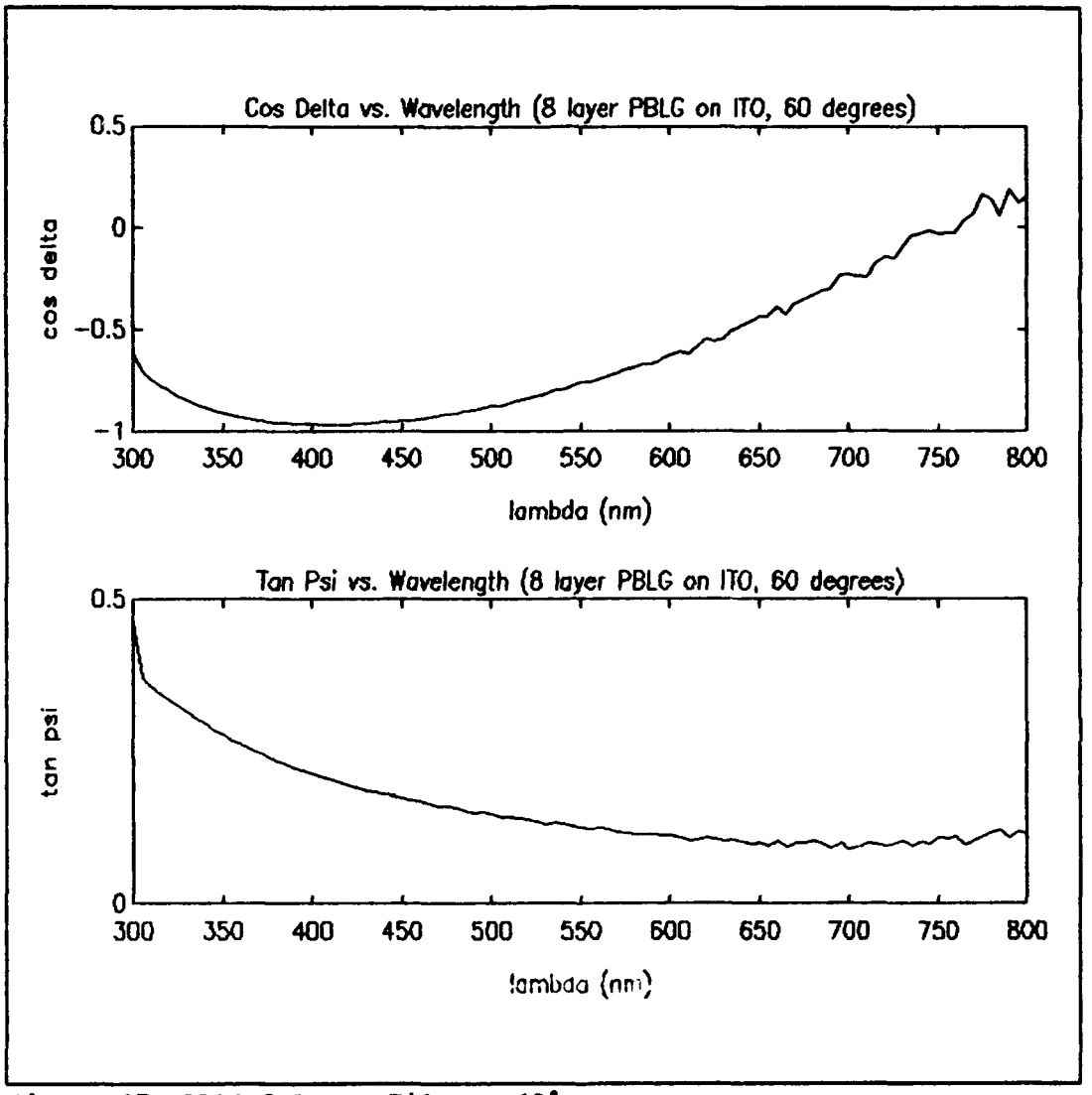

Figure 17 PBLG 8 Layer Film at 60°

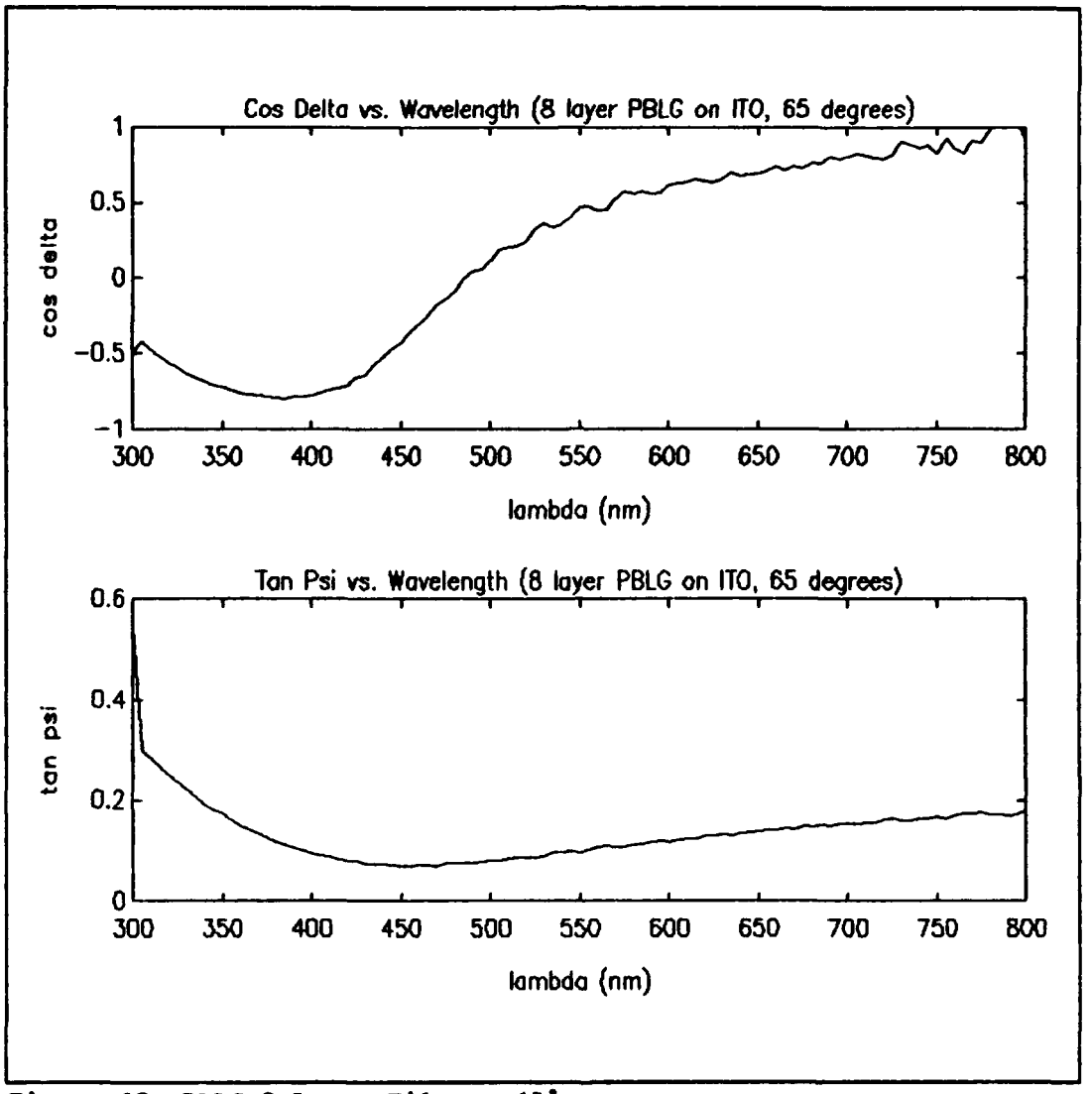

Figure 18 PBLG 8 Layer Film at 65°

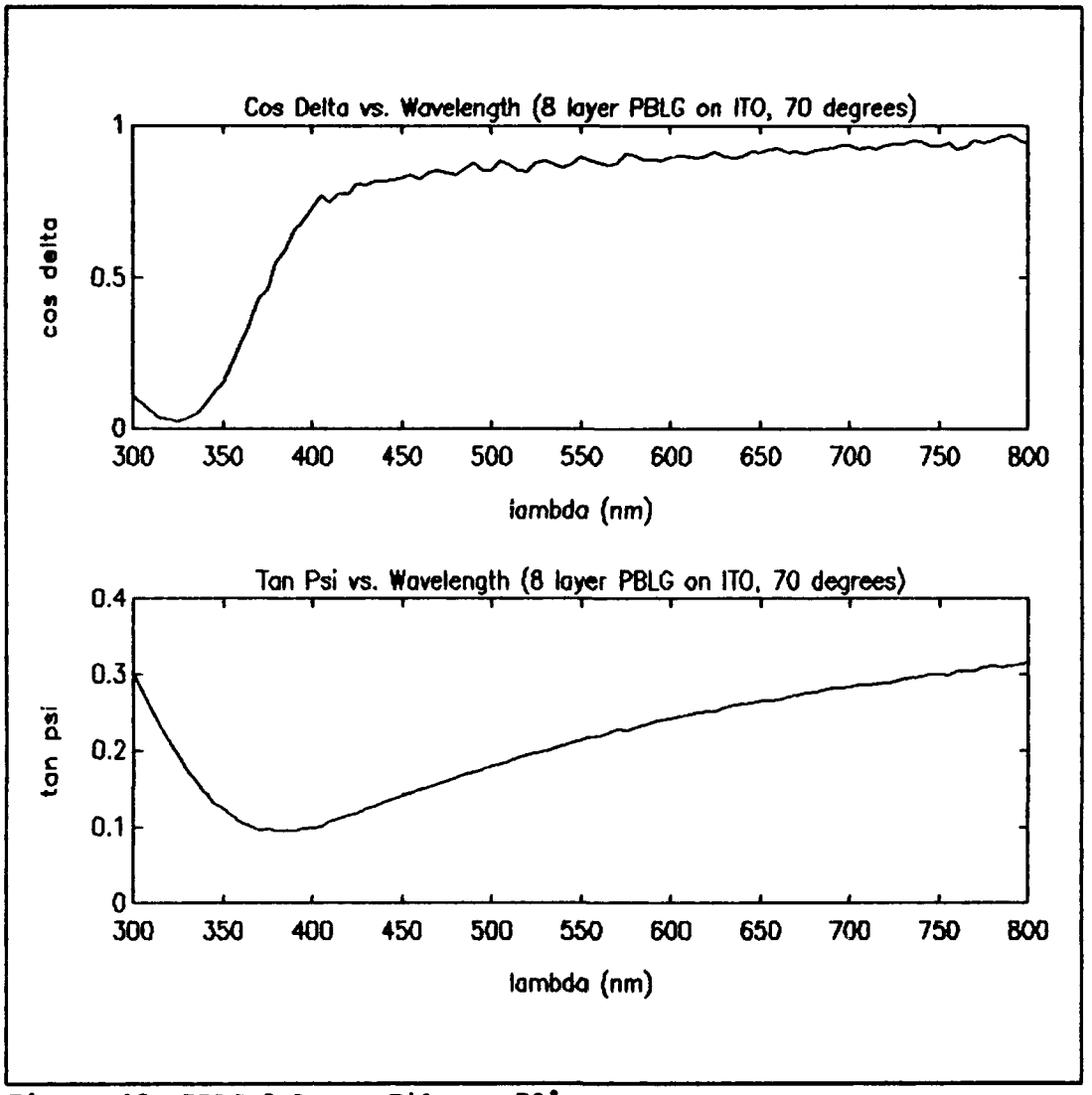

Figure 19 PBLG 8 Layer Film at 70°

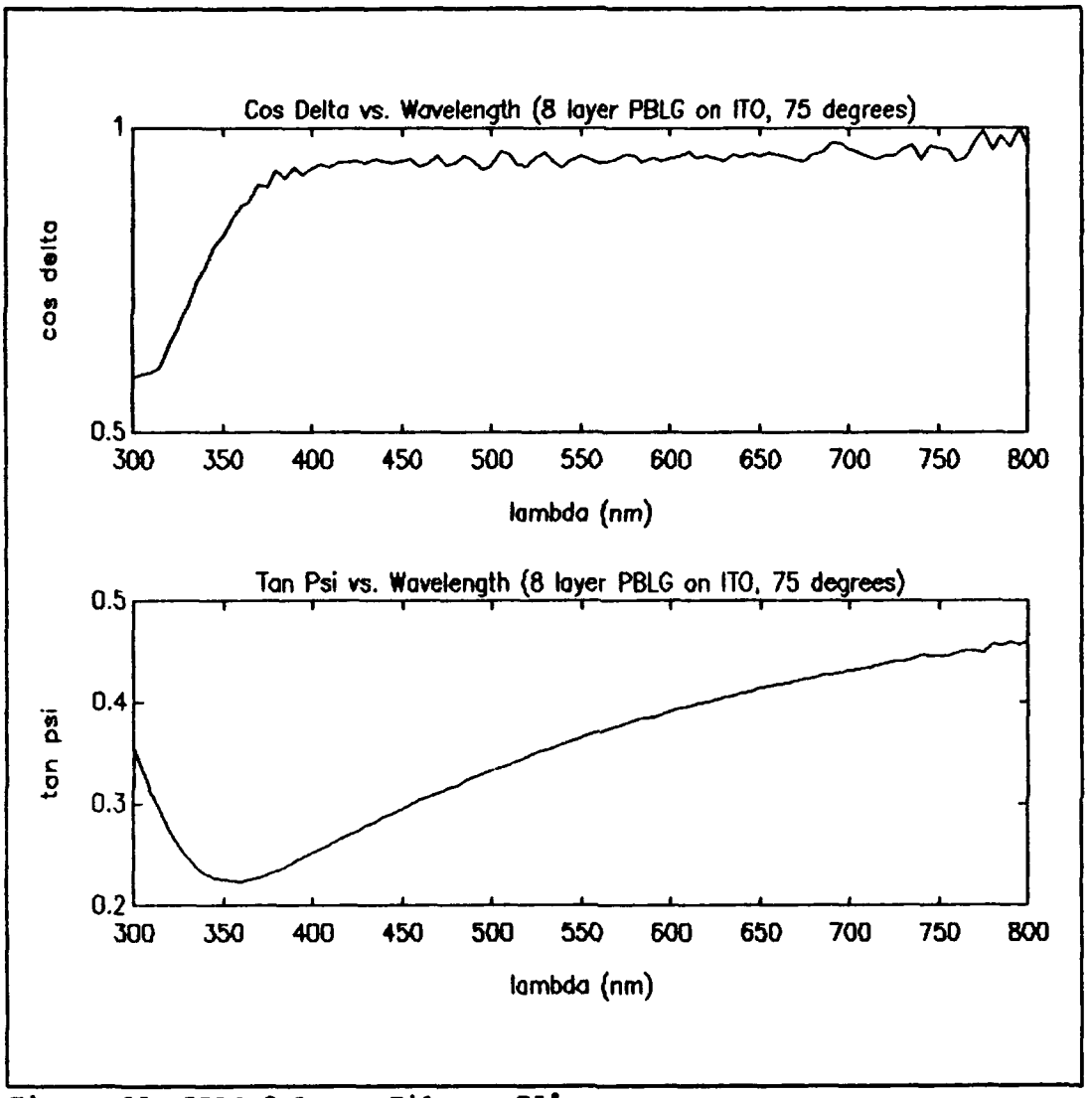

Figure 20 PBLG 8 Layer Film at 75°

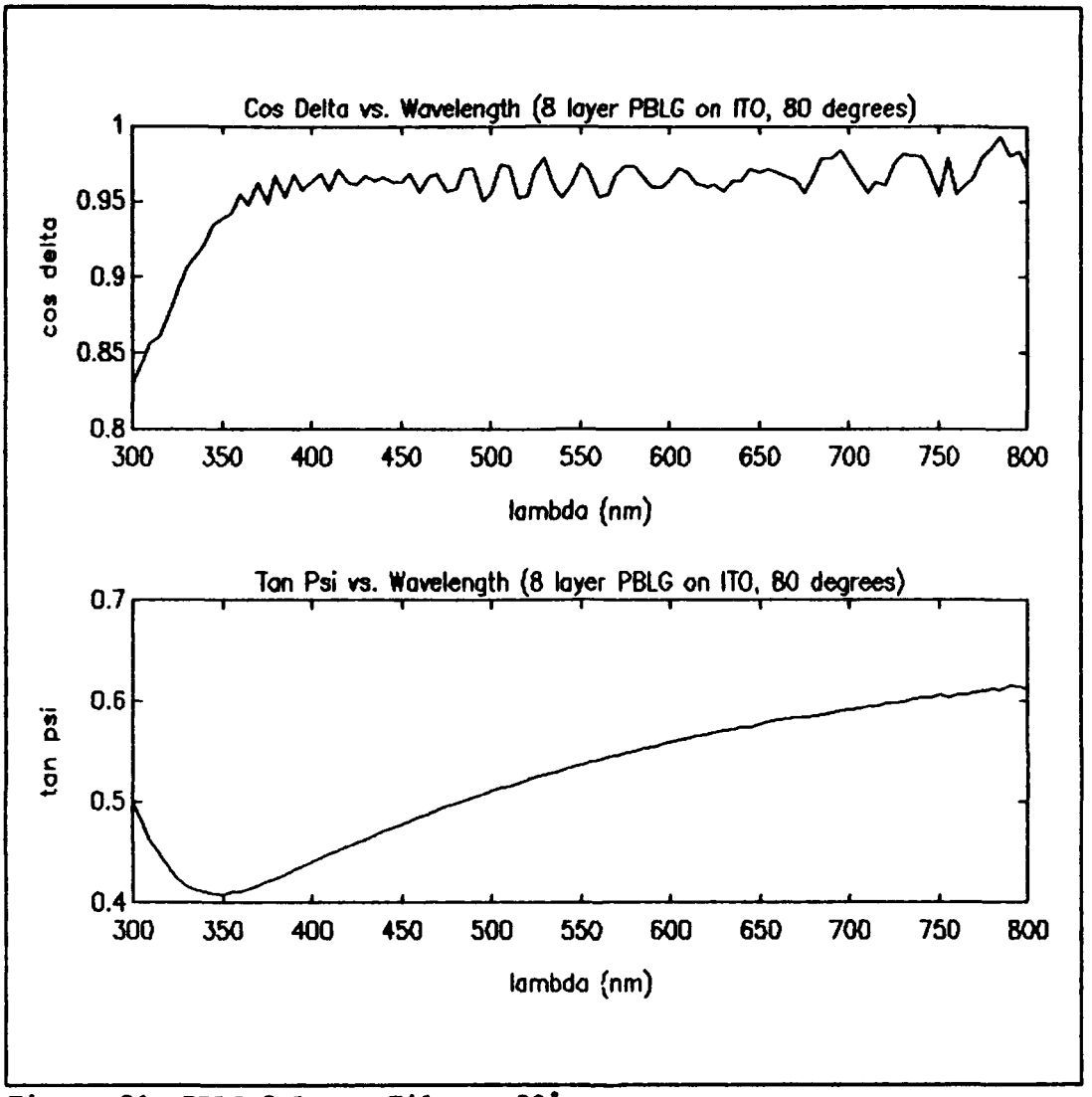

Figure 21 PBLG 8 Layer Film at 80°

Appendix D: Thiophene Spectroscopic Ellipsometry Data

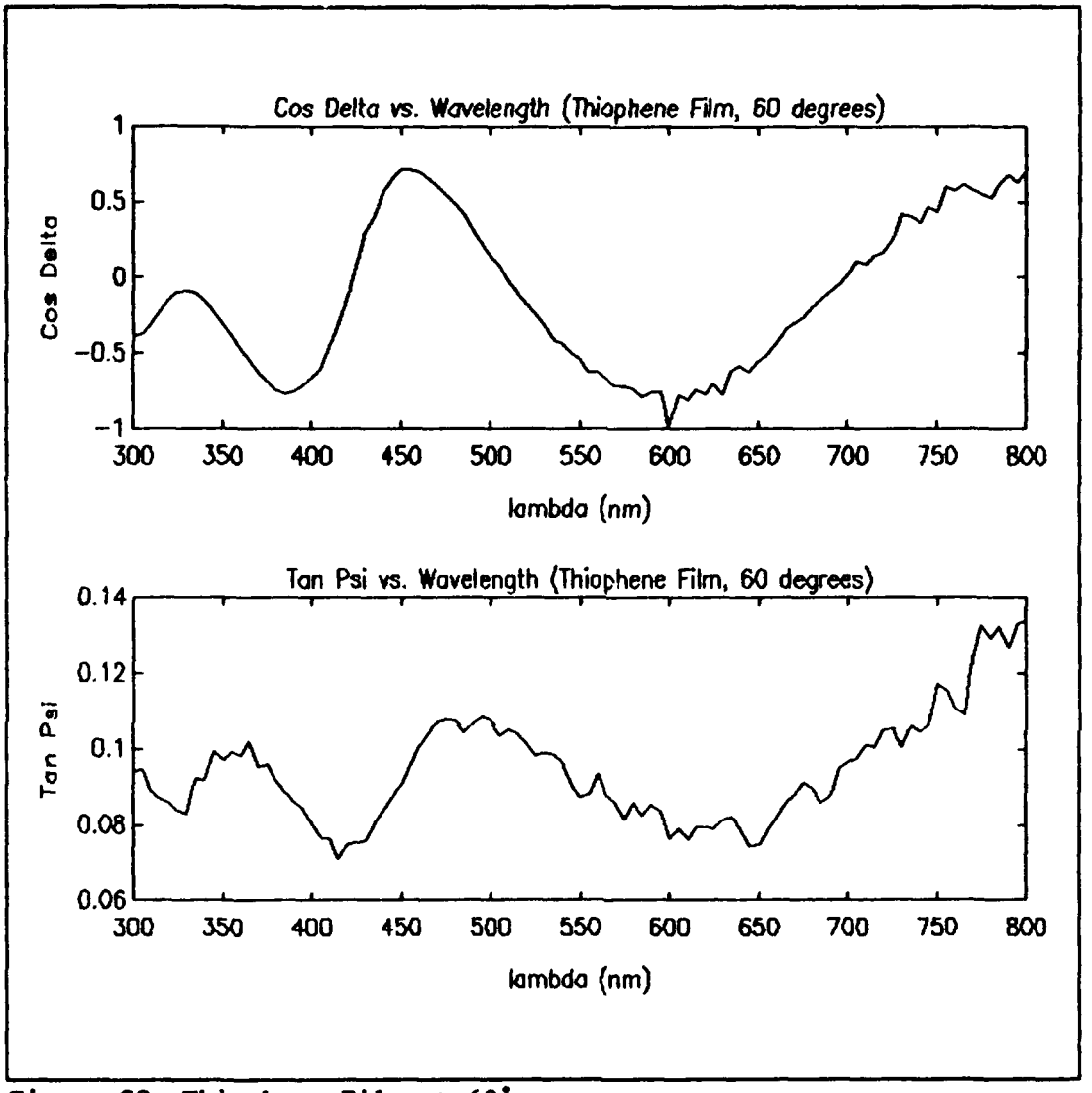

Figure 22 Thiophene Film at 60°

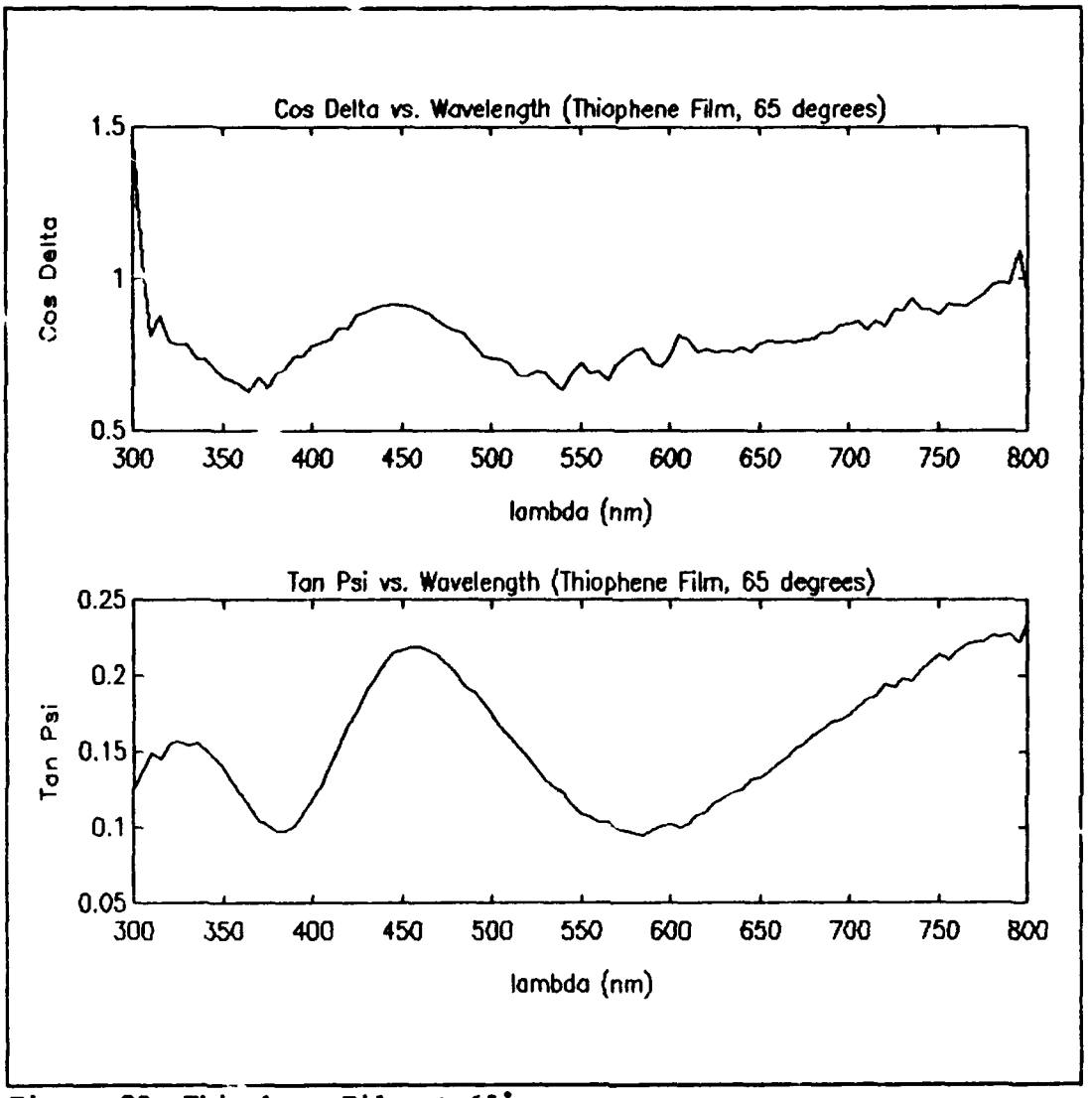

Figure 23 Thiophene Film at 65°

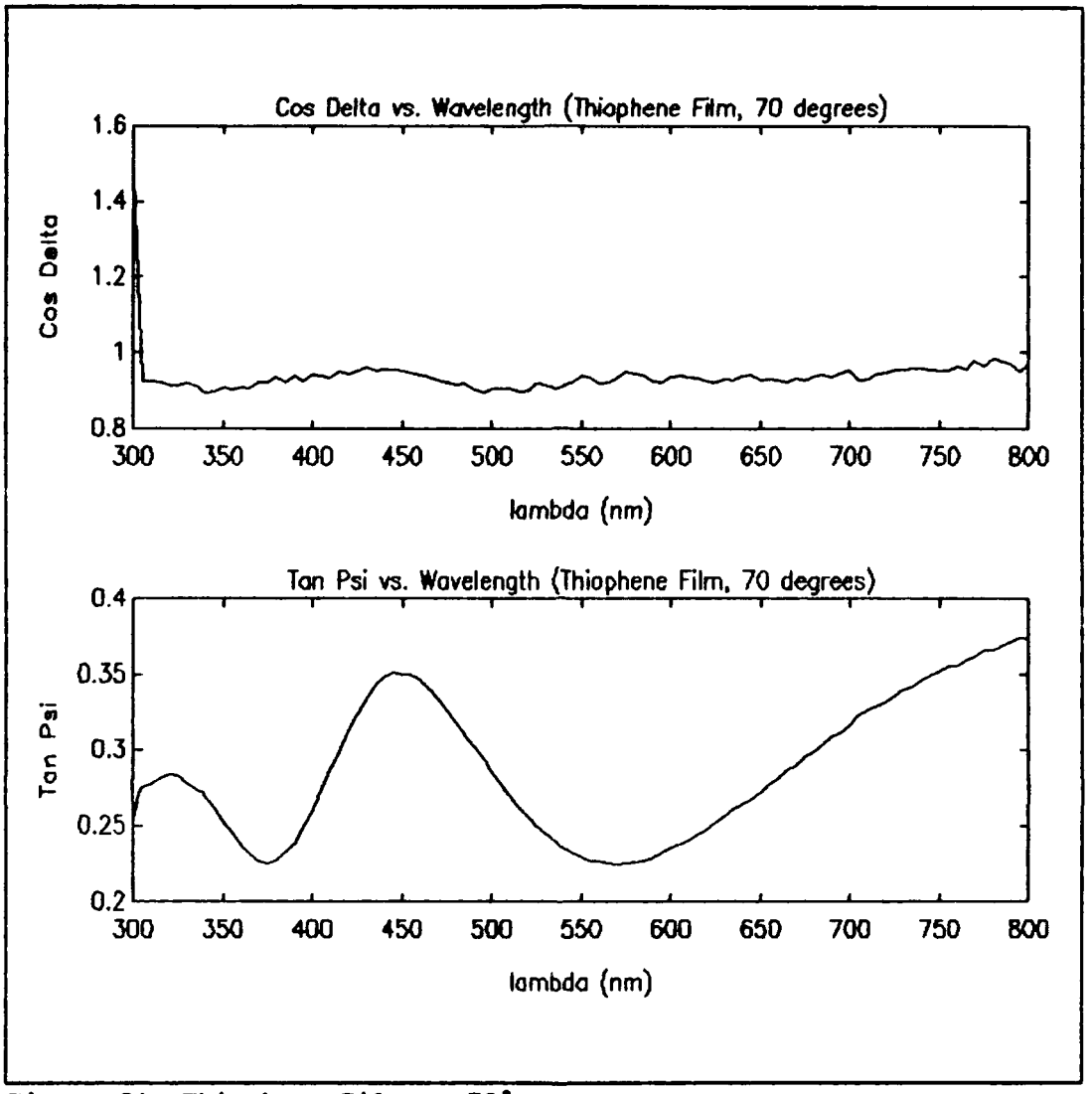

Figure 24 Thiophene Film at 70°

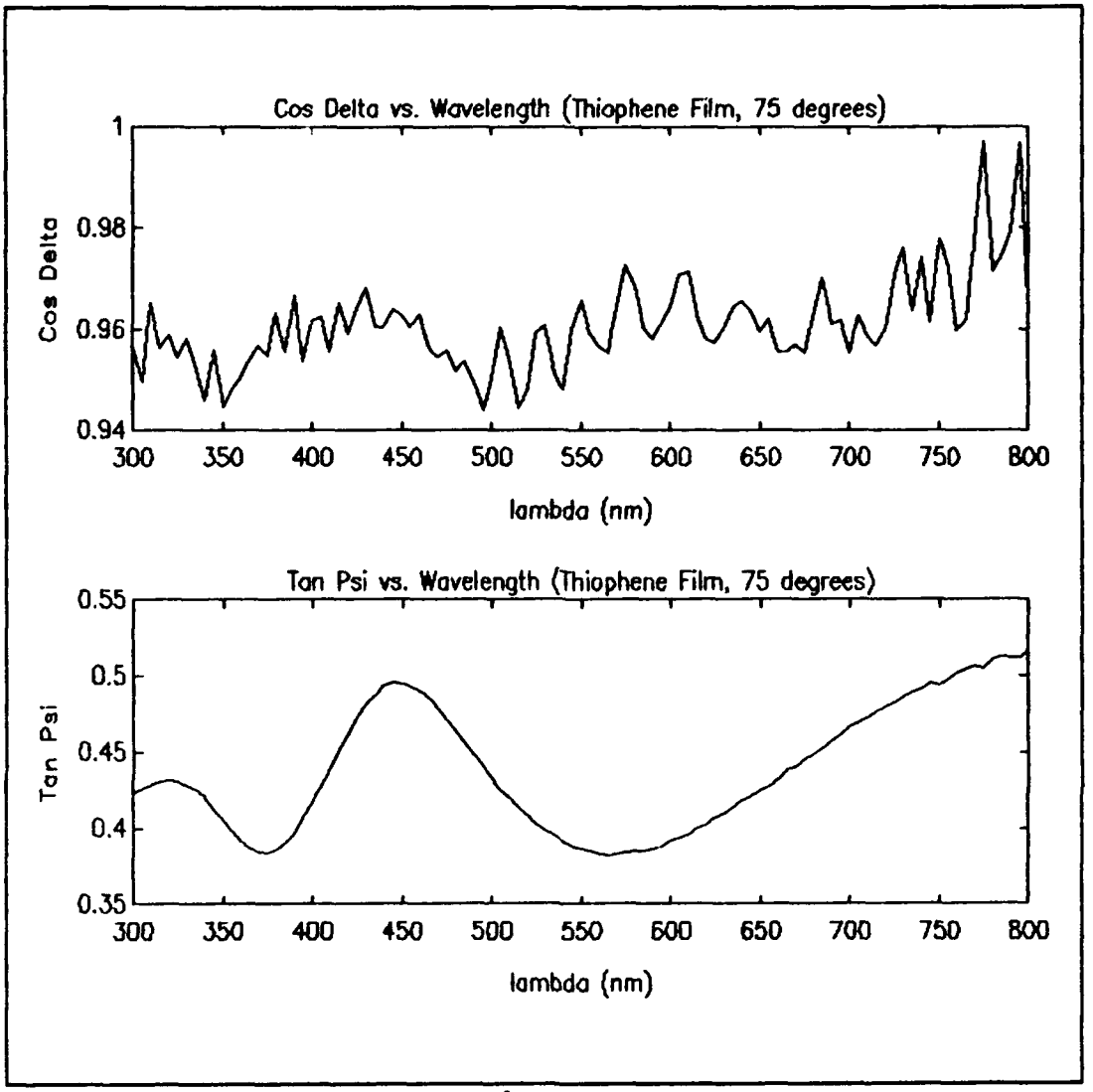

Figure 25 Thiophene Film at 75°

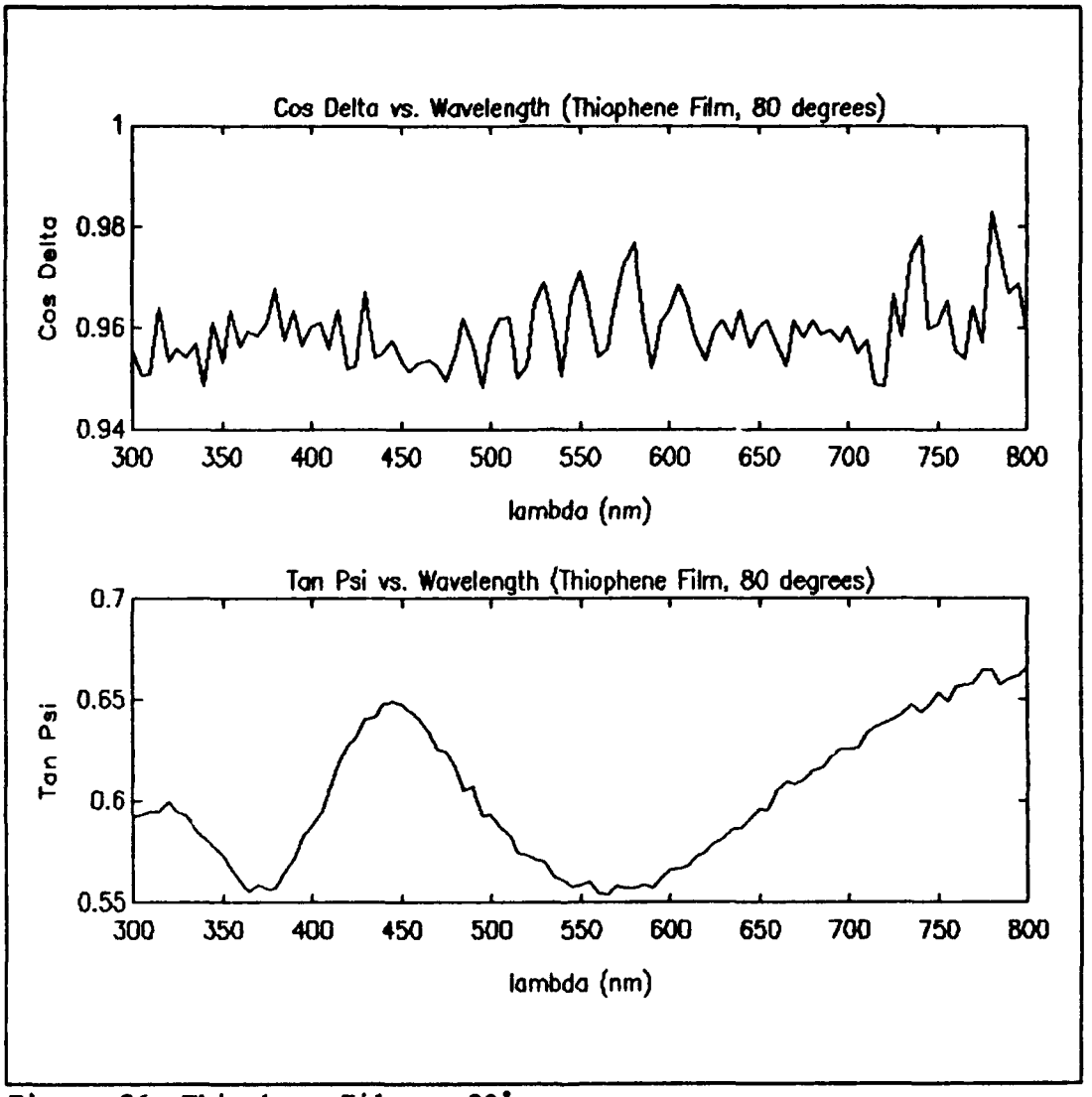

Figure 26 Thiophene Film at 80°

Appendices E, G-I

For each of these appendices, both experimental and calculated tan Ψ and cos Δ data is plotted versus wavelength. For Appendices E, G and H the data used in the fit was tan Ψ from 305-370 nm, for a total of 28 data points at each angle of incidence. For Appendix I, the data used was tan Ψ from 500-800 nm, for a total of 61 data points at each angle of incidence.

At the bottom of each of these appendices are the values used in the final fit, as well as the variance of that fit. Even though only tan Ψ data were used in the fits, and the variances were calculated with only the tan Ψ data, the calculated and experimental cos Δ data is also plotted versus wavelength for each data set.

Appendix E: ITO Fitted Data

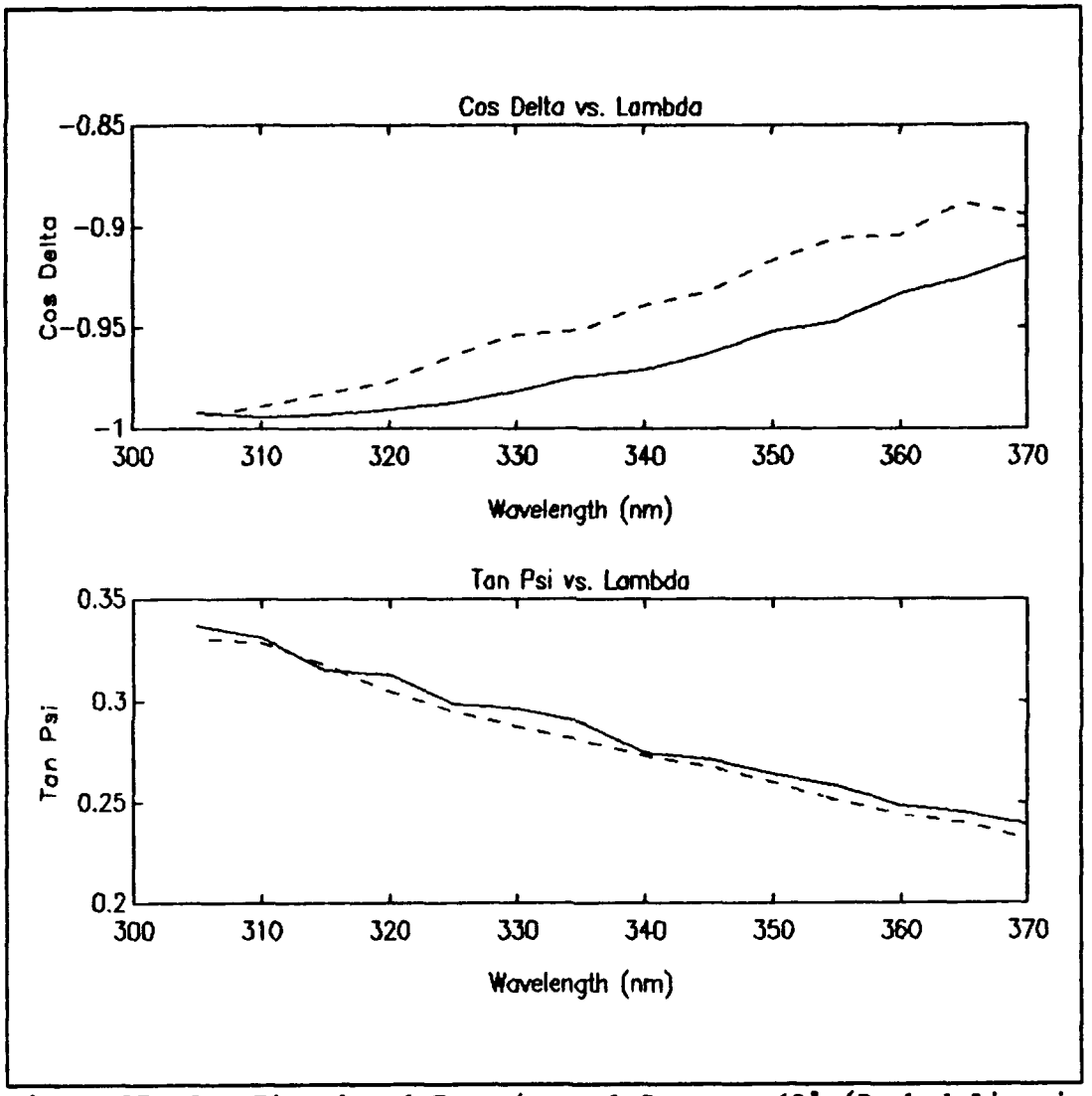

Figure 27 ITO Fitted and Experimental Data at 60° (Dashed Line is Fit)

T_f = 279 ± 3 Å

(N_f dispersive from N_{305} = 2.38 - 0.12*i to N_{370} = 2.15 - 0.07*i)

VARIANCE = 0.0093

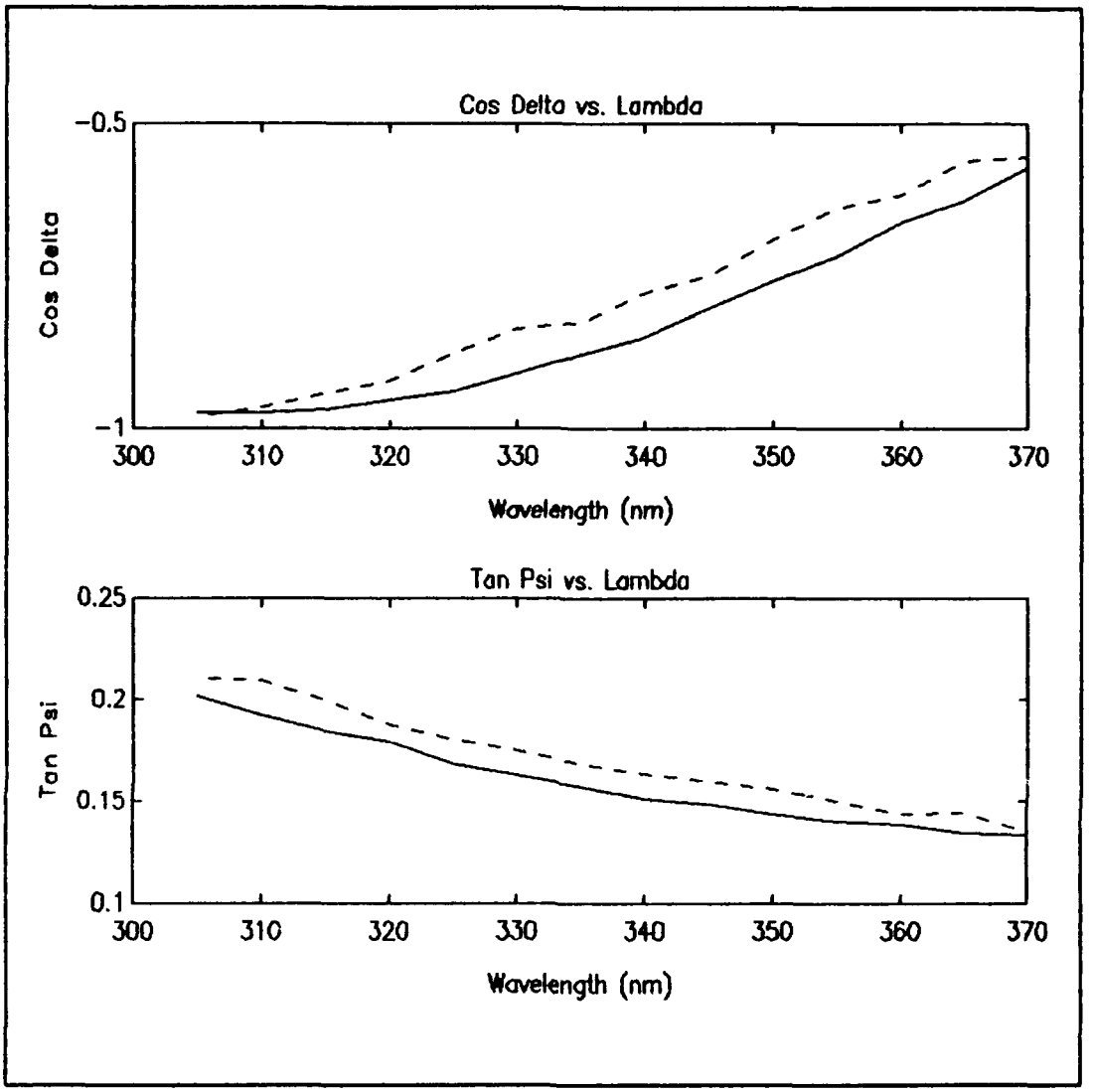

Figure 28 ITO Fitted and Experimental Data at 65° (Fitted Data is Dashed)

T_f = 279 ± 3 Å

(N_f dispersive from N_{305} = 2.38 - 0.12*i to N_{370} = 2.15 - 0.07*i)

VARIANCE = 0.0093

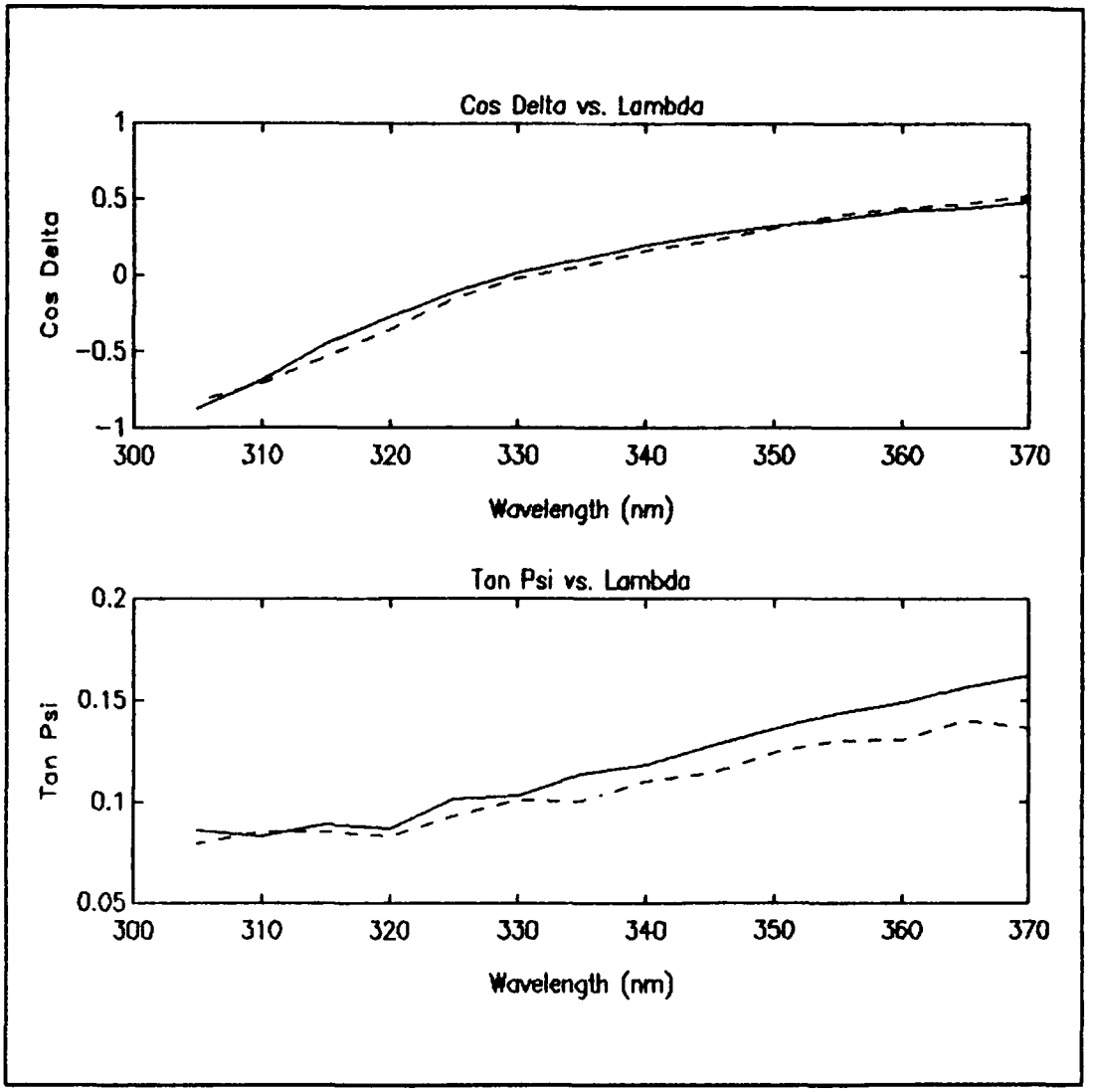

Figure 29 ITO Fitted and Experimental Data at 70° (Fitted Data is Dashed)

T_f = 279 ± 3 Å

(N_f dispersive from N_{305} = 2.38 - 0.12*i to N_{370} = 2.15 - 0.07*i)

VARIANCE = 0.0093

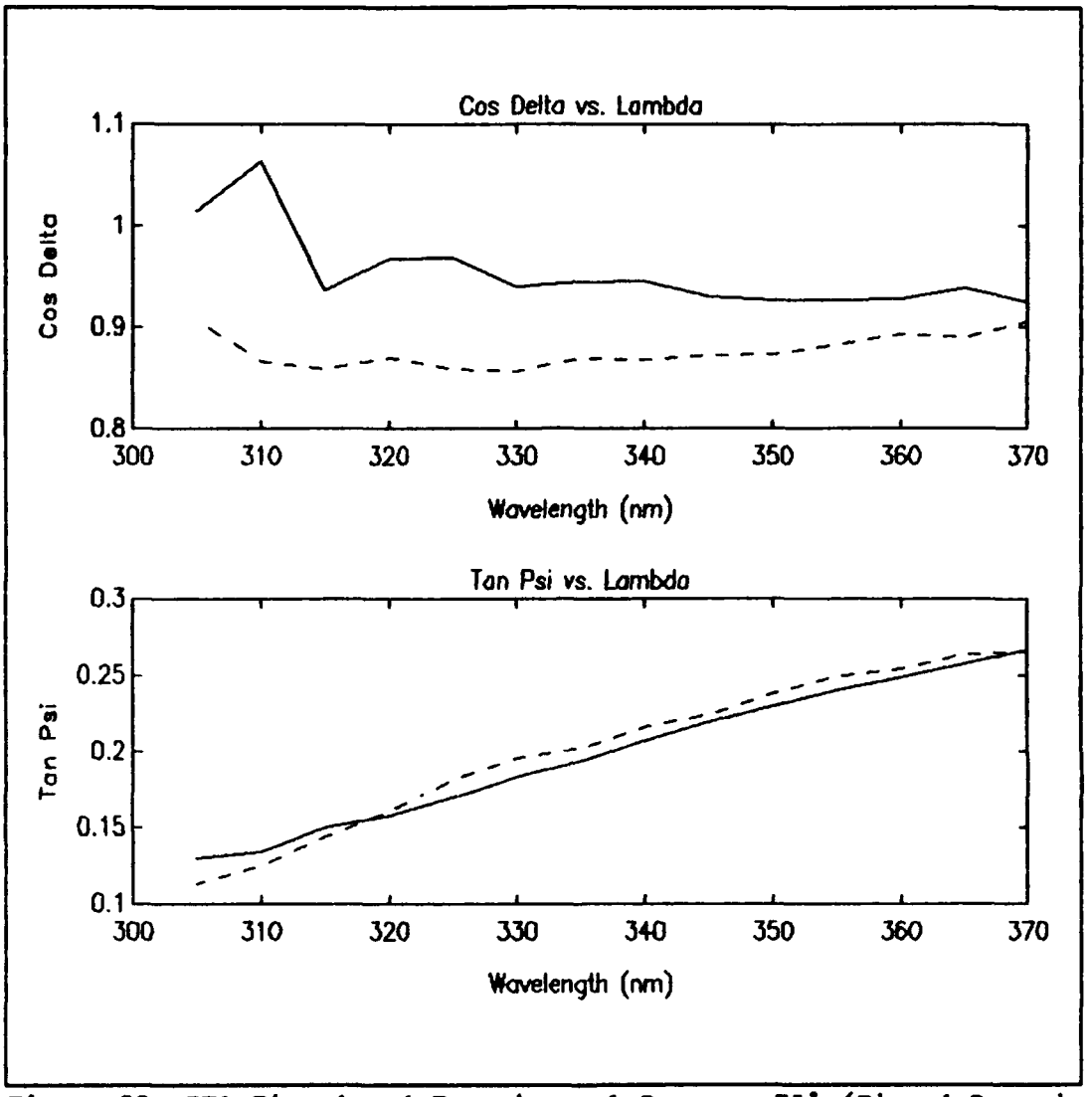

Figure 30 ITO Fitted and Experimental Data at 75° (Fitted Data is Dashed)

T_f = 279 ± 3 Å

(N_f dispersive from N_{305} = 2.38 - 0.12*i to N_{370} = 2.15 - 0.07*i)

VARIANCE = 0.0093

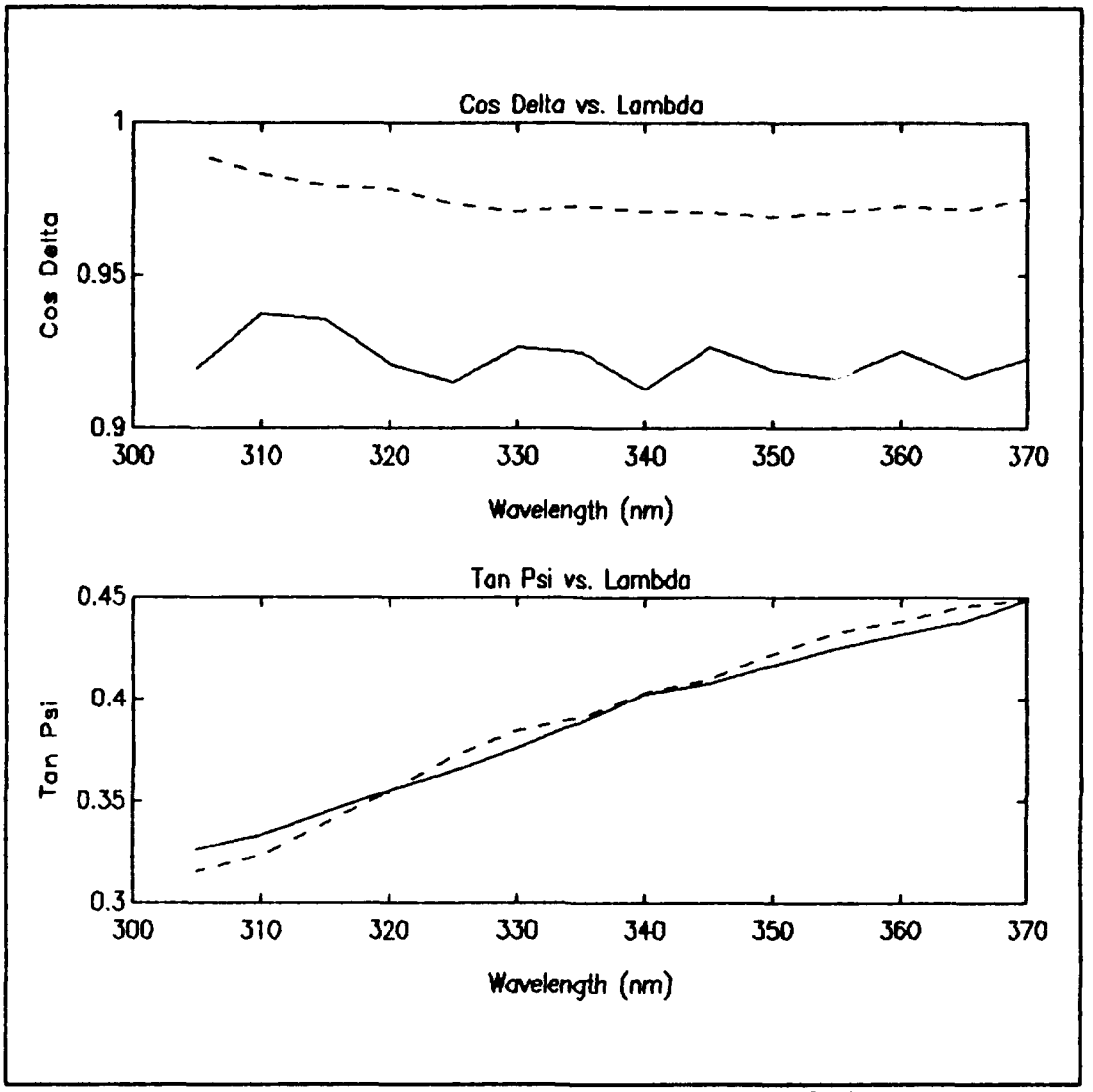

Figure 31 ITO Fitted and Experimental Data at 80° (Fitted Data is Dashed)

T_f = 279 ± 3 Å

(N_f dispersive from N_{305} = 2.38 - 0.12*i to N_{370} = 2.15 - 0.07*i)

VARIANCE = 0.0093

Appendix F: Dispersion of n,k vs. Wavelength (ITO)

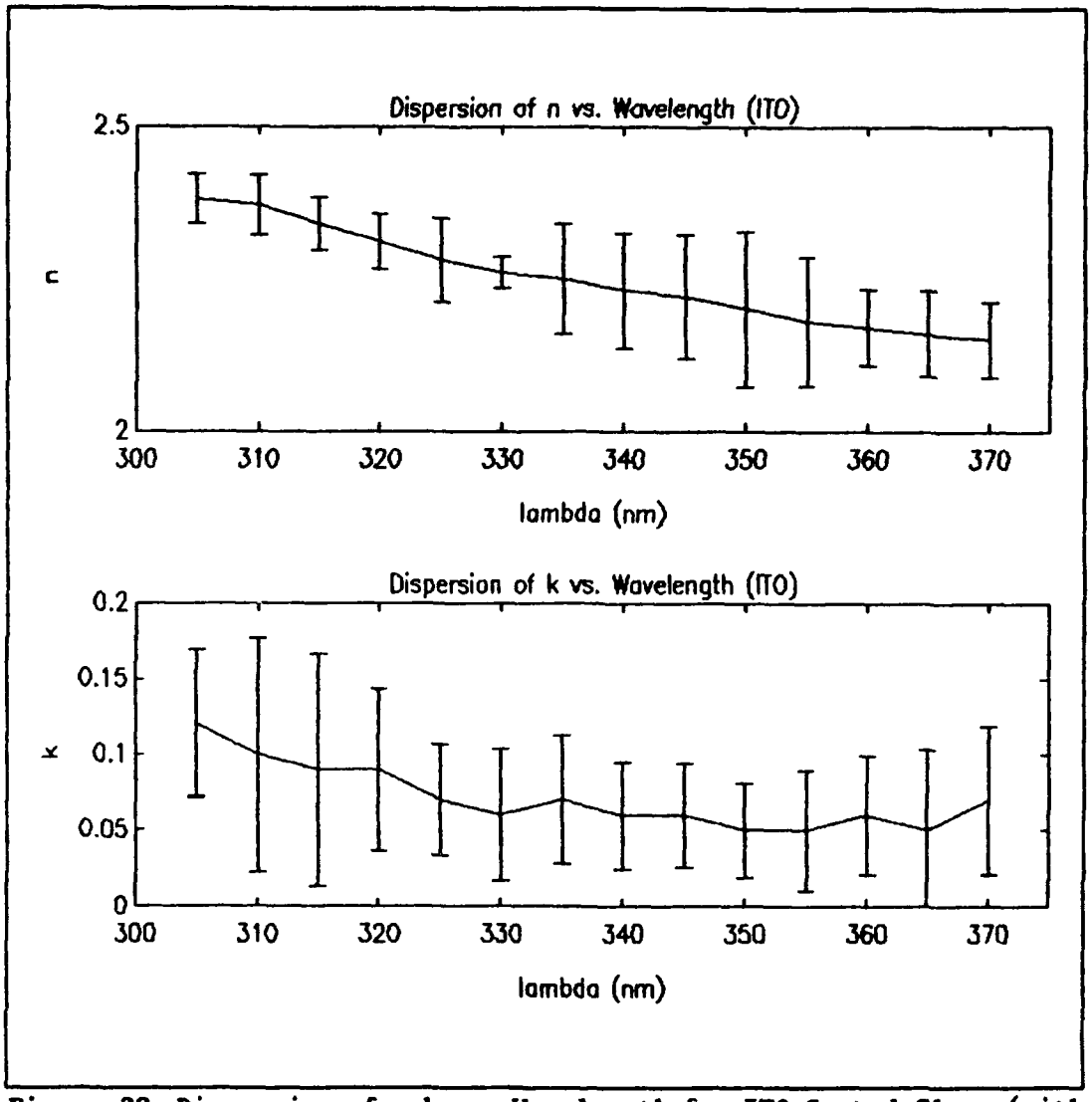

Figure 32 Dispersion of n,k vs. Wavelength for ITO Coated Glass (with 90% confidence intervals)

T_f = 279 ± 3 Å

VARIANCE = 0.0093

Appendix G: PBLG 5 Layer Fitted Data

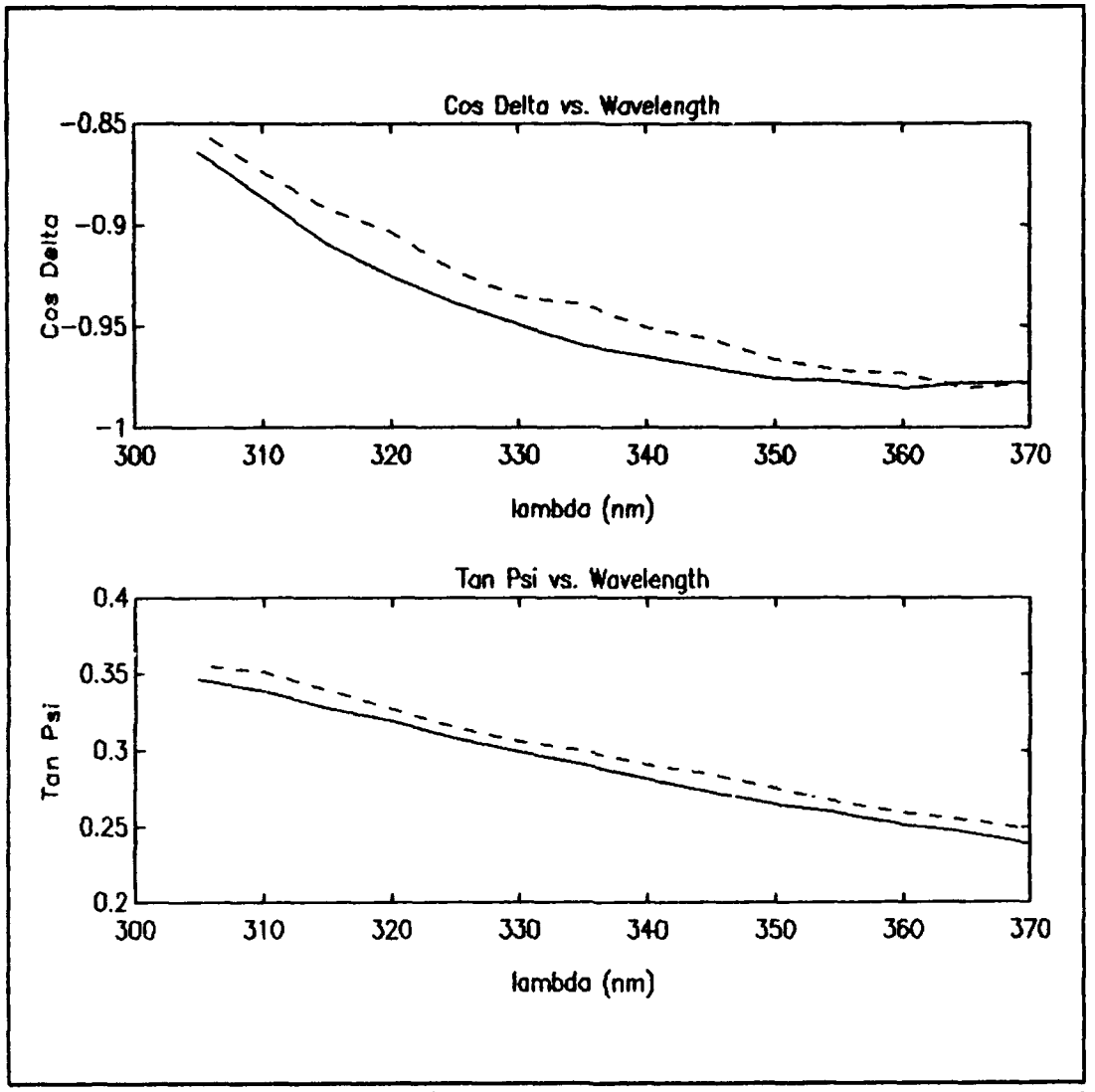

Figure 33 Fitted and Experimental Data for 5 Layer PBLG on ITO Coated Glass at 60° (Dashed line is fitted data)

T_{f1} = 164 ± 2 Å

(N_{i1} = 1.65 - 0.20*i and

N_{f1} = N_{i1} = 1.62 - 0.10*i for all wavelengths)

VARIANCE = 0.0075

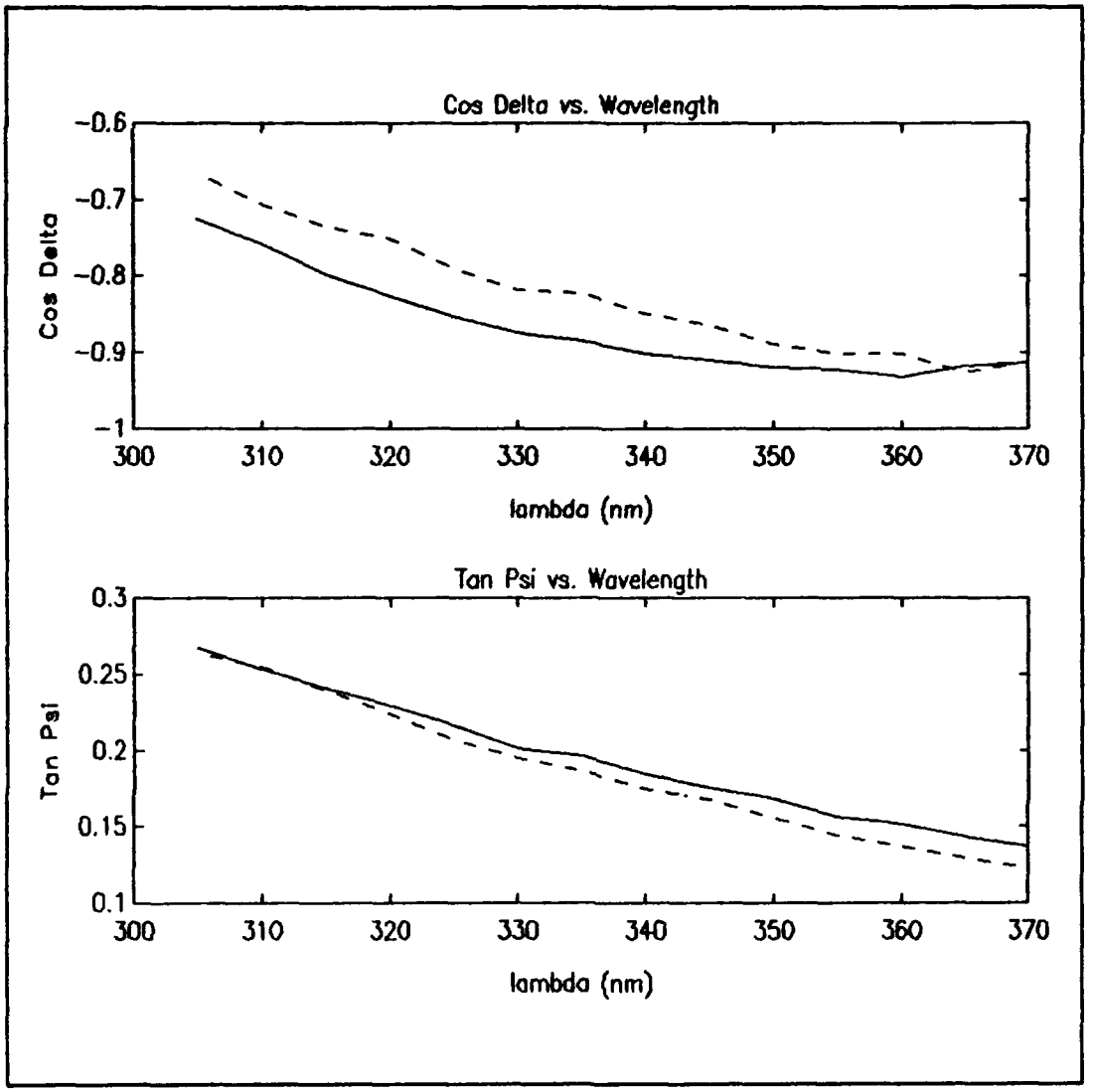

Figure 34 Fitted and Experimental Data for 5 Layer PBLG on ITO Coated Glass at 65° (Dashed line is fitted data)

T_{f1} = 164 ± 2 Å

(N_{s1} = 1.65 - 0.20*i and

N_{f1} = N_{s1} = 1.62 - 0.10*i for all wavelengths)

VARIANCE = 0.0075

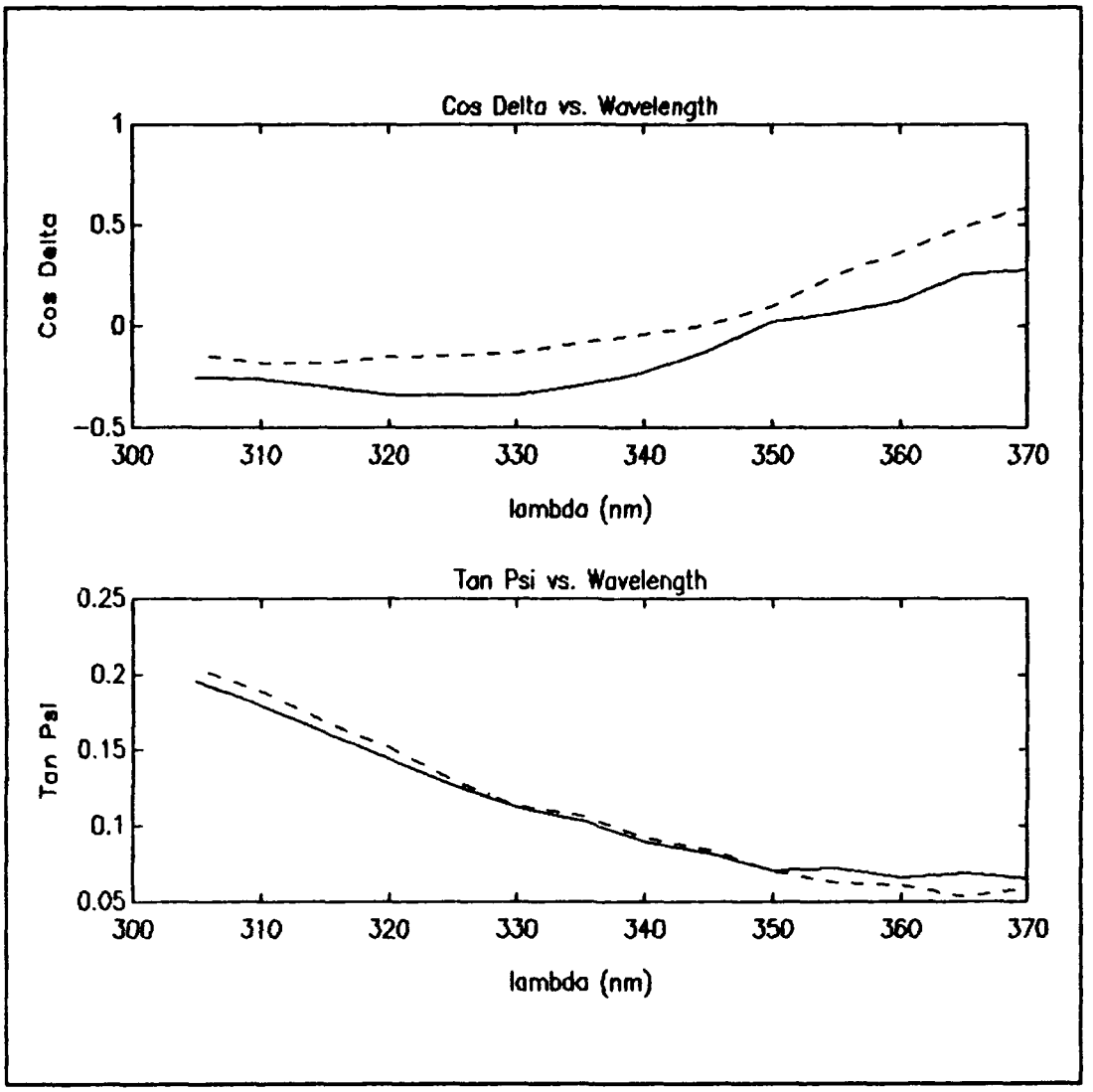

Figure 35 Fitted and Experimental Data for 5 Layer PBLG on ITO Coated Glass at 70° (Dashed line is fitted data)

T_{f1} = 164 ± 2 Å

(N_{i1} = 1.65 - 0.20*i and

N_{j1} = N_{i1} = 1.62 - 0.10*i for all wavelengths)

VARIANCE = 0.0075

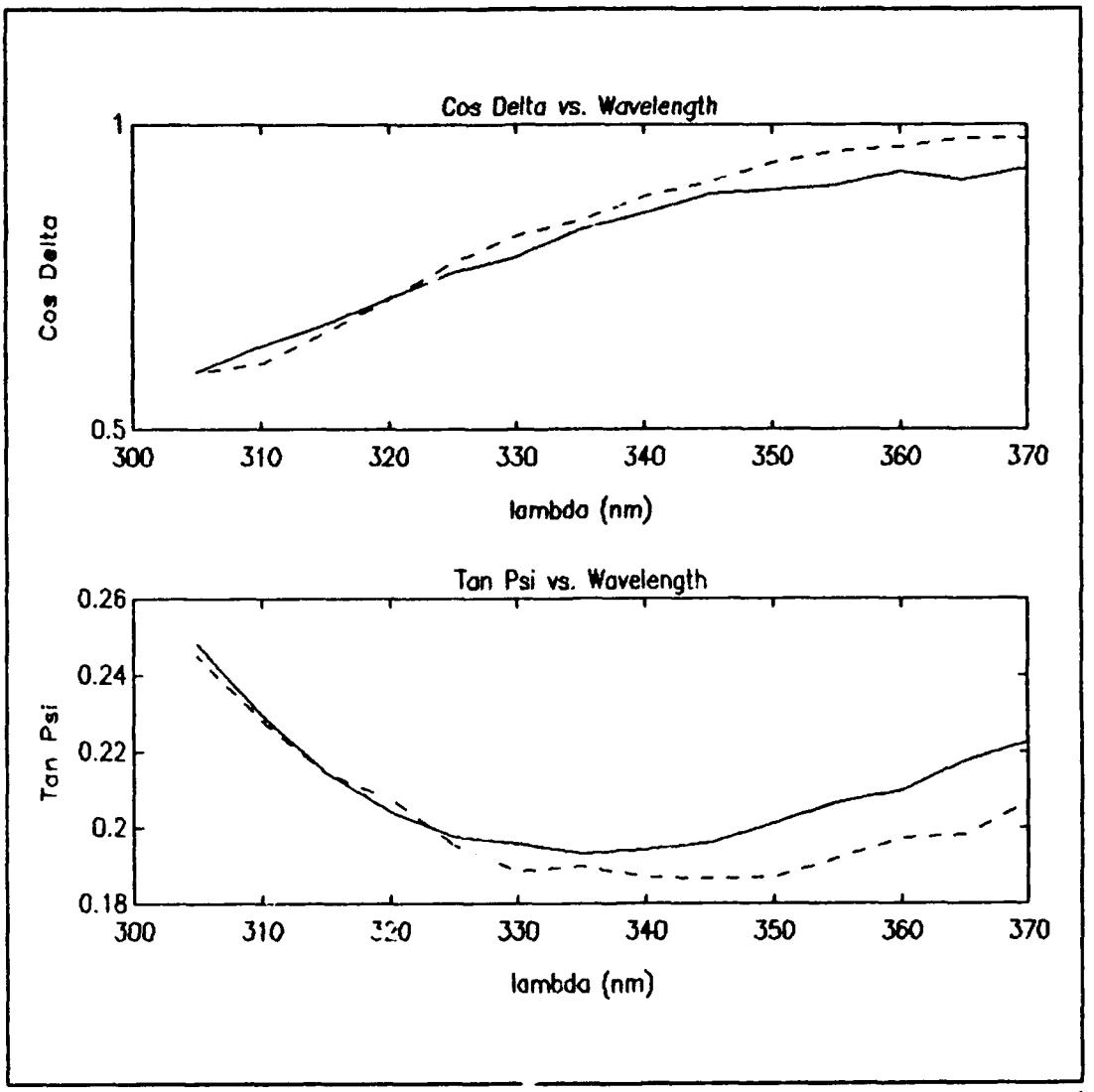

Figure 36 Fitted and Experimental Data for 5 Layer PBLG on ITO Coated Glass at 75° (Dashed line is fitted data)

T_{f1} = 164 ± 2 Å

(N_{x1} = 1.65 - 0.20*i and

N_{y1} = N_{z1} = 1.62 - 0.10*i for all wavelengths)

VARIANCE = 0.0075

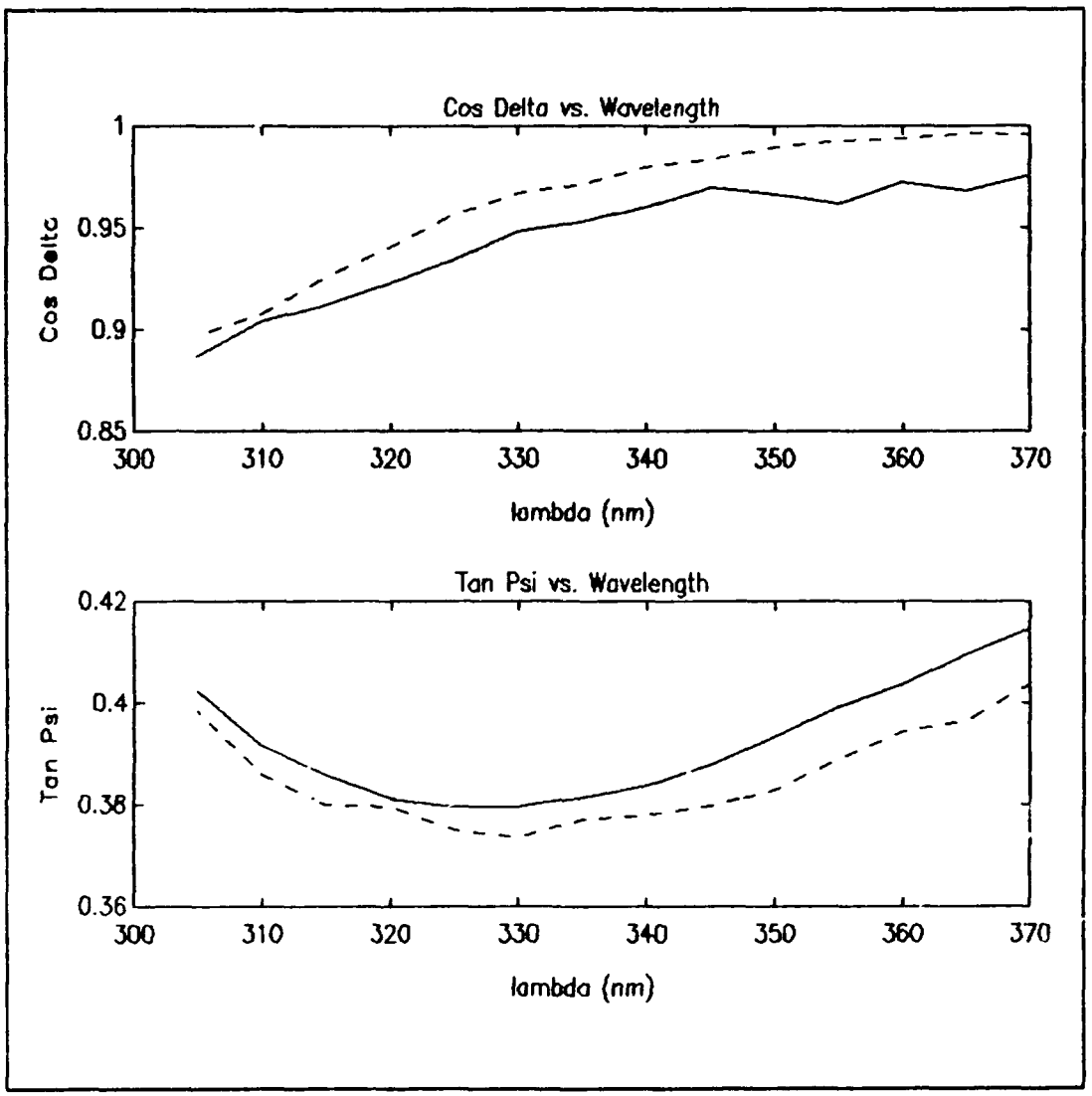

Figure 37 Fitted and Experimental Data for 5 Layer PBLG on ITO Coated Glass at 80° (Dashed line is fitted data)

T_{f1} = 164 ± 2 Å

(N_{x1} = 1.65 - 0.20*i and

N_{y1} = N_{z1} = 1.62 - 0.10*i for all wavelengths)

VARIANCE = 0.0075

Appendix H: PBLG 8 Layer Fitted Data

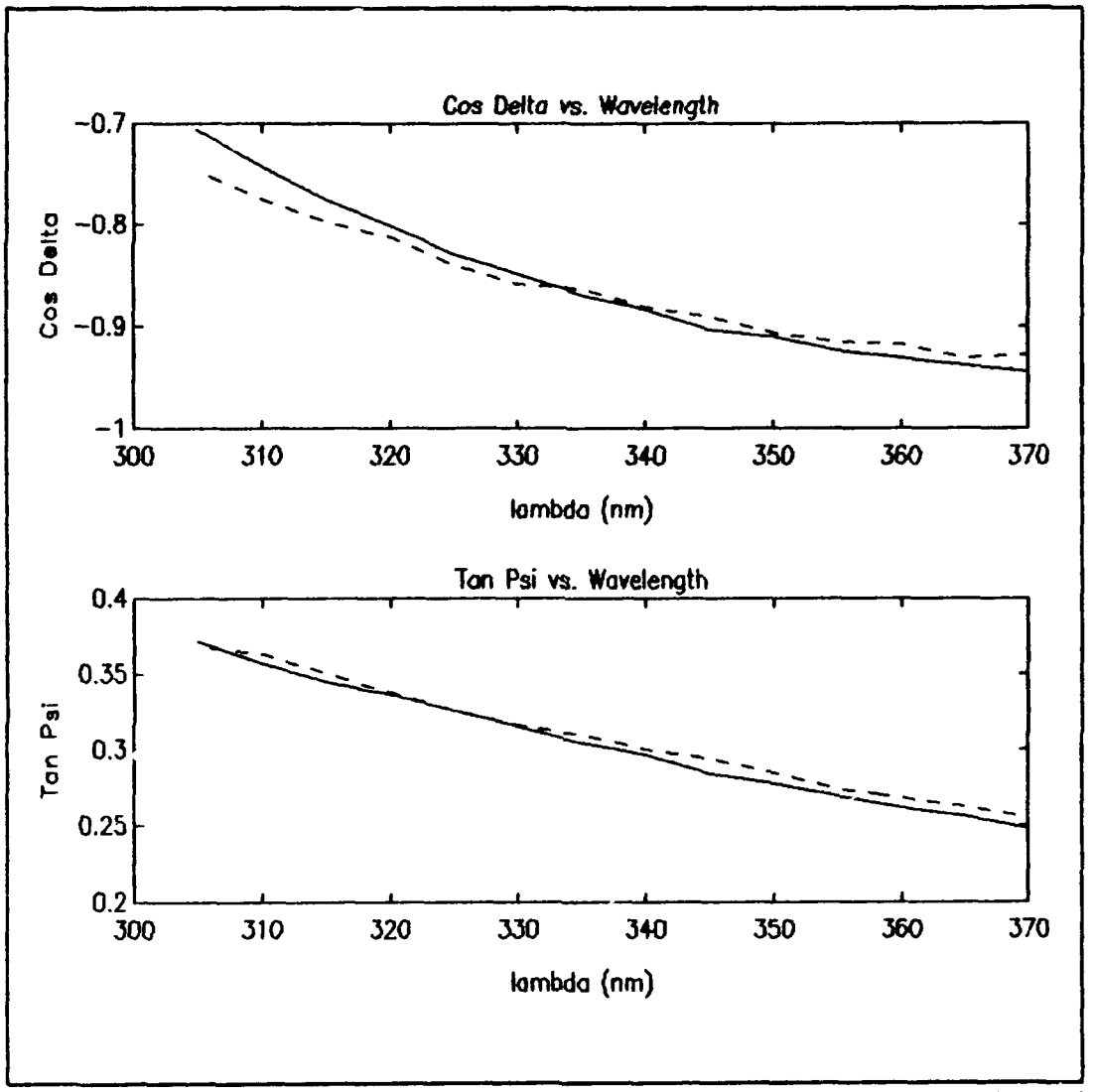

Figure 38 Fitted and Experimental Data for 8 Layer PBLG on ITO Coated Glass at 60° (Dashed line is fitted data)

T_{f1} = 216 ± 2 Å

(N_{s1} = 1.65 - 0.18*i and

N_{f1} = N_{s1} = 1.62 - 0.09*i for all wavelengths)

VARIANCE = 0.0056

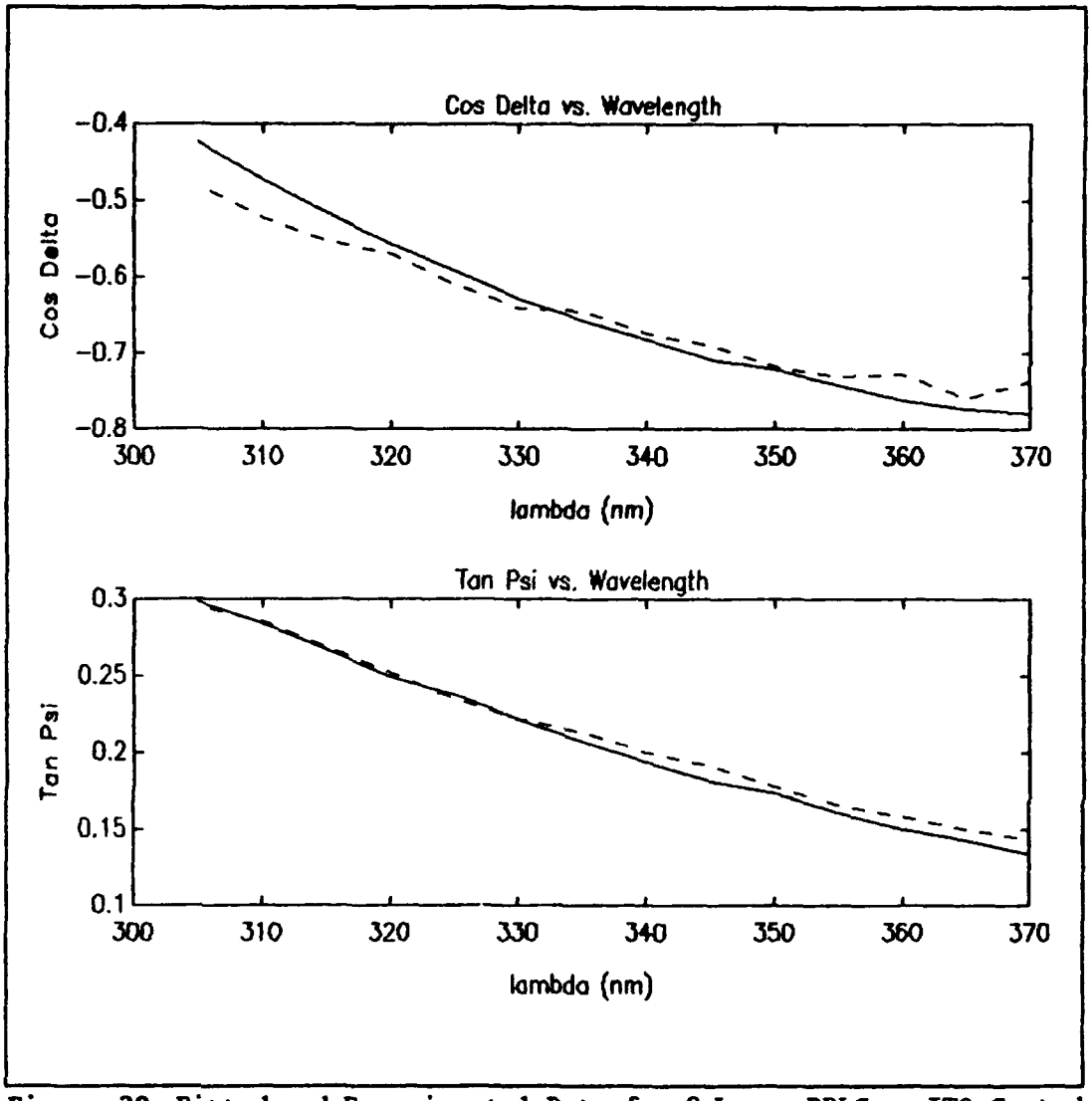

Figure 39 Fitted and Experimental Data for 8 Layer PBLG on ITO Coated Glass at 65° (Dashed line is fitted data)

T_{f1} = 216 ± 2 Å

(N_{x1} = 1.65 - 0.18*i and

N_{y1} = N_{z1} = 1.62 - 0.09*i for all wavelengths)

VARIANCE = 0.0056

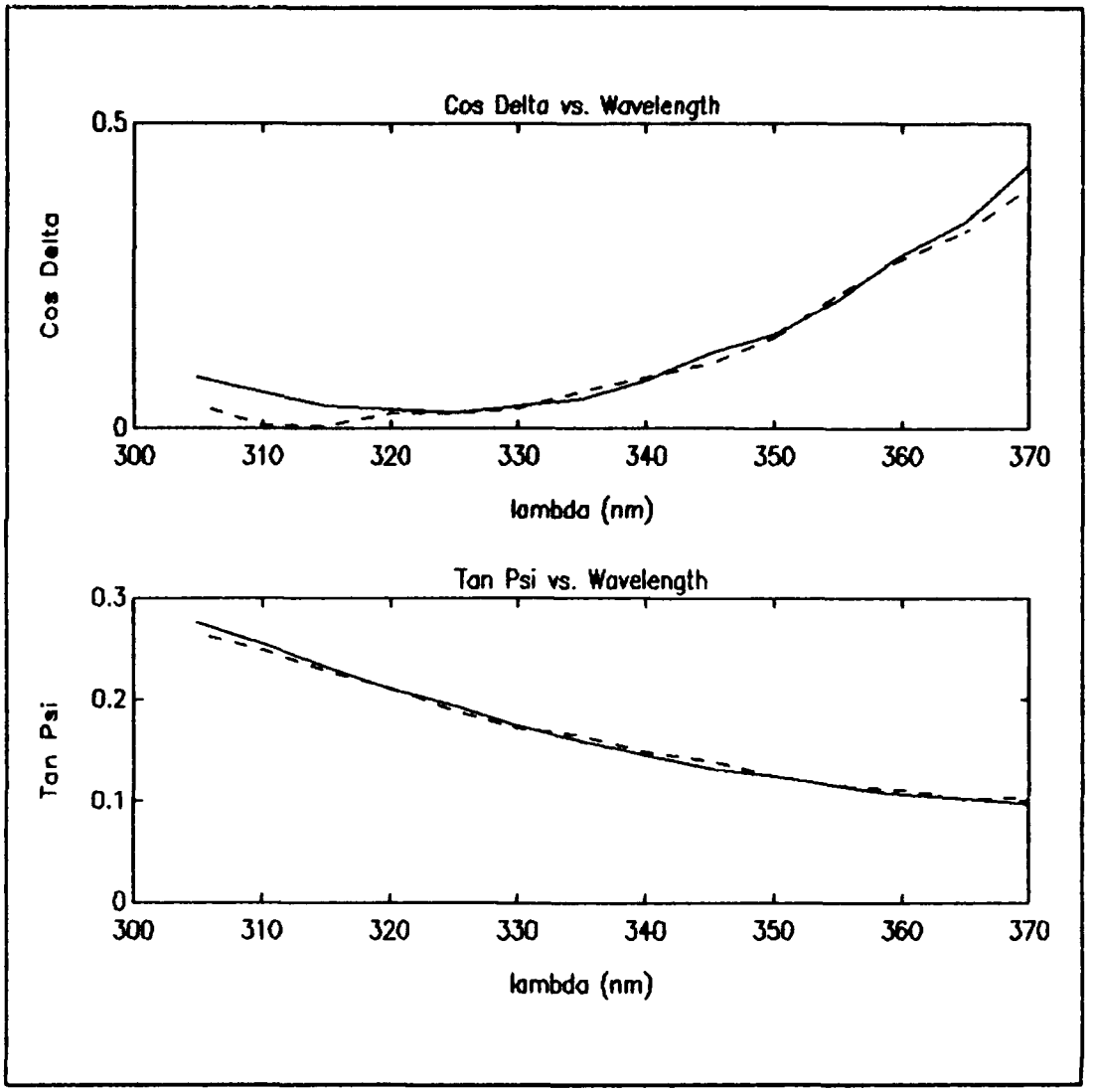

Figure 40 Fitted and Experimental Data for 8 Layer PBLG on ITO Coated Glass at 70° (Dashed line is fitted data)

T_{f1} = 216 ± 2 Å

(N_{z1} = 1.65 - 0.18*i and

N_{y1} = N_{z1} = 1.62 - 0.09*i for all wavelengths)

VARIANCE = 0.0056

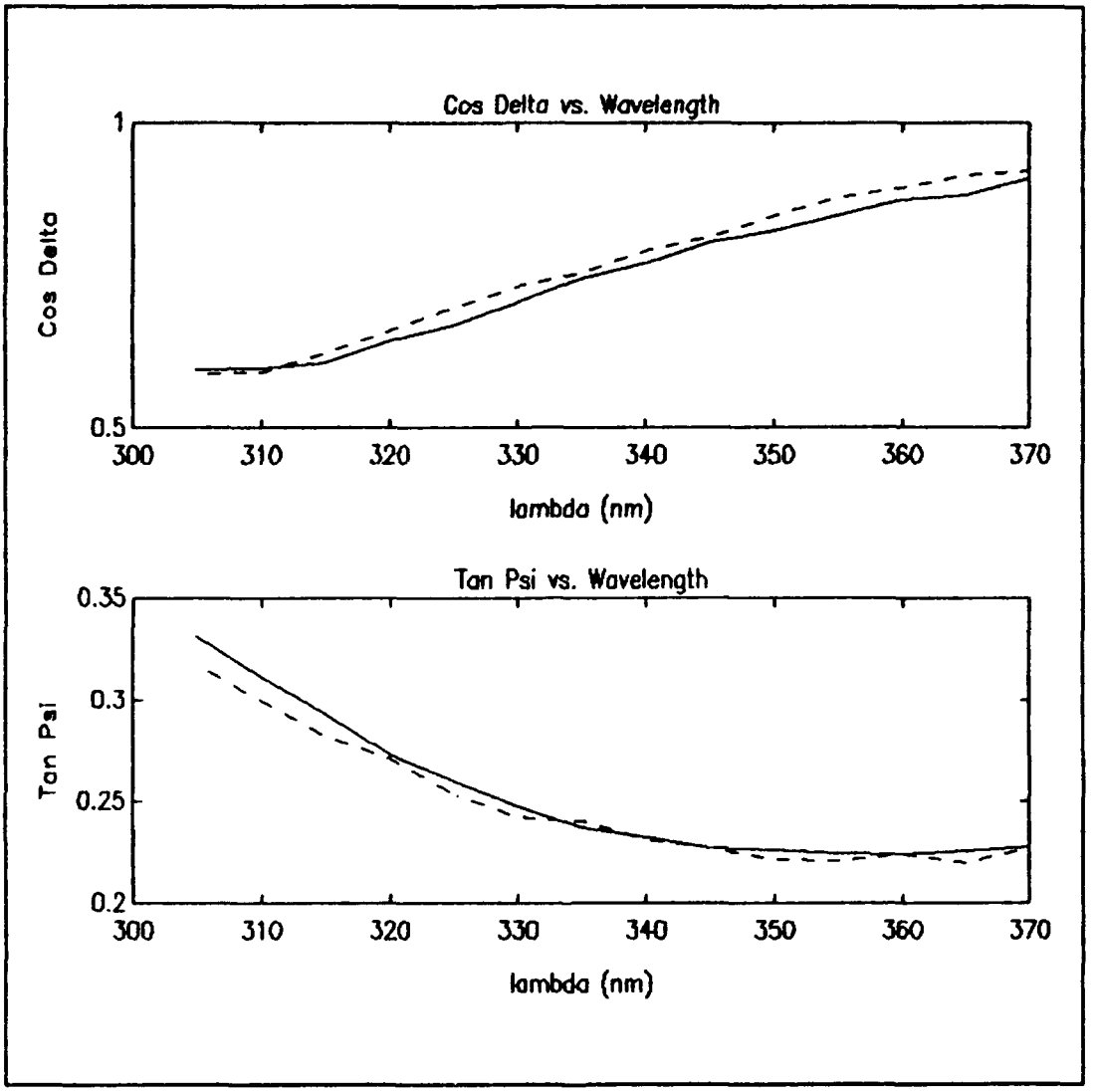

Figure 41 Fitted and Experimental Data for 8 Layer PBLG on ITO Coated Glass at 75° (Dashed line is fitted data)

T_{f1} = 216 ± 2 Å

(N_{z1} = 1.65 - 0.18*i and

N_{y1} = N_{x1} = 1.62 - 0.09*i for all wavelengths)

VARIANCE = 0.0056

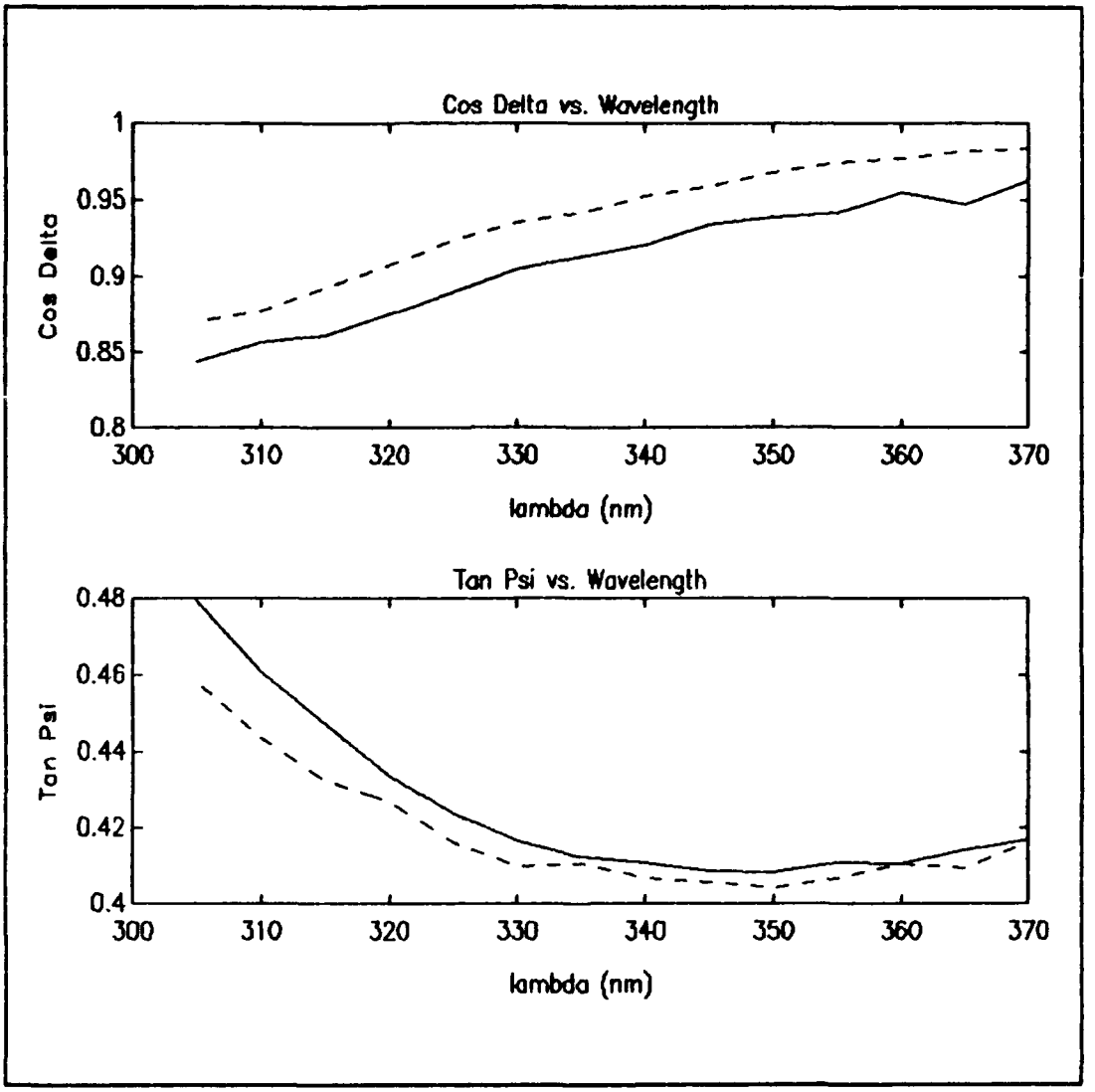

Figure 42 Fitted and Experimental Data for 8 Layer PBLG on ITO Coated Glass at 80° (Dashed line is fitted data)

T_{f1} = 216 ± 2 Å

(N_{x1} = 1.65 - 0.18*i and

N_{y1} = N_{z1} = 1.62 - 0.09*i for all wavelengths)

VARIANCE = 0.0056

Appendix I: Thiophene Fitted Data

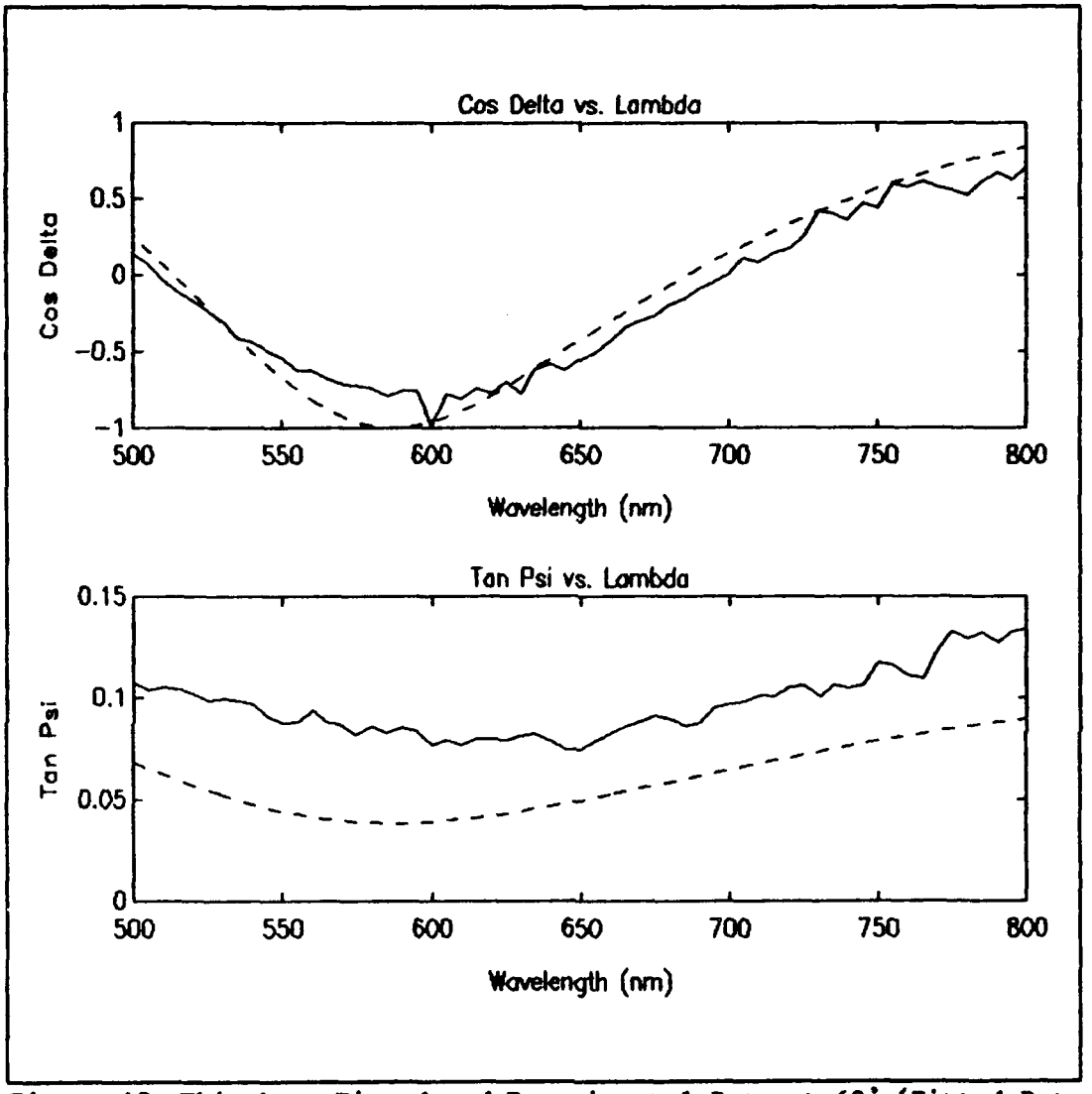

Figure 43 Thiophene Fitted and Experimental Data at 60° (Fitted Data is Dashed)

T_f = 3060 ± 7 Å

(N_f = 1.68 - 0*i for all wavelengths)

VARIANCE = 0.0075

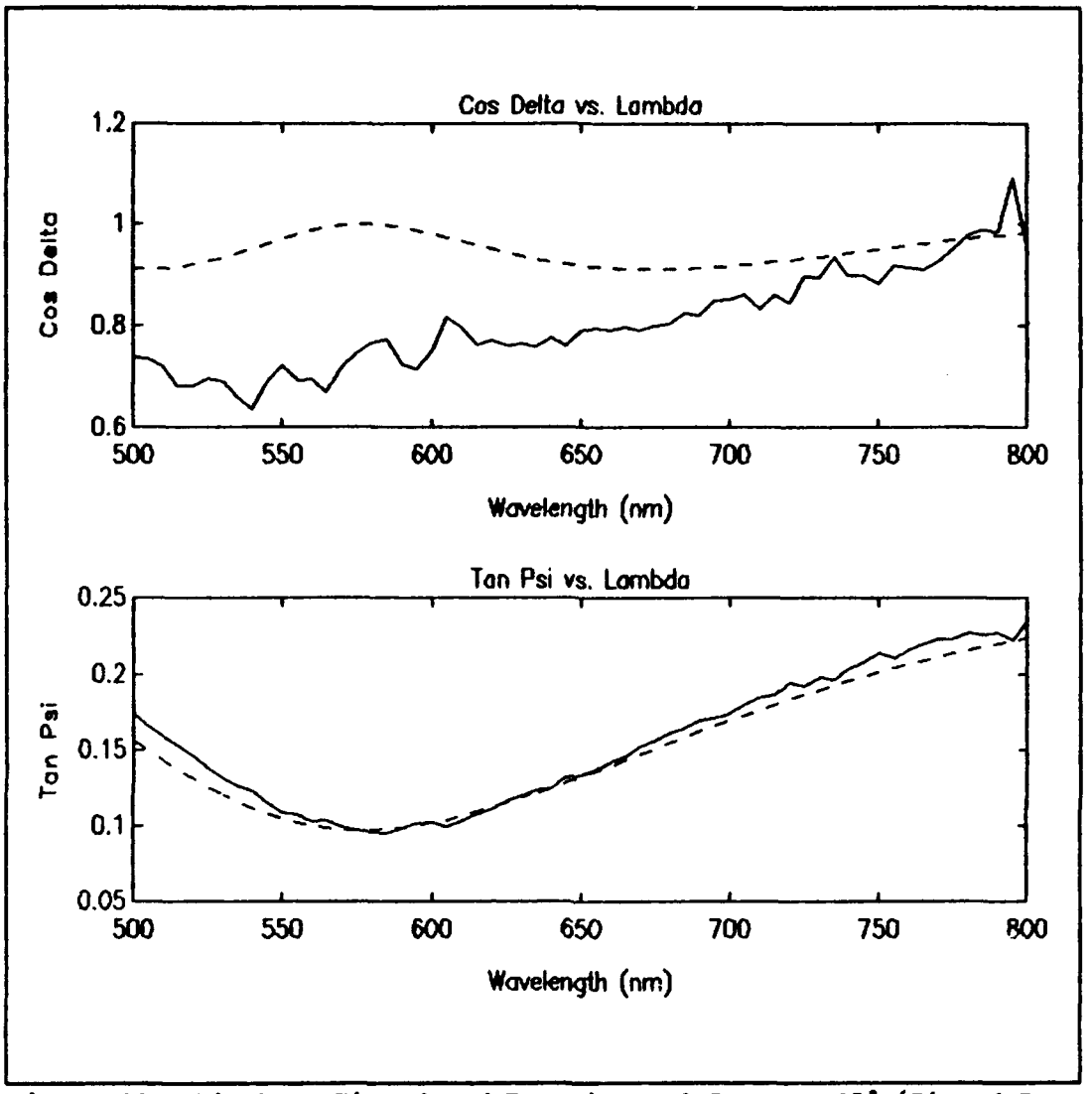

Figure 44 Thiophene Fitted and Experimental Data at 65° (Fitted Data is Dashed)

T_f = 3060 ± 7 Å

(N_f = 1.68 - 0*i for all wavelengths)

VARIANCE = 0.0075

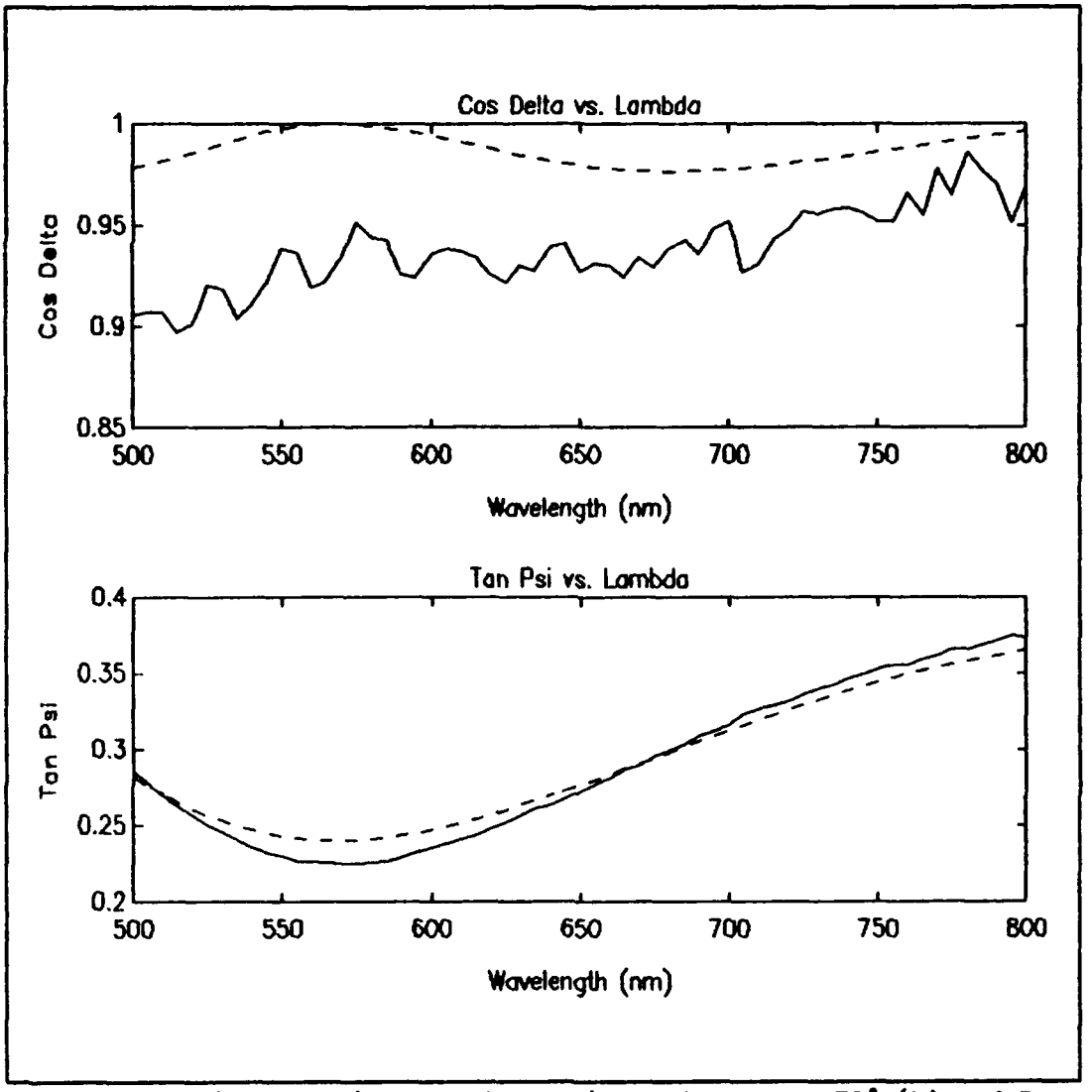

Figure 45 Thiophene Fitted and Experimental Data at 70° (Fitted Data is Dashed)

T_f = 3060 ± 7 Å

(N_f = 1.68 - 0*i for all wavelengths)

VARIANCE = 0.0075

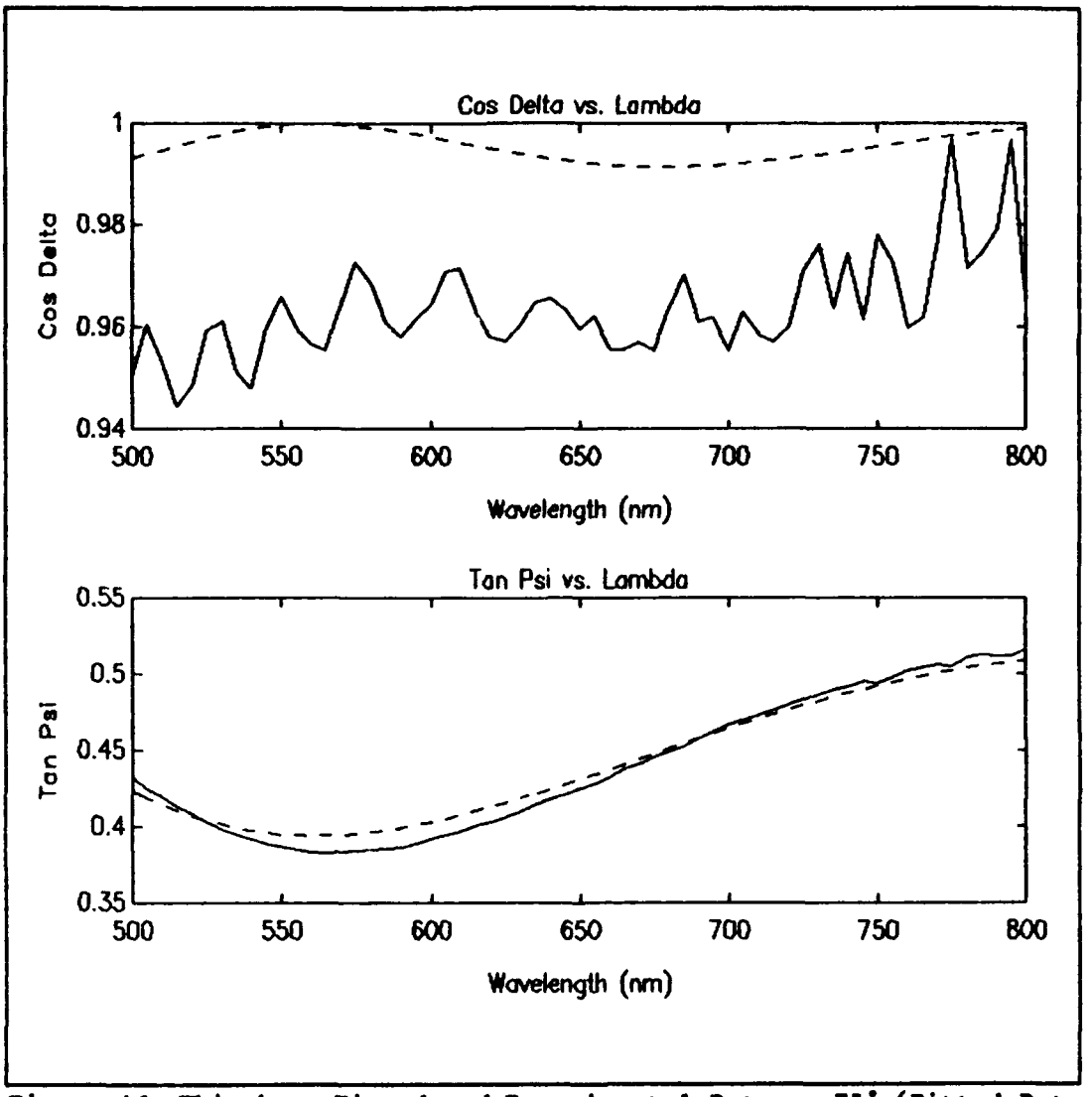

Figure 46 Thiophene Fitted and Experimental Data at 75° (Fitted Data is Dashed)

T_f = 3060 ± 7 Å

(N_f = 1.68 - 0*i for all wavelengths)

VARIANCE = 0.0075

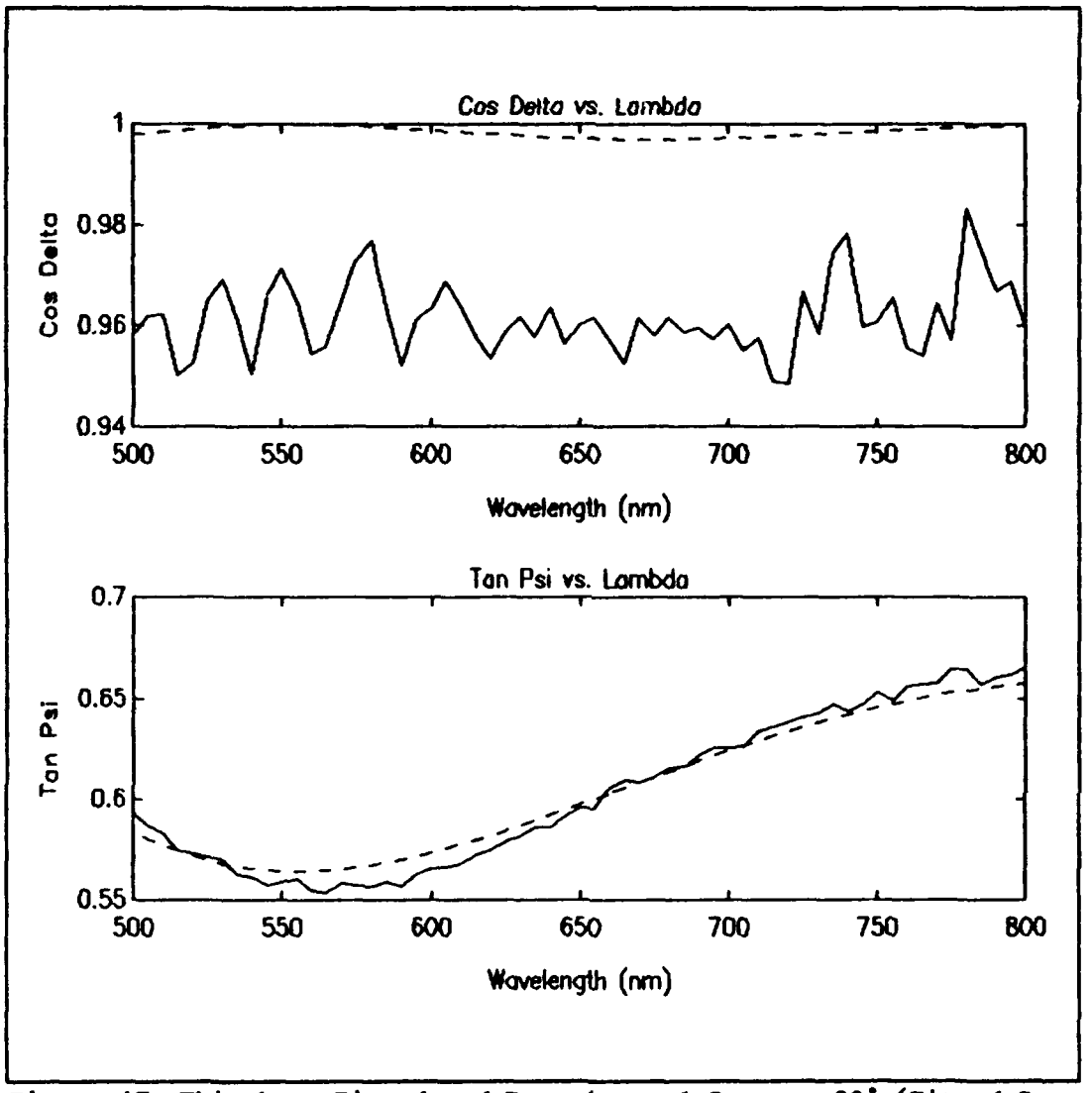

Figure 47 Thiophene Fitted and Experimental Data at 80° (Fitted Data is Dashed)

T_f = 3060 ± 7 Å

(N_f = 1.68 - 0*i for all wavelengths)

VARIANCE = 0.0075

Bibliography

1. Hann, R. and Bloor, D. (ed) 1989 *Organic Materials for Nonlinear Optics* Special Publication 69. (London: Royal Society of Chemistry).

2. Davis, R. et al. "Ellipsometric Observations of Surface Adsorption and Molecular Interactions of Native and Modified Fibrinogen and Factor VIII," *Surface Science*, 96: 539-554 (1980).

3. Ducharme, D. "Ellipsometric Studies of Rod Outer Segment Phospholipids at the Nitrogen-Water Interface," *Thin Solid Films*, 132: 83-90 (1985).

4. Gun, J. et al. "On the Formation and Structure of Self-Assembling Monolayers," *Journal of Colloid and Interface Science*, 101: 201-213 (September 1984).

5. Azzam, R. and Bashara, N. *Ellipsometry and Polarized Light*: New York, North-Holland Publishing, 1986.

6. Arfkin, G. *Mathematical Methods for Physicists*: New York, Academic Press, 1985.

7. Rudolph Research. *s2000 Spectroscopic Ellipsometer*. Rudolph Research Corporation, Flanders NJ, March 1990.

8. Householder, A. *The Theory of Matrices in Numerical Analysis*. New York: Dover Publishing, 1975.

9. Marquardt, D. "An Algorithm for Least-Squares Estimation of Non-Linear Parameters." *Journal of the Society for Industrial and Applied Mathematics*, 11: 431-441 (June 1963).

10. Press, W. et al. *Numerical Recipes: The Art of Scientific Computing*. New York: Cambridge University Press, 1986.

11. Thonn, T. and Azzam, R. "Determination of the Optical Constants and Thickness Profile of a Tapered Inconel Film by Reflection Ellipsometry," *Thin Solid Films*, 127: 215-222 (1983).

12. Aspnes, D. "Spectroscopic Ellipsometry of Solids," *Optical Properties of Solids - New Developments*, Chapter 15, edited by B. Seraphin. New York: New Holland, 1976.

13. Tomar, M. and Srivastava, V. "Anisotropic Effects in the Ellipsometry of Built-Up Films and Determination of Their Optical Constants," *Thin Solid Films*, 15: 207-215 (1973).

14. Den Engelsen, D. "Ellipsometry of Anisotropic Films," *Journal of the Optical Society of America*, 61: 1460-1466 (November 1971).

15. Boinovich, L. and Emel'Yanenko, A. "Ellipsometry of Free-Lying Films," *Surface Science*, 225: 206-216 (1990).

16. Tronin, A. and Kostantinova, A. "Ellipsometric Study of the Optical Anisotropy of Lead Arachidate Langmuir Films," *Thin Solid Films*, 177: 305-314 (1989).

Vita

Captain Mark L. Sward was born on 08 March 1963 in St. Paul, MN. He graduated from Cretin High School in St. Paul in 1981, and attended the University of Southern California. Upon graduation with a Bachelor of Science in Physics in 1985, he received a regular commission in the USAF. He was assigned as a Nuclear Research Officer at the Technical Operations Division (TOD), a subordinate unit of the Air Force Technical Applications Center (AFTAC), until entering the School of Engineering, Air Force Institute of Technology (AFIT), in May 1989.

Permanent Address: 687 O..io St.
St. Paul, MN 55107

REPORT DOCUMENTATION PAGE

Form Approved
OMB No 0704 0188

Public reporting burden for this collection of information is estimated to average 1 hour per response, including the time for reviewing instructions, searching existing data sources, gathering and maintaining the data needed, and completing and reviewing the collection of information. Send comments regarding this burden estimate or any other aspect of this collection of information, including suggestions for reducing this burden, to Washington Headquarters Services, Directorate for information Operations and Reports, 1215 Jefferson Davis Highway, Suite 1204, Arlington, VA 22202-4302, and to the Office of Management and Budget, Paperwork Reduction Project (0704-0188), Washington, DC 20503.

1. AGENCY USE ONLY (Leave blank)	2. REPORT DATE	3. REPORT TYPE AND DATES COVERED
	December 1990	Master's Thesis

4. TITLE AND SUBTITLE
DETERMINATION OF THE OPTICAL PROPERTIES OF ORGANIC THIN FILMS BY SPECTROSCOPIC ELLIPSOMETRY

5. FUNDING NUMBERS

6. AUTHOR(S)
Mark L. Sward, Captain, USAF

7. PERFORMING ORGANIZATION NAME(S) AND ADDRESS(ES)
Air Force Institute of Technology, WPAFB, OH 45433-6583

8. PERFORMING ORGANIZATION REPORT NUMBER
AFIT/GEP/ENP/90D-7

9. SPONSORING MONITORING AGENCY NAME(S) AND ADDRESS(ES)

10. SPONSORING/MONITORING AGENCY REPORT NUMBER

11. SUPPLEMENTARY NOTES

12a. DISTRIBUTION AVAILABILITY STATEMENT
Approved for public release; distribution unlimited

12b. DISTRIBUTION CODE

13. ABSTRACT (Maximum 200 words)

This thesis demonstrated the feasibility of determining the optical properties of organic and polymer thin films through the use of Spectroscopic Ellipsometry (SE). Tan Ψ and cos Δ data from 300-800 nanometers (nm) were taken with a Rudolph Research s2000 spectroscopic ellipsometer four samples: indium tin oxide (ITO) coated glass; five layer poly-benzyl-L glutamate (PBLG) organic film on ITO coated glass; eight layer PBLG film on ITO coated glass; and a thiophene polymer film on a microscope slide. The data sets were fit to a choice of four computer models based on a paper written by Dwight Berreman in 1972. The four models were written in MATLAB to take advantage of its matrix manipulative capabilities. The models were: a single layer isotropic film on an isotropic substrate; a single layer anisotropic film on an isotropic substrate; two isotropic films on an isotropic substrate; and two anisotropic films on an isotropic substrate. Using only tan Ψ data over a restricted wavelength region, all four data sets were fit to variances of 0.01 or less.

14. SUBJECT TERMS	15. NUMBER OF PAGES
Ellipsometry, Ellipsometry (Spectroscopic), PBLG, ITO, thiophene, MATLAB, Berreman, organic, thin films, polymer	95
	16. PRICE CODE

17. SECURITY CLASSIFICATION OF REPORT	18. SECURITY CLASSIFICATION OF THIS PAGE	19. SECURITY CLASSIFICATION OF ABSTRACT	20. LIMITATION OF ABSTRACT
Unclassified	Unclassified	Unclassified	UL